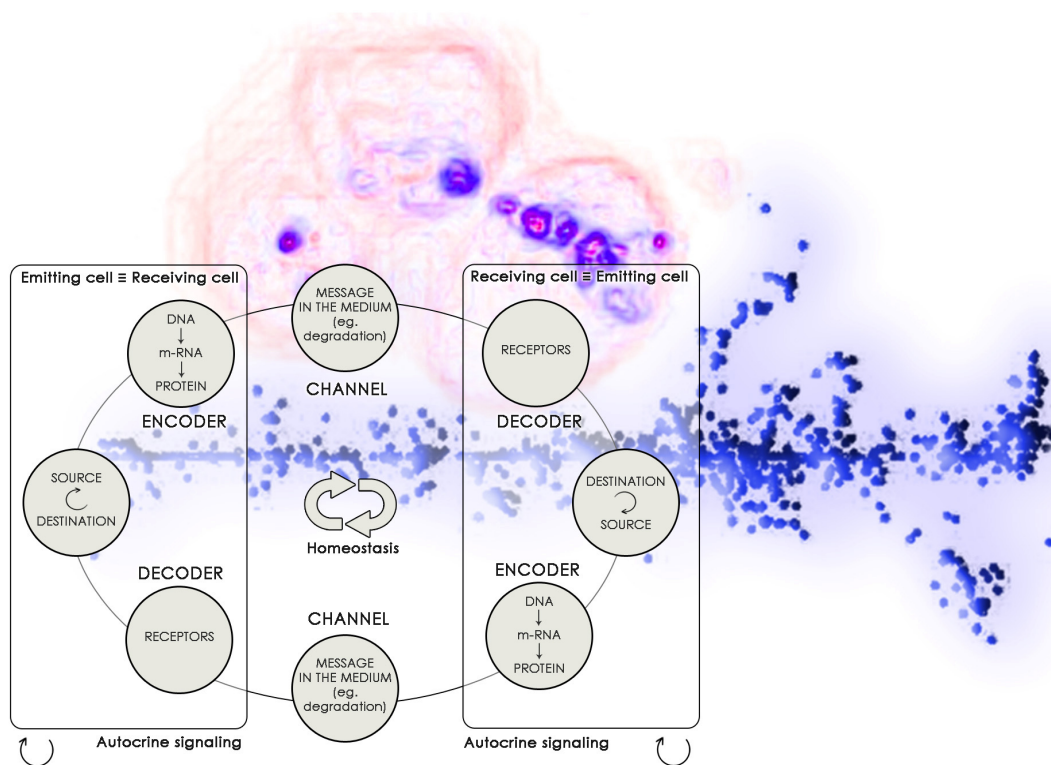


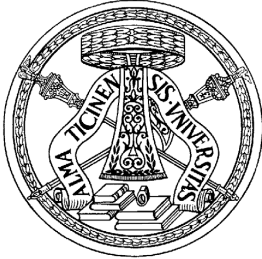
Multi-Scale Response of Cell Perturbation induced by different Radiation Qualities: a Systems Radiation Biology Approach

Luca Giovanni Mariotti

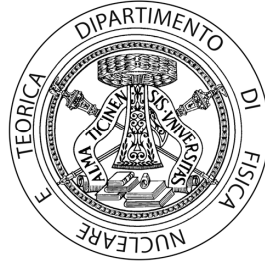


Tesi per il conseguimento del titolo

Università degli
Studi di Pavia



Dipartimento di Fisica
Nucleare e Teorica



Istituto Nazionale di
Fisica Nucleare



DOTTORATO DI RICERCA IN FISICA – XXIII CICLO

**MULTI-SCALE RESPONSE OF CELL PERTURBATION
INDUCED BY DIFFERENT RADIATION QUALITIES:
A SYSTEMS RADIATION BIOLOGY APPROACH**

dissertation submitted by

Luca Giovanni Mariotti

to obtain the degree of

DOTTORE DI RICERCA IN FISICA

Supervisor: Prof. Andrea Ottolenghi (Università degli Studi di Pavia)

Referee: Prof. Peter O'Neill (University of Oxford, Gray Laboratory)

Cover: Schematic representation of a multi-scale investigation:

Background: Gamma H2AX phosphorylation induced by transversal of a Alpha particle inside a cellular nucleus (pink dots); alpha track simulation realized with the PARTRAC code (blue dots) (courtesy of Dr. Friedlan, Helmutz center, Munich)

Foreground: Proposed model of cell communication in response to exposure to ionizing radiation

© Luca Giovanni Mariotti, Pavia

ISBN 978-88-95767-42-0

Dottorato di Ricerca in Fisica

Università di Pavia, Italy

Printed by Print Service, Pavia

November 2010

To mix up the models with reality is like going to the restaurant and eating the menu.

Anonymous

Contents

1	Introduction	1
2	From physical interactions to DNA damage	3
2.1	DNA as the biological target	4
2.1.1	Direct and indirect induction of DNA damage	7
2.2	Modelling Radiation Induced Double strand breaks	11
2.3	The PARTRAC code	14
2.3.1	The Structure of the code	15
2.3.2	DSB distribution as a function of the LET	29
2.3.3	Small Fragments analysis	37
2.4	Internal Exposure	39
2.4.1	Changes in the shape of the sources used and their location	40
2.4.2	Results	41
3	The evolution of DNA damage: protein recruitment at the damage site	47
3.1	Radiation Induced γ X2AX	47
3.2	Radiation Induced foci as a Function of radiation quality	50
3.2.1	Low LET irradiation: X-Rays	50
3.2.2	High LET irradiation: Alpha particles	53
3.2.3	Example of mixed Field Irradiation: Antiprotons	59
3.3	Theoretical analysis	64
3.3.1	Model Definition	65
3.3.2	Results	66
4	The irradiated cell as a <i>perturbed system</i> in its environment	73
4.1	Bystander effect	73
4.1.1	Bystander experimental techniques: The irradiated Conditioned Medium (ICM)	76
4.2	Cell Communication: general features	77
4.3	Cell Communication perturbation: A systems radiation biology approach	78

4.3.1	Communication model: A general formalization	80
4.3.2	Cytokine role in the bystander signalling	81
4.3.3	Preliminary experiments for signaling investigation	82
4.3.4	How do the experimental condition affect the cytokine release?	94
4.3.5	How does the cytokine release affect the cell behavior?	96
4.3.6	Theoretical analysis (I): the stochastic approach	98
4.3.7	Theoretical analysis (II): the analytical approach	100
4.3.8	Cell signaling modulation induced by different radiation qualities	110
4.3.9	IL-6 and IL-8: The role of oxidative stress	115
4.4	Expression of NF-kB	119
4.4.1	Activation and role of NF-kB	122
4.4.2	Experimental Detection of NF-kB	124
4.4.3	NK-kB activation: Experimental results	125
4.4.4	NF-kB and cytokine expression	127
4.4.5	Theoretical analysis	128
4.5	Receptor Expression as a function of Radiation Quality	139
5	Conclusions	145

Chapter 1

Introduction

The evaluation of the risk associated to low doses of ionizing radiation is still an open question in radiation research. For radiation protection purposes, the risk at low doses is generally obtained with a holistic approach through extrapolations from data at higher doses, mainly obtained from A-bomb survivors, in a *top down* fashion (where the basic mechanisms of a single element of the system can be described extrapolating the behavior of the emergent phenomena that characterizes the system itself).

The data coming from the epidemiological studies allow reliable extrapolation only for doses higher than 1 Gray. To understand the effect at lower doses, a mechanistic approach is needed to investigate radiation effect in a dose range (cGy) where epidemiological studies are not able to discriminate the radiation effect from the background fluctuations.

This reductionistic (based on the reductive nature of typical molecular biology approach), mechanistic approach (often referred as *bottom up*) needs to analyze all the details of the processes of the investigated phenomena, to try to infer the results obtained usually in *in vitro* controlled systems to the *in vivo* situation.

In this thesis the investigation of the low dose research was carried out following a mechanistic description of the radiation injury, according to the latter approach.

In the case of radiation biology, the induction of a radiological damage in humans is a complex process that starts with the energy deposition in the target and can lead to the formation of somatic and/or genetic effect in the organism. This process is characterized by a very wide time-scale and spatial-scale that goes from the initial processes of energy transfer right after the interaction between the radiation and the matter to the induced biological effects in the biological system (single cell, tissue, organs and so on) that can even take years (e.g. carcinogenesis).

With the increasing efficiency of the experimental biological techniques (and irradiation technology), an increasing number of mechanisms underlying the induction of the damage have been discovered and investigated, starting - just

to refer to the most famous one - from the analysis of gene expression in irradiated cells.

In the past few years, with the evolution of experimental detection techniques, also the vision of the biological damage evolved, passing from a focus on the damage in terms of the DNA molecule, to a new one, wherein the final results of the radiation insult is seen as a broader response of the system (single cell, tissue, organ etc) to the perturbation induced by the radiation exposure. Amongst all the mechanisms studied, to try to further enlarge the number of processes investigated, new attention has been devoted to the role of cell communication in the transmission of the effects also to cells not directly hit by radiation (i.e. bystander effect). This step is particularly important because, besides its crucial role in the understanding the *in vitro* situation, can be useful to understand the mechanism of carcinogenesis in 3-dimensional architecture or even *in vivo*, where the investigation of the micro environment characteristics is crucial.

In this thesis work the idea was to explore the different steps that lead to the formation of the radiobiological damage, starting from the early events occurring after irradiation (e.g. DNA damage), passing through the molecular response (DNA repair, mediated by the recruitment of the sensor proteins) to the investigation of the role of the signal transmission in the evolution of the cellular damage (focusing on low dose range). The adopted method was an integrated approach with the design of experiments useful for the development of models, that in turn conducted to the design of further experiments to test some of the mechanisms hypothesized.

One particular prominent aspect of our research was the characterization of robustness of the cellular system for different endpoints, that is their insensitivity to a wide range of possible perturbations (including irradiation). From these considerations on the robustness of the *in vitro* system, it was also possible to quantify the difference between some mechanisms examined with this research and their *in vivo* correspondents.

In this framework, particular attention was also devoted to the study of the effect that different radiation quality could have in the different steps of radio biological damage formation. The qualitative and quantitative differences between sparsely and densely ionizing radiation mainly reside on the cluster properties and the different temporal properties of the incident radiation. Due to the different pattern of energy deposition between low LET and high LET radiation (especially at low doses) the response mechanisms of each cell can be very different: for this reason all the investigations in this thesis covered systematically both low LET and high LET radiations.

In the first part of this thesis (Chapter 2) we studied the processes from physical interaction to DNA damage. In particular we present the biophysical Monte Carlo code PARTRAC (PARTicles TRACks) used in this work and developed by the Helmholtz Institute of Munich in collaboration with the University of Pavia that allows a reliable reproduction - at the nanometer scale - of the

passage of radiation inside biological target (the code also provides a detailed (atom-by-atom) description of the DNA and chromatin structure). In this chapter the study considered the initial radiation insult (with radiation characterized by the same LET or by the same specific energy) to inspect the role of the track structure in the formation of DNA breakages. The code was then developed in order to describe also the internal emitters behavior for different nuclide types and with different biophysical endpoints (dose released in the cell, varying the concentration of the nuclide in the cell nucleus, DSB formation and chromosomal aberrations induction)

In Chapter 3 we studied the evolution of DNA damage (protein recruitment), An investigation of the phosphorylation process was carried out (in collaboration with the radiation biology group at the Center for Cancer Research and Cell Biology at Queen's University of Belfast), in particular focusing on the kinetics of the protein recruitment leading to the induction of a visible focus. The study was carried out with 3 different radiation types (e.g. gamma, alpha and antiproton irradiation), starting with a qualitative study on the size and the properties of the foci. Furthermore an analytical model was developed to quantify the parameters involved in the foci induction (such as kinetics of phosphorylation, residual damage) as a function of the radiation adopted.

In Chapter 4 we studied the irradiated cell as a perturbed system in its environment. In particular we investigated the study of relevant signals - in our case, cytokines (i.e. IL-6 and IL-8) - after exposure of fibroblasts to different types of ionizing radiation. The investigation covered the whole pattern of signal transmission, from the quantification of the release of the molecules after irradiation, through the diffusion in the media (where they might be degraded by free proteases) and to a detailed study of receptors expression either in irradiated and bystander cells. We evaluated the release of these cytokines and their correspondent receptor expression after irradiation both in normal condition and in presence of scavengers (DMSO, c-PTIO) of the molecules involved in the early-steps of bystander transmission, such as NO, ROS and OH radicals. The investigation was carried out through the development of an integrated theoretical/experimental approach, with the construction of ad hoc models able to describe the underlying mechanisms of cell communication and its perturbation by radiation.

The results were discussed and hypotheses were formulated about the relationship between radiation exposure and the activity of the related transcription factor (e.g. NF-kB expression), in order to give an interpretation of the perturbation of the protein's signalling. A theoretical model based on feedback mechanisms were adopted and a best fit of the experimental data was considered. By using this technique, we observed and quantified the variation of the expression of nuclear NF-kB following a perturbation from low-dose gamma irradiation.

Chapter 2

From physical interactions to DNA damage

In order to understand and potentially prevent the effects of ionizing radiations on living systems, it is necessary to know all the mechanisms involved after the interaction of the radiation that lead to the final damage.

Considering that some effects can show up after years, the whole process could be divided temporarily. This process could be classified into three phases: physical, chemical and biological.

The physical phase consists of primary interaction events between ionizing radiations and the atoms and molecules of target. In this first part, charged particles excite or ionize the orbital atomic electrons of the material (usually low Z elements) whereas neutral radiation (e.g. gamma rays) produces charged particles through other processes [88].

These secondary charged particles will lose their energy with further ionizations or excitations of the atomic electrons of the materials until they reach thermalization. For this reason, depending on the involved processes, the physical phase can last from 10^{-18} s to 10^{-12} s.

The important aspect of this first step is given by the possibility to correlate the characteristics of the radiation with the amount of the (initial) damage. As will be shown later, this has important consequences on the relation between dose and cellular damage.

During the chemical phase, the excited atoms and molecules chemically react with other components present in the cell. Ionizing radiation can produce molecules electrically charged because because of the ejection of an orbital electrons during the ionization process.

As will be shown later, this may result in the production of reactive species known as free radicals (especially after the ionization of the water molecules), which contain an unpaired electron in the outer shell. Free radicals are produced in 10^{-12} s and their reactions are complete within approximately 1 ms after radiation exposure [166]. The development of this phase can be modulated by the action of the so called scavengers, molecules responsible for the

inactivation of free radicals.

The biological phase includes all the processes that happen before the final damage (which starts from the direct/indirect initial damage, the DNA damage repair, etc), which can show up even after years or generations after the irradiation. This process usually starts with the repair mechanisms that drive the cellular response to radiation. Considering the complexity of the biological system, in particular in the case of *in vivo* studies, the biological phase is the most unpredictable and complex (and complicated) part of the time scale of effects in radiation biology.

In this chapter we will focus our investigation on the initial events (physical and chemical processes) that characterize the interaction of radiation with biological target.

2.1 DNA as the biological target

Deoxyribonucleic Acid (DNA) is a large molecule (a polymer) that most commonly occurs in nature with a well-known double helix structure. The basic features of this structure were deduced by James Watson and Francis Crick in 1953. It consists of two strands, held together by hydrogen bonds between the bases. The backbone of each strand - primary structure - consists of alternating sugar and phosphate groups and the sugar involved is deoxyribose. Attached to this backbone are four bases, the sequence of which specifies the genetic code. The complex base+sugar+phosphate group is called nucleotide. Two of the bases are single-rings groups (pyrimidines); these are thymine (T) and cytosine (C). Two of the bases are double-ring groups (purines); these are adenine (A) and guanine (G). The structure of a DNA strand is illustrated in Fig. 2.1.

Two separate chains of DNA are wound around each other following a helical (coiling) path - secondary structure - resulting in a right-handed double helix (or duplex). The negatively charged sugar-phosphate backbones of the molecules are outside, and the planar bases of each strand stack on above the other in the center of the helix. Between the backbone strands run the major and minor grooves, which also follow a helical path. The strands are joined non-covalently by hydrogen bonding between the bases on opposite strands, to form the base pair (bp) and the distance between the two strands is maintained regular at 2 nm.

There are around 10 bp per turn in the DNA double helix. The distance between two successive bases on the backbone is about 0.34 nm, so the helix pitch is about 3.4 nm. The two strands are oriented in opposite directions (anti parallel) and, most crucially, the two strands are complementary in terms of base sequences.

The last feature arises because the structures of these bases and the constraints

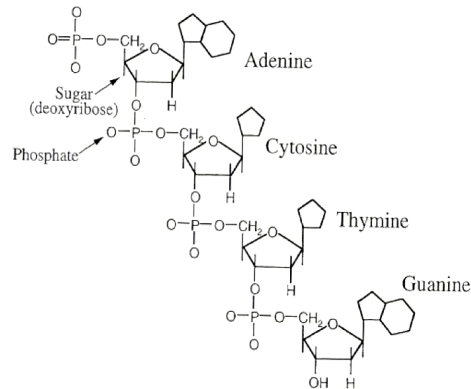


Figure 2.1: Structure of the DNA [118]

of the backbone dictate that the bases hydrogen-bond to each other as purine pyrimidine pairs which have similar geometry and dimensions. Guanine pairs with cytosine (three H-bonds) and adenine pairs with thymine (two H-bonds). Hence, any sequence can be accommodated within a regular double-stranded DNA structure (Figure 2.2).

The sequence in one strand uniquely specifies the sequence of the other, with

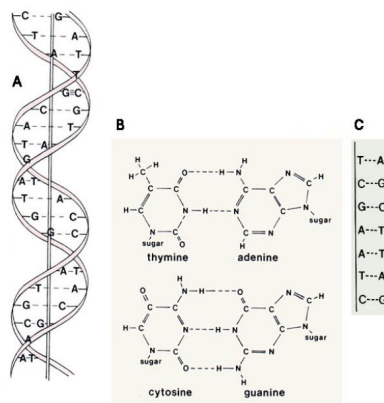


Figure 2.2: Structure of the DNA [118]

all that implies for the mechanism of copying (or replication) of DNA and the transcription of DNA sequence. In fact, a number of different forms of nucleic acid double helix have been observed and studied, all having the basic pattern of two helically-wound anti-parallel strands. The structure identified by Watson and Crick, as described above, is known as B-DNA, and is believed to be

the idealized form of the structure adopted by virtually all DNA *in vivo* (see Figure 2.3). It is characterized by a helical repeat of 10 bp/turn (although it is known that real B-DNA has a repeat closer to 10.5 bp/turn), by the presence of base pairs (bp) lying on the helix axis and almost perpendicular to it, and by having well-defined, deep major and minor grooves. DNA can be induced to form an alternative helix, known as the A-form, under conditions of low humidity. The A-form is right-handed, like the B-form, but has a wider, more compressed structure in which the base pairs are tilted with respect to the helix axis, and actually lie off the axis. The helical repeat of the A-form is around 11 bp/turn. Although it may be that the A-form, or something close to it, is adopted by DNA *in vivo* under unusual circumstances, the major importance of the A-form is that it is the helix formed by RNA (ribonucleic acid) and by DNA-RNA hybrids.

A further unusual structure can be formed by DNA. The left-handed Z-DNA is stable in synthetic double stranded DNA consisting purely of alternating pyrimidine/purine sequences (such as CGCGCG, with the same on the other strand of course respecting complementarity). This is because in this structure, the pyrimidine and the purine nucleotides adopt very different conformations, unlike in A-form and B-form, where each nucleotide has essentially the same conformation and immediate environment. The Z-helix has a zig-zag appearance, with 12 bp/turn. Z-DNA does not easily form in normal DNA, even in regions of repeating CGCGCG, since the boundaries between the left-handed Z-form and the surrounding B-form would be very unstable. Although it has its enthusiasts, the Z-form is probably not a significant feature of DNA *in vivo*. Each organism is characterized by its own proteic constitution: enzymes and structural proteins are different from one species to the other, and are faithfully reproduced in cells of the same species. DNA is the responsible of the transmission of these hereditary characteristics.

In the mammalian cell nucleus the DNA is always bound to stable proteins called histones. There exist five different classes of such proteins denoted by H1, H2A, H2B, H3, H4, and others quite rare. The complex made up by an histonic octamer and DNA coiled around octamer is called nucleosome (see Fig. 2.4). The part of DNA that connects two nucleosomes is called linker DNA and has a variable length in the interval 10-90 bp. Nucleosomes are the elementary subunits of the chromatin. The latter is made up of all the DNA contained in cell nucleus, divided into long and filamentous molecules, each of one constitutes a chromosome. Fig. 2.4 illustrates this three-dimensional quite complex situation.

At the beginning of mitosis, the chromosomic chromatin coils with the result of an enormous condensation and in the central phases of this process (metaphase and anaphase) the chromosomes adopt the famous stick-like conformation.

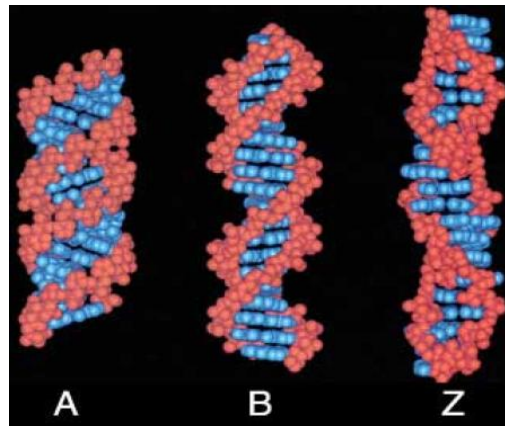


Figure 2.3: The three different structure of DNA [35]

2.1.1 Direct and indirect induction of DNA damage

As mentioned in the introduction, if any form of radiation is absorbed in a biologic material, there is a possibility that it will interact directly with the critical target in the cell, the DNA. The atoms of the target itself may be ionized or excited, thus initiating the chain of events that leads to biological change. This is called direct action of radiation, and the induced damage are called direct damage.

Alternatively the radiation may interact with other atoms or molecules in the cell (particularly water) to produce free radicals ¹ that are able to diffuse far enough to reach and damage the critical targets. This is called indirect action of radiation and the induced damage is called indirect damage.

Direct DNA damage

The direct interaction of radiation with the biological target (i.e. the DNA molecule) possibly induces DNA damage classified as *direct damage*. It is important to underline that intuitively the DNA damage distributions depend on the spatial distribution of energy deposition (for example in terms of event density) and on the DNA conformation and its distribution in the cell nucleus. LET (Linear Energy Transfer) is one of the most important physical quantity that characterizes the radiation, although often it is not sufficient to describe the effects in terms of induced damage distribution. Studies on DNA, and in particular on the repair phenomenon have considerably extended our knowledge on molecular biology, genetics, and carcinogenesis. The most significant

¹Radicals (often referred to as free radicals) are atoms, molecules, or ions with unpaired electrons on an open shell configuration. Free radicals may have positive, negative or zero charge.

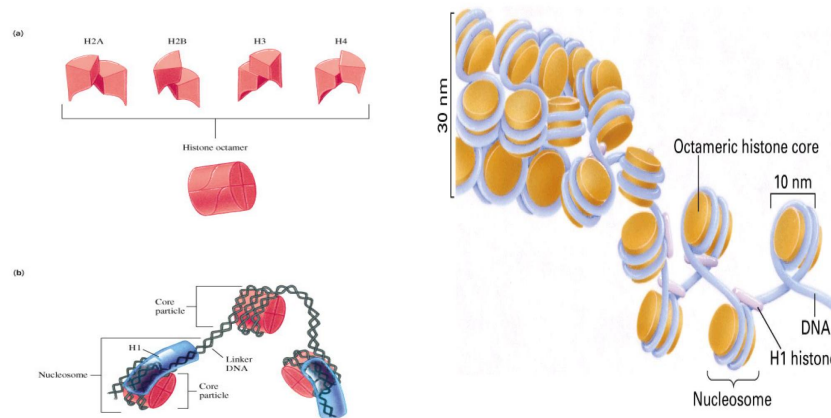


Figure 2.4: 3-Dimensional structure of the DNA [35]

progresses are related to the discovery of three principal radio-induced DNA damage: single-strand breaks (SSB), double-strand breaks (DSB), and base damage (BH).

Single-strand breaks (SSB) In general the number of SSB increases linearly with the radiation dose in a dose range quite large, usually from 0.1 Gy to 6×10^4 Gy. The value of the energy requested to induce one break is about 10-20 eV. A high percentage of SSB is induced through a mechanism that involves the OH water radical that reacts with sugar-phosphate causing the strand break. The repair of a SSB can be very quick and efficient. This repair mechanism begins with the removal of the nucleotidic chain containing the break, and uses the single non altered complementary strand as a print for the synthesis of the new chain. The process is controlled by enzymes and is temperature-dependent. The velocity of repair is exponential and generally about half of SSBs is repaired within fifteen minutes. Since a large part of this kind of breakage is repaired also in lethally irradiated cells, it is believed that SSBs are not determinant breakages for cell death with respect to more complex DNA breakages, such as DSBs.

Double-strand breaks (DSB) DSBs are produced when two SSBs are in two opposite strands, that is on complementary strands (separated by only few base pairs, say 10 bp). In this case the piece of chromatin snaps into two pieces. A DSB is believed to be the most important lesion produced in chromosomes by radiation: the interaction of two double strand breaks has a non-negligible probability to result in cell killing, mutation, or even carcinogenesis.

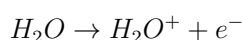
There are many kinds of DSB, varying in the distance between the breaks on the two DNA strands and the kind of end groups formed. Their yield in irradiated cells is about 0.04 times that of single-strand breaks. On the relation dose-number of DSB induced there is not a total agreement: in most experiments there is a linear response with dose, but other studies concluded that only the first part of the curve (at very low doses) is linear and at higher doses the number of DSB increases with the $(dose)^2$, and the dose-effect curve is linear quadratic, according to the formula $(DSB) = a + bD + cD^2$, where D represent the dose.

Base damage (BH) The damage induced in the DNA bases shows a linear increase with dose, and it is believed that this damage rises through the interaction between aqueous free radicals and DNA. Nevertheless, these type of damage have a very low probability to evolve to worse cellular damage.

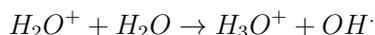
Indirect DNA damage

When the radiation interacts in close proximity to the DNA molecule but does not ionize any atom in the DNA chain, it is possible to produce a damage similar to the previous case, but in an indirect way. In particular, as already shown in the previous section, free radicals production can occur in the medium (e.g. water). Moving by diffusion in the cell, they can reach the DNA molecule and interact with it. This interaction can result in a damage that can be similar to a direct ionization of an atom in the DNA.

Since 80% of a cell is composed of water, it is interested to study how a H_2O molecule reacts to the stimulus of a radiation. As a result of the interaction with a charged particle, the water molecule may become ionized:



and the H_2O^+ ion can interact with other water molecules:



where $OH\cdot$ is the highly reactive hydroxyl radical. The $OH\cdot$ reactive specie has a lifetime of about $10^{-9}s$ in cells and can diffuse to DNA from a distance about twice the diameter of a DNA double helix (4 nm). It is estimated that about two thirds of the x-ray damage to DNA in mammalian cells is caused by the hydroxyl radical [11]. Unlike the first case, indirect action is dominant for sparsely ionizing radiation, such as x-rays.

The amount of ionization depends strongly on the nature of the particle. For example, γ -rays can be able to produce different clusters of ionization in the medium (e.g- blobs, spurs, etc), depending on the energy of the radiation deposits.

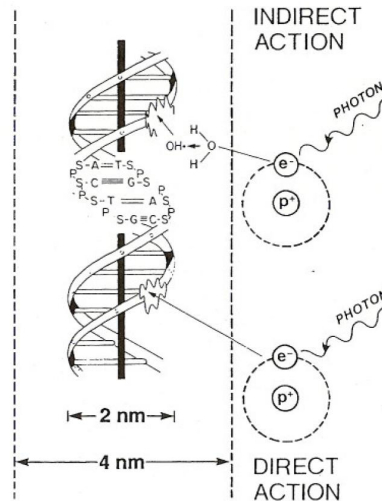


Figure 2.5: Direct and indirect action of radiation.[11]

Between the two stages of production and reaction of chemical species, the molecules resulting from the radiolysis of water are able to diffuse in the cellular environment before they react with DNA or other molecules. The diffusion process in the chemical stage after irradiation can be described with the usual theory of diffusion processes. Generally, in Monte Carlo codes the simulation of diffusion processes of chemical species after irradiation is based on the partition of time simulation into short time steps Δt . In few words, for each Δt , known the displacement of the radical during diffusion, it is necessary to determine the direction.

The random walk assumption is usually adopted, by which each direction is equally probable and there exists no type of correlation between the direction taken at a certain moment and the direction taken in the subsequent time step. At the end of each time step the chemical species formed in this process can interact with each other in the various modes previously listed, forming new radicals and molecules that can interact with other chemical species and DNA atoms.

Scavengers The principal obstacles for the action of radicals are the so called scavengers, which are molecules that can react with free radicals instead of DNA. Most of these molecules (except water) are composed by damaged DNA fragments and protein residues after synthesis. These molecules have a chemical composition similar to that of DNA and so these fragments are able to show similar reaction rates with radicals. In this way, scavengers are able to absorb a part of the chemical impact generated by ionizing radiation, reducing

the mean free path of free radicals and their mean life time.

The latter quantity is used to define the capacity of a compound to prevent the free radicals action. In fact, the scavenging capacity (SC) is the inverse of the mean life time of radicals, and the constant $\tau = 1/SC$ is called scavenging capacity time constant.

It is customary to associate the quantity τ to the mean life time of the OH radicals. This is because it produces damage of two order of magnitude larger than other radical species. The scavenging capacity can be defined as the number of reactions per unit time between OH radical and the scavengers substrate. The concept of SC allows a comparison between the effects of different scavengers. In general, some experimental studies demonstrated that the curve representing the life time of radicals in cellular environment decreases in the range 10^{-10} s to 10^{-8} s after irradiation, and for this reason they are not able to travel a distance longer than 4-5 nm. These results are extremely important for the implementation of Monte Carlo codes because they allow us to restrict the number of radicals to be monitored after their generation, that is less time required for computer calculations.

Damage repair mechanisms The cell possesses different mechanisms to repair DNA breakage. This occurs also because DNA is affected by continuous endogenous damaging reactions like oxidations, methylations, protein errors, and so on. For this reason, the cell has developed defense and repair mechanisms against the endogenous damaging agents and exogenous agents like ionizing radiation.

The simplest case is the mechanism of chemical repair where the ionized molecule has the possibility to capture the missing electron leak from the substrate and to reform the broken bond.

This kind of repair is surely the most immediate type of recombination. However, frequently it is necessary the help of some appropriate proteic structures. The SSBs are repaired by enzymes involved in SSB repair with ligases required to join the strand.

These enzymes are able to reattach the chain using the intact complementary chain as a print. errors. This also happens when there is the junction of incorrect fragments, for example following chromosome aberrations.

2.2 Modelling Radiation Induced Double strand breaks

Ionizing radiation can induce several different types of damage on the DNA, the key molecule for the transmission of the genetic information and for the maintenance of all the processes of a living organism. Broadly speaking, despite the classification we made in the previous section, DNA lesions can be also

classified in two categories on the basis of their effect on chromatin integrity [8]. The first category, which includes base and nucleotide damage as well as single interruptions of the sugar phosphate backbone, does not overly risk chromatin integrity or function, and error-free repair can be accommodated with limited, local modification of the chromatin structure using the complementary DNA strand as a template. The second category, however, which is mainly comprised of DNA double strand breaks (DSBs), but may also include some types of DNA-protein crosslinks, can bring chromatin to a state severely undermining its integrity and function [19] [81].

This type of DNA lesion may be partly recognized by the resulting destabilization of chromatin with the resulting signaling and repair coordinated by associated modifications in chromatin structure. In comparison with other types of DNA lesions, DSBs generate the additional complication that error-free restoration is possible only through copying of lost sequence information from a different DNA molecule (or a different part of the same molecule), as the complementary strand is also damaged.

In view of the specific requirements for error-free DSB repair, as well as the immediate risks a DSB generates to chromatin stability, it is not surprising that the DSB is among the most severe DNA lesions. Unrepaired or misrepaired DSBs induced by physical agents such as ionizing radiation, chemical agents such as topoisomerase inhibitors, oxidative stress, aberrant DNA replication, aberrant V(D)J or class switch recombination, etc., can cause genomic instability and cancer if the cell escapes death altogether.

Particular signature of the ionizing radiation is the ability in the formation of clusters of ionization (e.g. at the end of the ejected electron tracks after the ionization due to the interaction of the incident radiation). These clusters are such that many ionizations can occur within a few base pairs of the DNA. These very severe type of damage seems to be unique characteristics of ionizing radiation, in contrast to other forms of radiation such as UV or DNA-damaging drugs such as topoisomerase inhibitors.

The probability of a given late cellular effect does not depend only on the number of DSBs produced; it also depends strongly on their spatial distribution [75]. In particular, if two or several DNA damage are close, they will be repaired with less efficiency than isolated molecular damage [138]. The sites of these damage may be geometrically close even if their genomic distance (as measured in terms of base pairs) is not small due to the chromatin conformation. The DSB distribution will be determined not only by this conformation but also by the radiation track structure at length scales down to the nanometer level, that is the scale of the DNA double helix. Therefore, it is expected that the cellular effects induced by a given dose will depend on the radiation quality. This has been found experimentally in studies of cell death, mutation induction and chromosome aberrations [45]. Thus the biological effects of ionizing radiation are strongly related to the complexity of DNA damage, which affects all of the mechanisms of repair.

The determination of a relationship between radiation quality and late cellular effects needs a quantitative characterization of the early molecular (DNA) damage caused by the energy deposition events. This issue has been the focus of experimental, theoretical and simulation studies. Studies on radiation-induced DNA fragment size distributions can measure the yield of DNA DSBs and provide an estimation of the correlation between DSBs. It has been found that the DSB yield is only mildly dependent on radiation quality; on the other hand, the expected DSB correlation for high-LET radiation has been confirmed, together with an LET dependence of the DSB repair kinetics [18] [74] [94] [115] [138]. On the theoretical side, both phenomenological approaches and analytical treatments have been pursued: The former tried to evaluate the DSB correlation from the analysis of fragmentation data [145] [146] [141] [153], while the latter proposed a derivation of the pattern of DSB production as determined from the interaction of the ionizing radiation with the chromatin structure [154] [146]. Simulation calculations with the Monte Carlo code PARTRAC (PARTicle TRACKs) have been performed for about a decade [77] [30] [6] to study the dependence of DNA fragmentation pattern on radiation quality. A lot of studies have been performed in which the results of PARTRAC calculations were compared with experimental fragmentation data for different radiation qualities [29] [43], with the main focus on the very large production of very small DNA fragments after high-LET irradiation, in particular smaller than 1 kbp, which usually are not detected experimentally. Campa et al [29] showed that the relative biological effectiveness (RBE) for DSB production can be significantly larger than 1. Among the cases considered so far, Campa and coworkers found the largest RBE value of about 2.4 for iron ions with LET in water of 442 keV/mm [29]. This result is in contrast with the previously mentioned mild dependence of the DSB yield on radiation quality in the experimental data; however, these data do not include the contribution of the very small fragments to the total number of DNA fragments.

Following this line of research, in this work we made a comparison among the fragmentation patterns obtained from the PARTRAC code for a number of different radiation qualities. The comparison with the experimental data, where available, offers the opportunity to validate the code, both for the earlier version devoted only to protons and for the more recent version in which irradiations with heavy charged particles (at non-relativistic energies) are treated (see Section 2.2.1). Therefore, the data obtained can be reasonably trusted even without an experimental counterpart. [1] [29] [30] [43] [146]

We give special attention to the production of DNA fragments smaller than 1 kbp. These are probably very important for late cellular consequences. As such, they are relevant both (1) when the radiation damage to the cells is produced with low or very low doses, as in the situations relevant for radiation protection, and (2) when high doses are delivered, as in hadron therapy. The case of small doses delivered by high-energy heavy particles is also relevant in for radiation protection during long-term manned space missions. It should

be emphasized that the fragmentation pattern is not expected to depend only on LET, since ion beams can have the same LET but a very different track structure: A low-energy light particle can have a LET similar to that of a high-energy heavy particle, but these two particles will produce secondary electrons (delta rays) with very different energy distributions and different secondary ions. This implies that the energy deposition sites, and therefore the possible sites of the DNA damage, both direct and indirect, will have rather different spatial distributions. For irradiation with high energy ions, we expect, in particular, a production of DSBs at large distances from the primary track. On the other hand, ions with similar specific energies (i.e., kinetic energy per nucleon) but different charges may have similar distributions for the energy of the secondary electrons, but the different LETs give rise to different fragmentation patterns.

2.3 The PARTRAC code

Track structure theory gives detailed information on the spatial and temporal aspects following irradiation, and at the same time these theories need, as input, the knowledge of the cross sections relative to the physical processes [43]. All stages of the radiation action are stochastic in nature, therefore mechanistic models, possibly applied as Monte Carlo simulations, can be of great help for a better understanding of the various steps of radiobiological damage induction. Such models mainly rely on the knowledge of track structure features and geometrical and biochemical properties of the target. Indeed, one of the main problems concerning the present status of radiobiological damage modeling is that different approaches can, in principle, lead to equally acceptable results, thus making it difficult to identify and reject erroneous working hypotheses. These kinds of problems are emphasized by the fact that several orders of magnitude, both in the time and in the space scale, are involved in the induction of radiobiological damage. Moreover, mechanisms involved at different levels are strictly interrelated, thus implying that the uncertainties in a certain step of the process can propagate in subsequent steps, and as a consequence, acceptable approximations might evolve, leading to unacceptable uncertainties in the final results.

The recent improvement of physicochemical cross-sections in track-structure simulations and of geometrical models of the DNA and chromatin structure makes it possible to test separately different assumptions on the mechanisms, leading from the initial radiation insult to the induction of certain endpoints. It is therefore of utmost importance to develop models capable of describing each single step of the process of interest in a testable way, so that contributions from distinct mechanisms to the same endpoint can be identified and uncoupled. The basic idea of the models regarding the interaction between

radiation and biological matter is the assumption that the knowledge of the initial energy depositions (spatial and temporal coordinates, interaction types, deposited energies, and produced species) is the key for the comprehension of the various biological end-points like cellular inactivation and chromosome aberrations induction.

In this research work we used the biophysical Monte Carlo code PARTRAC, developed in collaboration with the GSF Institute of Munich; it constitutes the evolution of the codes MOCA 8 (electron transport code) and MOCA 14 - MOCA 15 (protons and Helium ions transport code). With the current PARTRAC code version it is possible to simulate electron and photon tracks with energy in the range 10 eV-100 MeV, and proton and heavier ions tracks with an energy per nucleon in the non relativistic regime.

These powerful techniques are used to simulate the enormous number of physical processes that happen during irradiation. Starting from the physics of matter radiation interactions, this code allows us to reproduce and study the consequences and the effects of various types of radiation. Some of the available codes are only able to reproduce the physical stage of irradiation, while others, like PARTRAC code, are able to simulate various stages starting from the physical one (following the primary and secondary particle energy deposition) to the chemical stage where the diffusion of radical species produced in the irradiated medium is simulated.

This code also provides a detailed (atom-by-atom) description of the DNA and chromatin structures, thus making it possible to test working hypotheses on the radiation action mechanisms in a quantitative way and to perform extrapolations safer than hitherto possible to parameter regions where no experimental data exist (e.g., at low doses). In previous works [28, 29, 32], PARTRAC has been used to model the spectra of various types of DNA damage induced by different radiation fields. In this work we used the PARTRAC code in two different studies on radiation-induced DNA damage. The first one is presented in section 2.3 and is focused on the study of DNA damage induction - DNA fragmentation - by different ions with the same LET and/or with the same specific energy. In the second one, we focused on the comparison between experimental and theoretical results, in the region of very small fragments after irradiation with Nitrogen ions ($125 \text{ keV}/\mu\text{m}$)

2.3.1 The Structure of the code

The PARTRAC code includes an accurate representation of the chromatin and of the physical and physico-chemical processes associated with the energy deposition by radiation. Different modules of the code simulate the various stages after the passage of an ionizing particle. Further details on the PARTRAC code can be found elsewhere [78] [76] [77].

Recently, the transport of ions in the physical module of the PARTRAC code, based on cross sections for interactions of protons in water [43], has been

suitably extended to reproduce the physics of any type of primary ion in the non-relativistic regime using scaling laws related to the mean free path of the primary ion and to the ion effective charge (Barkas formula). The results that have already been published concerning simulation with different ions are of interest for basic radiobiology, hadrontherapy and space radiation protection. The comparison with experimental fragmentation data provided a validation of the code [77].

The complexity of the spatial energy deposition is related to the physical characteristics of the particle track structure.

As an example of the ion tracks produced in this work, Fig. 2.9 shows three dimensional track-structure portions in liquid water iron ions at different LET ($155\text{keV}/\mu\text{m}$ Vs $414\text{keV}/\mu\text{m}$) obtained with the physical modules of the PARTRAC code; this module generates an output with the coordinates of each interaction point as well as the energy involved in each type of interaction.

As expected, the track structure produced by the ion with higher LET, is more *dense* with respect to the lighter ion track with the lower LET. The track with the lower LET is thus less clustered, but delta rays are energetic enough that they can travel far away with respect to the primary ion track core.

This can have important consequences in terms of radiobiological damage, because energetic delta rays can reach the neighboring cells.

Structure of the code

The PARTRAC code used in this work is structured in modules that act sequentially using as input the output files generated by the previous module. These modules are (in order of action)

- *p*trac (for photons); *pro*trac (for protons); *hion*trac (for Helium ions, recently modified also for heavier ions)
- *e*trac (for electrons, primary or secondary)
- *dn*ahit
- *chem*ie
- *dam*cheninfn
- *chrom*tracks

The first two modules (*e*trac after *p*trac for secondary electrons, *pro*trac or *hion*trac) simulate the physical stage of the energy release by primary particles in liquid water (the medium) and the interaction stage of the produced secondary particles (electrons).

In this way these modules terminate the construction of the physical tracks. This physical stage ends about 10^{-15} s after irradiation.

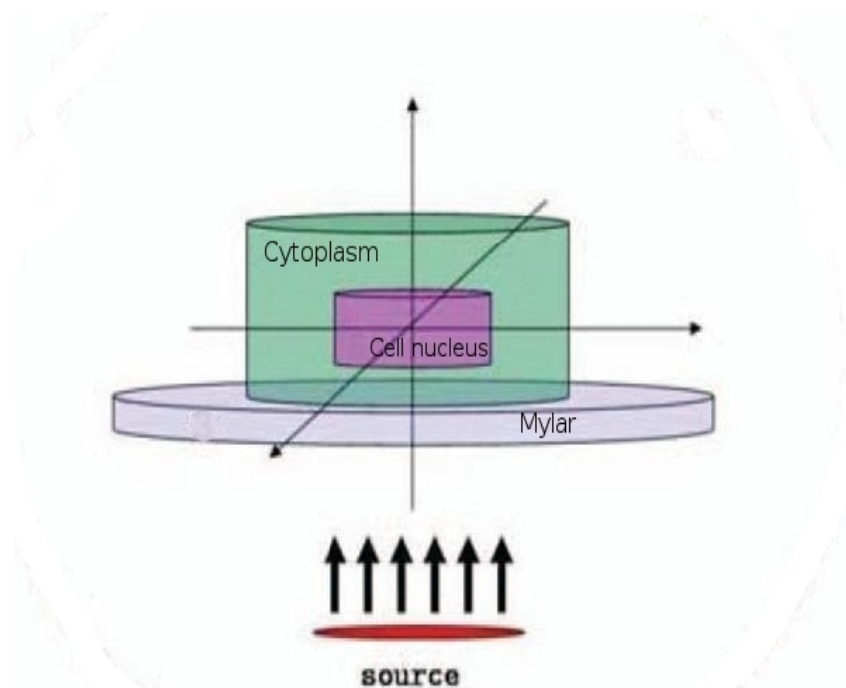


Figure 2.6: Irradiation Set-up. [67]

In the output files of the PARTRAC physical modules it is possible to check which primary particle has interacted, and at the same time the code also follows and processes the first and higher generation electrons. Through the output files, it is possible to know which was the type of interaction and the energy deposited where the interaction took place; besides the spatial coordinates of the event, it is possible to check the hit chromosome, the genomic position (in terms of base pairs), and the atom of the specific hit nucleotide. The fundamental object for the study of radiation effect is the target and its structure inside the cell nucleus. One of the most important features of the code is the use of geometric algorithms that allow to describe and build the principal target at different organization levels starting from single atom that constitute the DNA double helix to chromosome territories of cell nucleus (see next Section).

The third module *dnahit* simulates the prechemical phase of the process (starting from $10^{-15}s$ to $10^{-12}s$ after irradiation). In this phase the excited and ionized water molecules dissociate, relax and autoionize, while the electrons produced by ionizations recombine or thermalize (that is, they reach thermal energies $E = kT$, where k is the Boltzmann constant and T the absolute temperature of the medium) and become *aqueous electrons*, that is surrounded by a cloud of water molecules bound by ion-dipole interaction.

The dissociation schemes for water molecules are not yet determined experimentally in a quite reliable manner. In general different simulation codes use different values for the relative probabilities of the different dissociation modes. The fourth module (chemie) simulates the chemical phase: the products of the previous stages diffuse and react, both between each other and DNA; in particular, radicals like OH and e-aq can directly attack the DNA. To be able to simulate these processes, the PARTRAC code has input files containing information such as reaction constants and diffusion coefficients of the chemical species described here [67].

Physics

It is well known that the features of radiation track structure at the nanometer level have important implications in terms of radiation effects in biological targets. This is especially true for energetic ions, which have complex track structures characterized by energy depositions not only along the primary-particle path, but also projected out radially with respect to the track ‘core’. This is due to the so-called ‘delta rays’, i.e. high-energy secondary electrons which can travel distances of the order of tens of micrometres in biological targets. The effects of heavy ions, especially for high-energy primary ions, are further complicated by nuclear interactions, which can give rise to both projectile and target fragments including neutrons. On this subject, it is worth mentioning that while in nuclear physics, carbon ions are generally classified as ‘light ions’, in radiobiology and hadron therapy ions heavier than He—thus including carbon—are generally referred to as ‘heavy’. A detailed discussion on heavy-ion-induced nuclear interactions is beyond the scope of the present thesis. However, it is worth mentioning that projectile fragments have a high probability to proceed with the same direction and velocity as the primary particle, whereas target fragments (including carbon, oxygen and lighter particles such as protons and helium ions) generally have lower velocity—and thus higher LET—and can be significantly scattered with respect to the primary-ion trajectory.

Models and codes based on the Monte Carlo techniques represent very good tools to simulate ‘event-by-event’ radiation track structure at the nanometer level, taking into account each single energy-deposition event. In view of radiobiology applications, most of these codes are based on cross sections in liquid water, which is considered to be a good surrogate for biological targets. Older codes, based on water-vapor cross sections, are now considered obsolete because of the significant differences between liquid and vapor phase water. Although heavy-ion cross sections in liquid water are known with less detail with respect to light-ions, significant advances have been achieved in the last few years.

Energy deposition by charged particles mainly occurs via the Coulomb-field interaction, and the formal theoretical description of this kind of interaction is well developed. The numerical evaluation of cross sections is very

difficult in condensed media, where one deals with many-body systems containing a large number of targets. In contrast to the gas-phase, where isolated molecules or atoms have to be taken into account, for condensed matter it is not possible to obtain with sufficient accuracy the target wave functions and the eigenvalues with methods such as the Hartree-Fock techniques [43]. The main phase-specific difference between condensed and gas-phase matter is that condensed matter is characterized by collective (coherent) excitations induced by the charged-particle passage. These quanta are delocalized and cover a macroscopic spatial region, and then decay by single-particle excitations.

For energy values below the relativistic threshold, such inelastic processes are well described by the non-relativistic first Born approximation (NR-FBA) coupled with the dielectric theory (DT). While the NR-FBA is a perturbative treatment valid only for projectiles that are sufficiently fast but still in the non-relativistic regime, the latter is adopted to describe the condensed medium collective response to external perturbations that is the charged-particle passage.

Using the quantum mechanical approach, it is possible to obtain the general expression of the differential cross section in the solid angle $d\Omega = \sin\theta d\theta d\varphi(\theta)$ is the angle between the initial and final particle momenta \mathbf{k} and \mathbf{q} for the transition of the projectile (plus target) system from the initial state $|i\rangle = |\mathbf{q}, E_i\rangle$ to the final state $|f\rangle = |\mathbf{k}, E_f\rangle$

$$\frac{d\sigma_{i \rightarrow f}}{d\Omega} = \frac{k}{q} \left| \frac{2m}{4\pi} \langle \mathbf{k}, E_f | V | \mathbf{Q}, E_i \rangle \right|^2 \quad (2.1)$$

where V is the interaction potential between the projectile and the target, m is the mass of the projectile and E_i and E_f refer to the initial and final energy configurations of the target. The quantity $\sigma_{i \rightarrow f}$ is the total cross section that can be obtained after integration of equation (2.1) over the entire range of angular variables. Energy conservation allows only particles with energy $\omega = E(f) - E(i)$ to emerge from the collision process. The double-differential cross section into the solid angle and for energy transfer $d\omega$ can then be written as

$$\frac{d^2\sigma_{i \rightarrow f}}{d\omega d\Omega} = (2\pi)^6 \frac{k}{q} \left| \frac{2m}{4\pi} \langle \mathbf{k}, E_f | V | \mathbf{Q}, E_i \rangle \right|^2 \delta(\omega + E_i - E_f) \quad (2.2)$$

where the Dirac delta-function ensures energy conservation. Assuming that the potential V depends only upon the coordinates of the projectile \mathbf{r} and of targets (atomic electrons) \mathbf{r}_j (like in the case of the Coulomb potential, once the charges involved are known), equation (2.2) can be further simplified leading to an expression rewritten in terms of energy ω and transferred momentum $\mathbf{p} = \mathbf{q} - \mathbf{k}$

$$\frac{d^2\sigma(\mathbf{p}, \omega)}{dp d\omega} = \frac{2\pi p}{q} |V(\mathbf{p})|^2 \mathbf{S}(\mathbf{p}, \omega) \quad (2.3)$$

where the term $S(\mathbf{p}, \omega)$ is by definition the dynamic form factor (DDF) [43].

In principle, this expression contains all the information needed for the calculation of scattering probabilities, and is given as a product of two factors: $|V(\mathbf{p})|^2$ contains information on the projectile-target interaction, whereas the DDF describes the target.

Expression (2.3) can be provided in a form which is more convenient for the calculations. This is obtained replacing the DDF with the dielectric response function (DRF) $\varepsilon(\mathbf{p}, \omega)$ of the system (the medium), allowing for an easier interpretation. The DRF is defined in terms of the electric field \mathbf{E} and the dielectric displacement \mathbf{D} induced by a charged projectile of charge density $\rho_P(\mathbf{r}, t)$

$$E(\mathbf{p}, \omega) = \mathbf{D}(\mathbf{p}, \omega) / \varepsilon(\mathbf{p}, \omega) \quad (2.4)$$

From the Maxwell equations, it is possible to obtain an expression for $1/\varepsilon(\mathbf{p}, \omega)$ in terms of the projectile charge density and of the target charge-density fluctuation induced by the projectile itself

$$\frac{1}{\varepsilon(\mathbf{p}, \omega)} = 1 + \frac{\langle \Delta \rho_T(\mathbf{r}, t) \rangle}{\rho_P(\mathbf{r}, t)} \quad (2.5)$$

To calculate $1/\varepsilon(\mathbf{p}, \omega)$, we need to obtain an expression for the ratio containing the densities. The general lines to obtain the ratio consider the medium linear response to projectile perturbation, where ‘linear’ response means for sufficiently weak perturbations described by the interaction potential representing the Coulomb interaction between the two charge densities. To evaluate the system (medium) charge-density fluctuation under the influence of the projectile, the target wave function is also needed. This is achieved starting from the Schrodinger equation describing the target subject to the interaction potential and solving the problem by Green’s functions techniques. The final expression obtained for $1/\varepsilon(\mathbf{p}, \omega)$ (which contains the target eigenvectors) allows one to express its imaginary part in terms of the DDF

$$Im \left\{ \frac{1}{\varepsilon(\mathbf{p}, \omega)} \right\} = \frac{4\pi}{p^2} [S(\mathbf{p}, -\omega) - S(\mathbf{p}, \omega)] \quad (2.6)$$

Besides these calculations, we are interested in the final expression of the double-differential cross section (in energy and momentum transfers) for positive energy transfers ($\omega > 0$)

$$\frac{d^2\sigma(\mathbf{p}, \omega)}{dpd\omega} = \frac{2}{q^2} \frac{1}{p} Im \left\{ -\frac{1}{\varepsilon(\mathbf{p}, \omega)} \right\} \quad (2.7)$$

Here, q is the projectile initial momentum, whereas \mathbf{p} and ω are the transferred momentum and energy, respectively. For a particle of charge Z and velocity v , we can rewrite equation (4) in the more familiar form of double-differential cross section per atomic electron

$$\frac{d^2\sigma(\mathbf{p},\omega)}{dpd\omega} = \frac{2Z^2e^2}{\pi N h v^2 p} \frac{1}{p} \text{Im} \left\{ -\frac{1}{\varepsilon(\mathbf{p},\omega)} \right\} \quad (2.8)$$

The calculation of $\varepsilon(\mathbf{p},\omega)$ is beyond the current computational capabilities, since it requires a quantum mechanical description of the system band structure and its wave functions, and atomic hydrogen is the only system for which $\varepsilon(\mathbf{p},\omega)$ is exactly known. A number of different approaches [43] have been proposed for the modellization of $\varepsilon(\mathbf{p},\omega)$. Such approaches are based on the experimental optical data $\varepsilon(\mathbf{p} = 0,\omega)$ and are focused on the extrapolation of the expression of $\varepsilon(\mathbf{p},\omega)$ to nonzero momentum transfer ($\mathbf{p} \neq 0$) (the Bethe surface) and to large momentum transfer (the Bethe ridge).

In the initial version of the PARTRAC code, it was possible to perform irradiation simulations only with photons, electrons, protons and alpha particles. Recently, the code physical module has been suitably modified to adapt the code to reproduce the physics (i.e. the track structure) of basically any type of primary ion in the non-relativistic regime [37]. As an example, taking into account the Z^2 dependence of equation (2.5) (valid for protons and electrons), the mean free path (MFP) λ of the primary ion was obtained rescaling the proton MFP

$$\lambda_{ion} = \lambda_{proton} \frac{1}{(Z^*)_{ion}^2} \quad (2.9)$$

where Z^* is the ion effective charge, which takes into account charge-exchange processes via the Barkas formula (see Fig. 2.7)

$$(Z^*)_{ion} = Z_{ion} [1 - \exp(-125\beta/Z^{2/3})] \quad (2.10)$$

A first validation of the correctness of the adopted method was obtained by preliminary tests reproducing radial distributions of energy and dose following irradiation with different ions of interest for basic radiobiology, hadron therapy and radiation protection, including heavy ions [171]. Figure 2.8 shows two-dimensional (2D) projections of sample tracks of H-, He-, C- and Fe-ions with the same energy per nucleon (115 MeV/n), and thus the same velocity, as calculated with the PARTRAC code in liquid water. As expected, heavy-ion track structures are more ‘dense’ with respect to light ions with the same velocity, due to the fact that the LET is directly proportional to the square of the particle (effective) charge. These results are consistent with the earlier work by Chatterjee and Schaefer .

Geometry

DNA helix and nucleosomes The DNA target model that has been developed includes six levels of DNA organization (deoxynucleotide pair, double helix, nucleosome, chromatin fiber structure, chromatin fiber loop, and chromosome territories) and the model completely reproduces the human genome

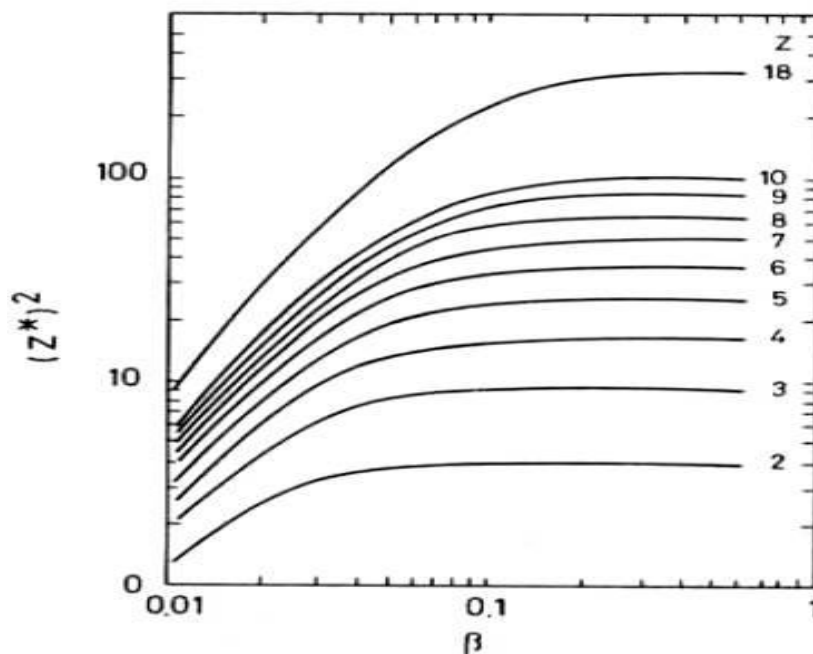


Figure 2.7: Z^2 values according to equation 2.10 [29]

(about 6 billion bp). Deoxynucleotide pairs are stacked in either a preselected or a random sequence with a z -shift of 0.3375 nm and a 90 helical turn of 36 degrees, yielding a linear double helix in B-DNA form. The coordinates of the atoms of the deoxynucleotides are taken from [30], and the van der Waals radii (P: 0.19 nm, C: 0.17 nm, N: 0.15 nm, O: 0.14 nm, H: 0.12 nm) are from [31]. In the simulation of higher-order structures, the atomic positions are applied to a local Cartesian coordinate system moving along the DNA axis with its helical rotation and subsequently transformed to a Cartesian coordinate system in which the chromatin fiber axis is coincident with the z axis.

The helical rotation of the moving coordinate system is varied slightly to fit the ends of the helices seamless when the modeled nucleosomes are stacked together. The simulation of the nucleosome core particle is based on the model reported in [33]. The core particle comprises 146 nucleotide pairs of a DNA helix wrapped in a left-handed superhelix 1.8 times around a histone octamer, which is represented geometrically by a cylinder with a diameter of 6.4 nm and a height of 6 nm. The radius of the axis of the superhelix is taken to be 4.4 nm. Thus the radius of about 1.1 nm for the DNA helix results in a total diameter of 11 nm for the core particle.

The pitch is 2.7 nm per turn. A hydration shell is implicitly modeled by increasing the van der Waals radius of all DNA atoms by a factor of two. No

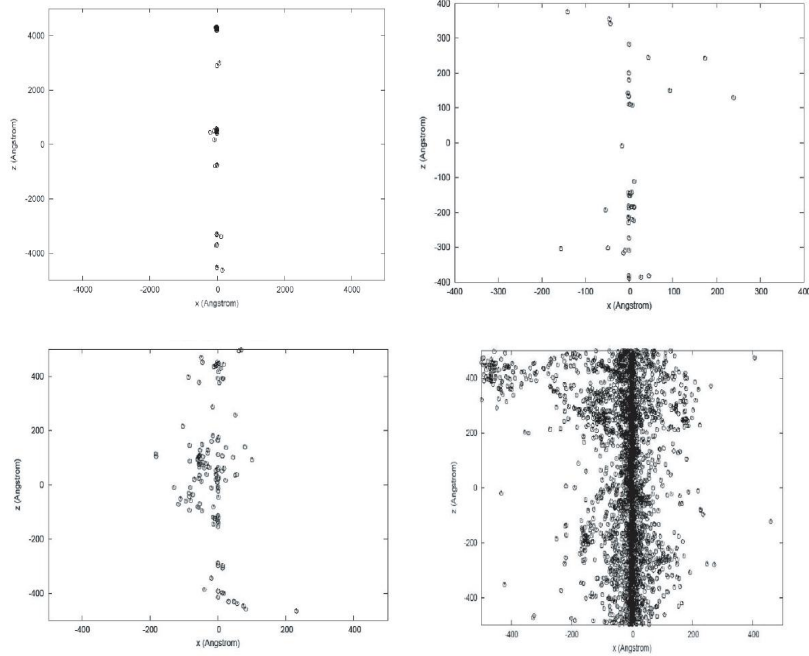


Figure 2.8: 2-D projection of track-structure segments in liquid water for different ions with the same velocity (115 MeV/nucleon) as calculated with the PARTRAC code. From top and bottom and from left to right: H, He, C and Fe; note the different scale for the proton track

further DNA environment (e.g. the stabilizing Na ions) is included in the model.

Chromatin fiber structure The position and the orientation of each nucleosome core particle in a chromatin fiber are determined by three cylindrical coordinates describing the position of the nucleosome center and three angles describing the orientation of the nucleosomes with respect to the fiber axis. In the input data set of the model, the outer radius of the chromatin fiber, the angle and the shift along the z axis between succeeding nucleosomes are given.

These data are constant for regular arrangements of nucleosomes since the positions of two succeeding nucleosomes relative to one another target and and protons and their interconnections are repeated identically. For the determination of the position and orientation of the linker DNA, the number of deoxynucleotide pairs between succeeding nucleosome core particles is an additional input of the model. The linker length must be selected as not

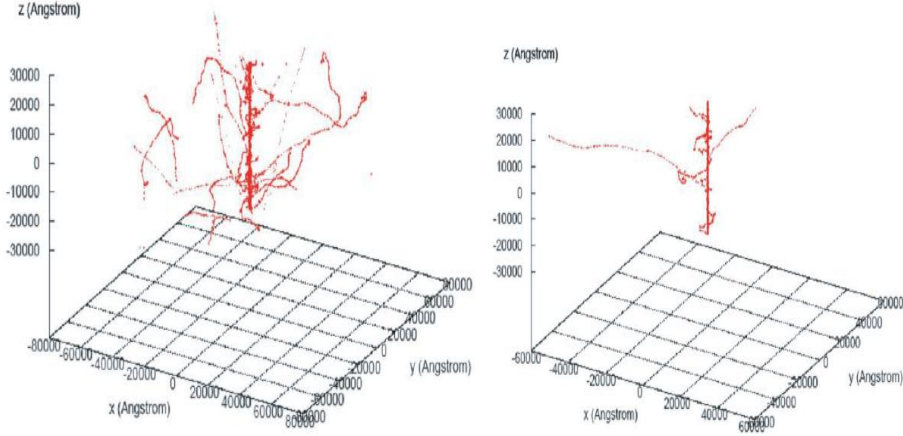


Figure 2.9: 3-D representation of track-structure segments in liquid water for iron ions with different energies as calculated as calculated with the PARTRAC code. Left panel: 115 MeV/u Fe ion, right panel: 414 MeV/u Fe ion. The corresponding LET values are 442 keV/micron and 201 keV/micron, respectively

below a minimum number of base pairs corresponding to the shortest connection. On the other hand, to avoid major bending of the DNA helix, the linker length must be chosen as not much higher than this minimum value, especially for short interconnections.

Finally, the number of nucleosomes per chromatin fiber element must be specified. The last nucleosome in a fiber element must allow for a seamless connection with the first nucleosome or an identical element stacked on top of the other element. This number of nucleosomes multiplied by the angle between them corresponds to the number of turns around the fiber axis per fiber element.

For a description of stochastic structures of the chromatin fiber, it is necessary to permit some variation of one or more parameters of the model. To generate a stochastic fiber, the position and orientation of each core particle are determined with random selection of variable parameters according to their ranges. The core particle is accepted if a sufficient smooth linker DNA connection with the former core particle is found and no overlap occurs of the DNA helix with itself or with the histone cylinders previously positioned.

If this is not achieved within a large number of trials, the formerly accepted core particles are rearranged. If only the final connection between the last core particle and the first one of a stacked fiber element is not met, the first nucleosome of the chain is discarded and the position of the last nucleosome for which all conditions are fulfilled is sought.

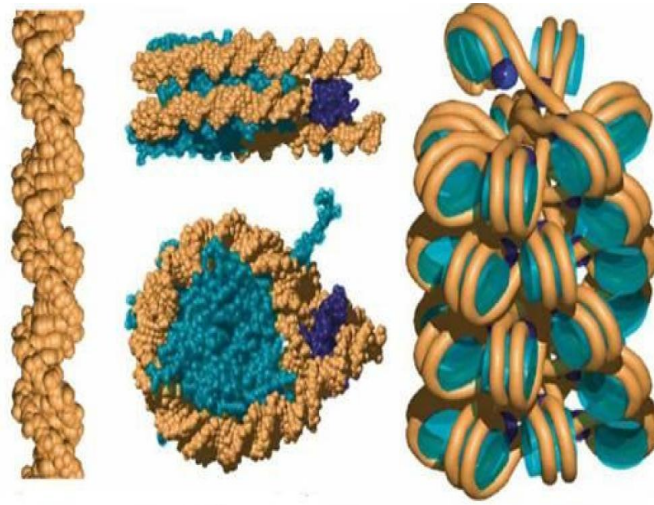


Figure 2.10: Different level of organization of the DNA simulated with PARTRAC [67]

This procedure is continued until all nucleosomes inside a fiber element are positioned and connected smoothly without overlap, or until no solution is found for the given set of parameters within a specified time. In the calculation of the stochastic fiber structure given below, more than 200.000 nucleosome core particles had to be positioned and tested (see FIG. 2.10).

Geometrical input parameters describe three regular fiber structures with solenoidal, crossed-linker and zigzag formation and one stochastic structure. The parameters used for the three condensed formations are compatible with the structure of the 300 Angstrom chromatin filament described in [34], apart from the orientation of the nucleosomes in the stochastic fiber for which a greater angular range was permitted in the model.

Correspondingly, the zigzag model is in accord with the 100 Angstrom nucleosome filament structure [34]. In Fig. 2.11, an illustration of the zigzag model of a chromatin fiber is given by spheres with single van der Waals radii of all atoms of the DNA and cylinders describing the histones.

In Fig. 2.12, the three types of condensed fibers are displayed in a top and a side view. The solenoidal structure is similar to that which was used in [36]; however, the linker DNA is somewhat longer and thus comes closer together in the center of the fiber (the figures were generated by the Persistence of Vision™ Raytracer (POV-Ray™) software package).

The straight chromatin fiber structure can be divided into linear chromatin fiber boxes consisting of all atoms with a z-coordinate along the fiber between 0 and the repeat length of the fiber. For the construction of looped chromatin fibers, two curved chromatin fiber boxes are introduced in which the axis of the

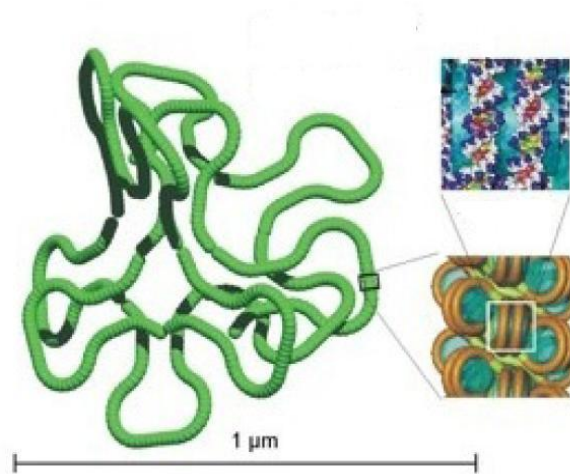


Figure 2.11: Different level of organization of the chromatin fiber [67]

linear box is changed to an arc of a circle to the left and to the right, and the cylindrical shape is altered into two torus sectors with all atomic coordinates inside the cylinder transformed.

The three types of boxes can be stacked with smooth interconnections of the DNA helices at their borders. Since the repeat lengths differ noticeably for the fiber structures considered, the bending angles of the curved elements are chosen to be about proportional to the box height which yields similar fiber curvatures of about 65 nm radius. Flat chromatin fiber loops with comparable sizes were constructed for the four fiber structures by stacking linear and curved boxes together in a selected sequence.

The advantage of this loop model is that the same atoms are found in each of the three boxes, and one coordinate of these atoms remains unchanged upon the transformation which reduces storage space and simplifies starting algorithms. Its limitations, however, are that the model describes only flat loops, that the cylindrical shape of the histones is distorted in the curved segments, that the distortion of the nucleosomes in the curved elements is unpleasant and unrealistic, and that the method is not capable of describing tight bends in the chromatin fiber (further work is in progress to remove these limitations).

Chromatin fiber loops In the present implementation of this DNA target model in PARTRAC, the entire DNA in the nucleus of a human cell is modeled by small identical chromatin fiber loops (see Fig. 2.11). These loops are considered to be distributed randomly and oriented randomly inside a cylinder describing the cell nucleus. To cope with such an amount of data, the spatial

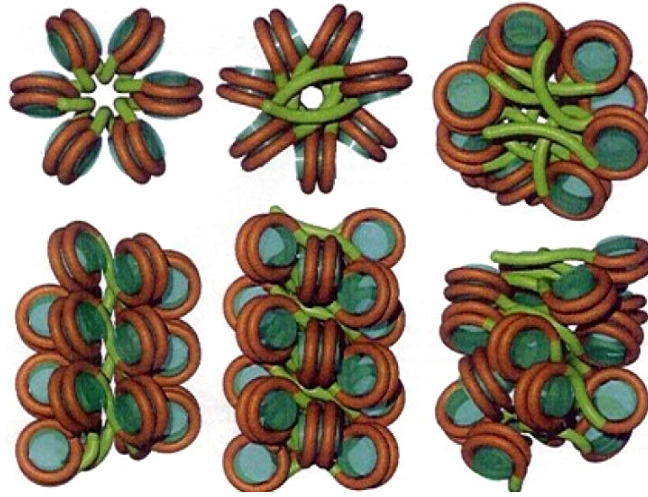


Figure 2.12: Different organization of the nucleosomes in the chromatin fiber simulated with the PARTRAC code [67]

information about the DNA is separated into two sets of data arrays. The first data set describes the fiber structure with all DNA atoms in the chromatin fiber boxes including Cartesian coordinates in the three types of fiber elements described above: atoms, deoxynucleotide pairs and strands.

The second data set describes all chromatin fiber loops by the origin, the direction of the axis and a polar angle of the first box in the fiber. The origin is chosen randomly inside the nucleus with random direction of the axis and random polar angle. A particular selection is discarded if parts of the loop are found outside the nucleus. Presently the fact that some of the chromatin fiber loops overlap with each other is not taken into account. However, the overlapping volume is less than 0.1% of the total DNA volume of each chromatin fiber structure, and thus its influence on the results is negligible. The amount of computer memory needed for implementation of the DNA target model is in the range of 100 MB. Some effort was necessary to limit the computing times to an acceptable level.

Besides sorting of both databases, this was achieved by a hierarchical test sequence for spatial coincidences and by using lists of possibly hit chromatin fiber loops for all events within a distance of 5 nm.

Chromosomal territories In order to simulate human chromosomes with a territorial organization, the total volume of the cell nucleus is divided into 46 domains with a volume corresponding to the real size of the chromosomes.

These chromosomal domains are defined on a regular grid of $101 \times 101 \times 101$ cubic elements, each with a side length of 130 nm, forming a cube surrounding the cell nucleus (See Fig. 2.13 and 2.14).

Only those grid elements which are totally inside the spherical cell nucleus were included in the following procedure. The algorithm starts with 42 elements near the surface and 4 elements in the central region of the nucleus which are the first assigned elements of each chromosome. The free elements around these assigned elements are marked as border elements of the domains. The next assigned element of each domain is selected randomly from the border elements with the highest number of neighboring assigned elements. This growth of domains is carried out element by element proportional to their volume. If the number of border elements around a domain happens to be short in relation to the number of missing elements of the domain, then adjacent border elements or even adjacent assigned elements from neighboring domains are redistributed.

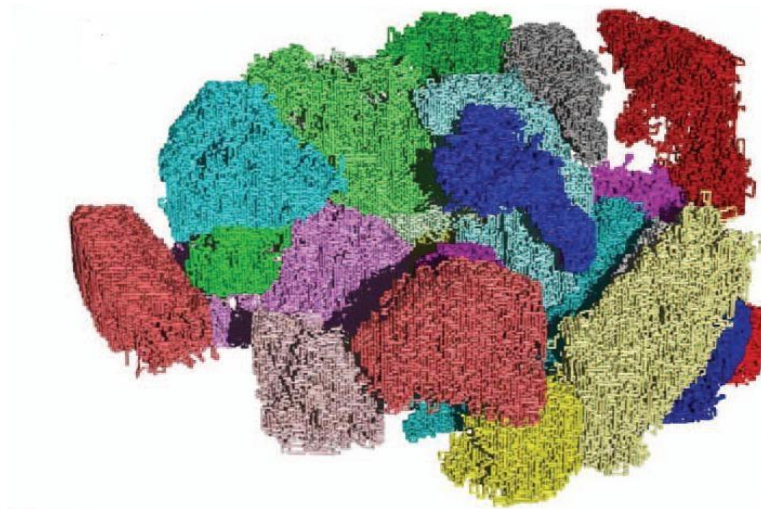


Figure 2.13: Chromatin fiber structure [67]

The procedure is finished when 95% of the grid elements are assigned to domains since the algorithm then starts to produce frayed borders. The total number of chromatin fiber loops is distributed to the 46 chromosomes proportional to their size, and the construction of connected fiber loops is limited to the volume of the grid elements assigned to the domain of the chromosome actually under construction, until the generation of the next chromosome starts at a corresponding grid element.

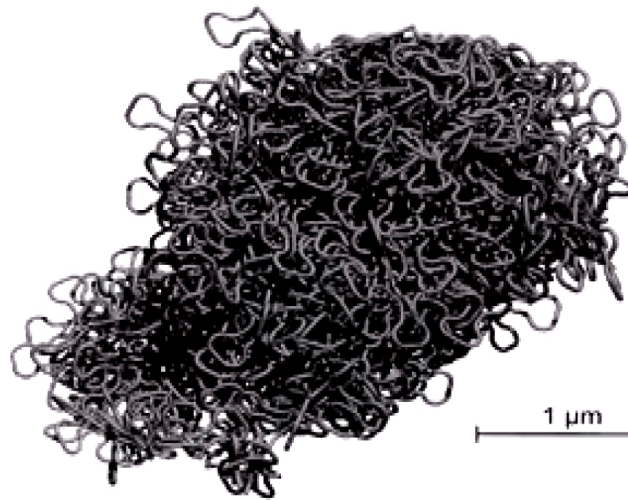


Figure 2.14: A Chromosome territory simulated with PARTRAC [67]

2.3.2 DSB distribution as a function of the LET

We simulated the irradiation of human fibroblasts with γ rays, protons and helium, carbon and iron ions at a fixed dose of 5 Gy. From the output of the code, containing in particular the genomic positions of the radiation-induced DNA double-strand breaks (DSBs), we obtained the DNA fragmentation spectra.

Very small fragments, in particular those related to *complex lesions* (few tens of base pairs), are probably very important for the late cellular consequences, but their detection is not possible with the common experimental techniques. We paid special attention to the differences among the various ions in the production of these very small fragments; in particular, we compared the fragmentation spectra for ions of the same specific energy and for ions of the same LET (linear energy transfer).

We present the results concerning DNA fragmentation occurring in human fibroblasts after they have been traversed by the following radiations (Same *Specific energy*):

- Co-60 gamma-rays(1),
- Protons with energy of 250 MeV , LET equals to $0.4 \text{ keV}/\mu\text{m}$ (2)
- Helium ions with energy 250 MeV/u, LET equals to $1.6 \text{ keV}/\mu\text{m}$ (3)
- Carbon ions with energy 250 MeV/u, LET equals to $13.8 \text{ keV}/\mu\text{m}$ (4)
- Iron ions with energy 250 MeV/u, LET equals to $260 \text{ keV}/\mu\text{m}$ (5)

and by (Same *LET*)

- Helium ions with energy 1.75 MeV/u, LET equals to 100 keV/ μm (6)
- Carbon ions with energy 18.33 MeV/u, LET equals to 100 keV/ μm (7)
- Carbon ions with energy 8.33 MeV/u, LET equals to of 201 keV/ μm (8)
- iron ions with energy 414 MeV/u, LET equals to of 202 keV/ μm (9)
- Carbon ions with energy 2.71 MeV/u, LET equals to of 201 keV/ μm (10)
- iron ions with energy 115 MeV/u, LET equals to 442 keV/ μm (11)

where the numbers between parenthesis represent the reference number of irradiation used.

We emphasize that it is possible to assign a LET also to gamma-rays, of about 0.3 keV/ μm , equal to an average of the one induced by the secondary electrons.

As found previously for iron ions, we found that the RBE (relative biological effectiveness) for DSB production was considerably higher than 1 for all high-LET radiations considered. This is at variance with the results obtainable from experimental data, and it is due to the ability to count the contribution of small fragments.

It should be noted that for a given LET this RBE decreases with increasing ion charge, due mainly to the increasing mean energy of secondary electrons. A precise quantification of the DNA initial damage can be of great importance for both radiation protection, particularly in openspace long-term manned missions, and hadrontherapy.

Figure 2.15 shows the simulation results for the cumulative DNA fragment distributions induced by irradiation with different ions with the same energy of 250 MeV/nucleon at the same dose of 5 Gy. The results for the same dose of γ rays are included for comparison. The plots indicate that the largest cumulative distribution is produced by iron ions, confirming the role of high-LET radiation in the induction of DNA fragmentation.

The data are presented in the form of histograms showing the number of fragments (per Mbp) with lengths in given size ranges, after irradiation with a dose of 100 Gy. For gamma-rays and for protons the experimental data concern the number of fragments in the ranges 23 - 1000 kbp and 1000 - 5700 kbp. For the two iron ion beams, in addition to the two previous ranges, data are available also for the ranges 1 - 9 kbp and 9 - 23 kbp.

In this and in the following cumulative distributions, the abscissa denotes the largest size of the fragments represented by the corresponding point.

The lines are a guide to the eye. Error bars are standard deviations and are often smaller than the symbols. In this and in the following graphs of the cumulative distributions, a log-log representation is used to obtain readable

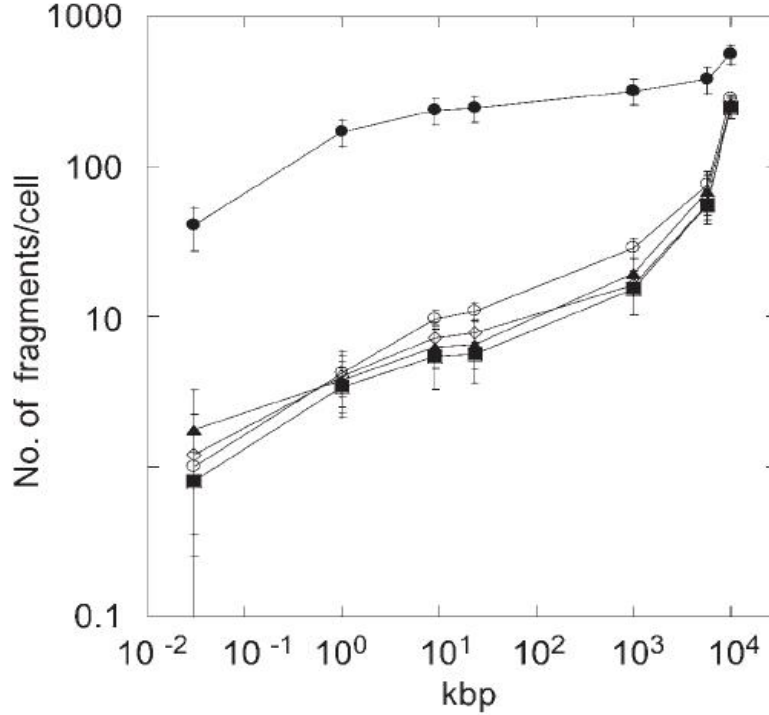


Figure 2.15: PARTRAC simulation results for cumulative DNA fragment spectra induced by 5 Gy irradiation with different 250 MeV/nucleon ions: protons (0.4 keV/mm, solid squares), helium ions (1.6 keV/mm, open diamonds), carbon ions (13.8 keV/mm, open circles), iron ions (260 keV/mm, solid circles). Gamma-ray results for the same dose are shown for comparison (solid triangles)

plots.

The fragmentation induced by the other three ions of relatively low LET do not differ considerably from that induced by γ rays. The histogram of the fragment distribution presented in Fig. 2.16 shows that the large fragment production due to iron ions is due mainly to the production of short fragments; for clarity, only the spectra of the iron and carbon ions are presented.

In particular, large numbers of fragments are found for iron ions in the first three size ranges, i.e., 0- 30 bp, 30-1000 bp and 1-9 kbp. Comparisons between ions with the same LET but different charge and therefore different specific energy are presented in Figs. 2.17, 18 and 19 for LET values of 100, 201 and 442 keV/ μ m, respectively.

As listed above, two different ions are considered for each LET. In the next Figure, the left panels show the histograms of the fragment distributions, while the right panels presents the plots of the cumulative fragment distributions.

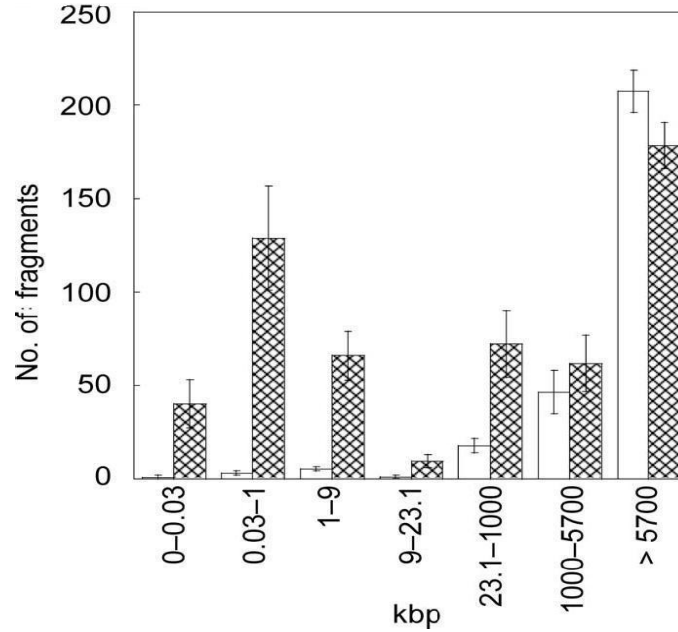


Figure 2.16: Comparison between simulation results for DNA fragment spectra induced by irradiation with 250 MeV/nucleon iron ions (filled bins) and carbon ions (empty bins) with a dose of 5 Gy. Error bars are standard deviations.

In all cases, from the histograms in the upper panels we see that, for two ions with the same LET, the one with smaller specific energy produces many more small fragments, belonging to the first two size ranges. The relative difference is somewhat attenuated for the last pair of ions, those with the highest LET of 442 keV/mm (Fig. 2.20).

In contrast, the ions with the larger energy within each pair produce more large fragments.

These results can be explained as follows. The ion with the lower charge (and thus with the lower specific energy for the same LET) generates delta rays with an energy distribution shifted toward lower energies. In terms of track structure, this results in a narrower track with an enhanced production of smaller fragments. On the other hand, the more energetic delta rays generated by the ion with the higher charge are more likely to produce larger fragments.

The rightmost points of the cumulative distributions shown in the bottom panels give the total number of fragments. The two effects just mentioned tend to compensate as far as this total number is concerned, but the first effect, i.e., the larger production of small fragments, appears to be more important. In Fig. 2.20 we present in a single histogram the total number of fragments for the 11 radiation qualities considered in this work. Each number on the ab-

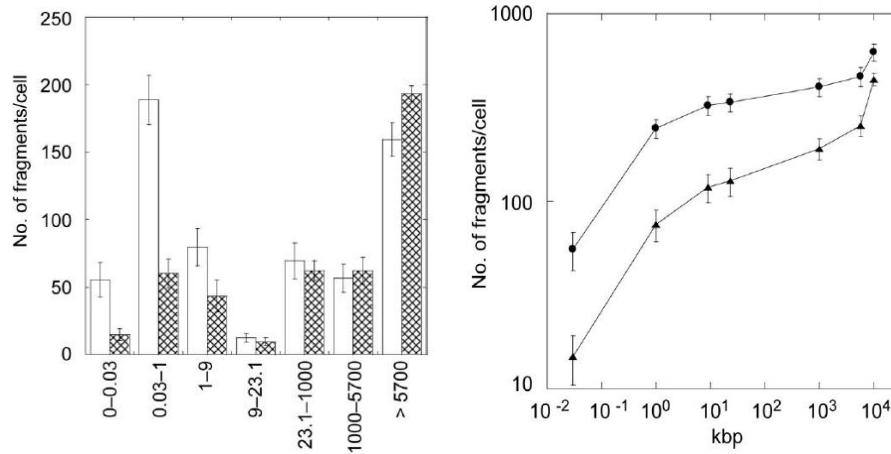


Figure 2.17: Comparison between DNA fragmentation spectra induced by irradiation with 100 keV/mm helium and carbon ions with a dose of 5 Gy. Left panel: Histogram of the fragment distribution (empty bins for helium ions and filled bins for carbon ions). Right panel: Cumulative fragment distributions (solid circles for helium ions and solid triangles for carbon ions); the lines are a guide to the eye. Error bars are standard deviations

scissa refers to the progressive number listed at the beginning of this Section; the left y axis gives the absolute values of the fragments produced by the 5-Gy irradiations, while the right y axis gives the RBE for fragment production, i.e., the values normalized to that of the c rays (given the large total number of fragments produced by even a relatively low dose of 5 Gy, one can safely define this RBE also as the RBE for DSB production).

The following features can be deduced from this plot: (1) As long as the LET is small (e.g. of the order of 10 keV/ mm or less, as for the ions in positions 2, 3 and 4), the RBE is very close to 1; (2) for a given ion, the RBE increases with LET (helium ions in positions 3 and 6, carbon ions in positions 4, 7, 8 and 10, iron ions in positions 9, 5 and 11); (3) for a given LET, the RBE increases for decreasing charge, as shown by the three pairs in positions 6 and 7, 8 and 9, and 10 and 11, although in the last case the difference is very small relative to the error bar.

Monte Carlo techniques with a realistic DNA target model describing its three-dimensional complex distribution and substructures such as the winding of DNA around histones are a necessary complement to the experimental determination of radiation-induced DNA DSBs and the consequent DNA fragmentation. This is especially valid for the study of the production of small fragments (smaller than 1 kbp) production. Although generally outside the possibility of experimental detection, methodologies have nevertheless been optimized that are able to count fragments of size as small as 100 bp . However, it should be

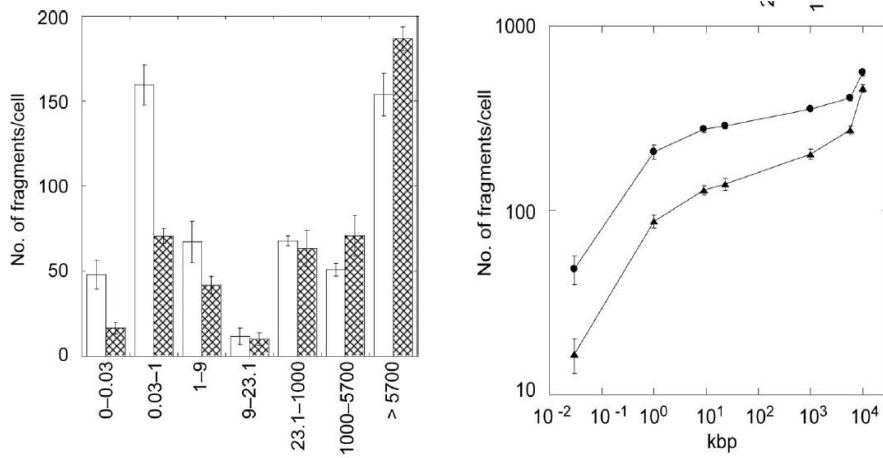


Figure 2.18: Comparison between DNA fragmentation spectra induced by irradiation with 201 keV/mm carbon and iron ions with a dose of 5 Gy. Left panel: Histogram of the fragment distribution (empty bins for carbon ions and filled bins for iron ions). Right panel: Cumulative fragment distributions (solid circles for carbon ions and solid triangles for iron ions); the lines are a guide to the eye. Error bars are standard deviations

taken into account that several difficulties are associated with this task. First, the problem of the background fragmentation that plagues the experimental determination of a genuinely radiation induced fragment size distribution is particularly relevant for small fragments; this forces the use of high doses (of the order of 100 Gy) to have a reliable signal above the noise (i.e., the background fragmentation) level [74]. However, one is generally interested in the small fragment production by single tracks, i.e., small fragments produced by correlated events; at low doses the probability of small fragments produced by different tracks is negligible. When performing irradiations with high doses, this probability becomes meaningful (although it is always smaller than for large fragments);

therefore, one has to subtract the contribution from different tracks. Second, the passage from the DNA mass determination in a given size range, the experimentally measured quantity, to the number of fragments, is not without pitfalls, again especially for small fragments. One is forced to deduce this number from the ratio of the mass to a mean molecular size of the range, and generally the middle size of the range is taken. Even assuming that the middle size is the actual average size of the fragments, this does not guarantee that one obtains the correct number. These arguments should be convincing about the usefulness of the Monte Carlo evaluation of the small fragment number. In any case, apart from the ref. [74], we are not aware of experimental determinations of number of fragments with size smaller than 1 kbp, since the upper

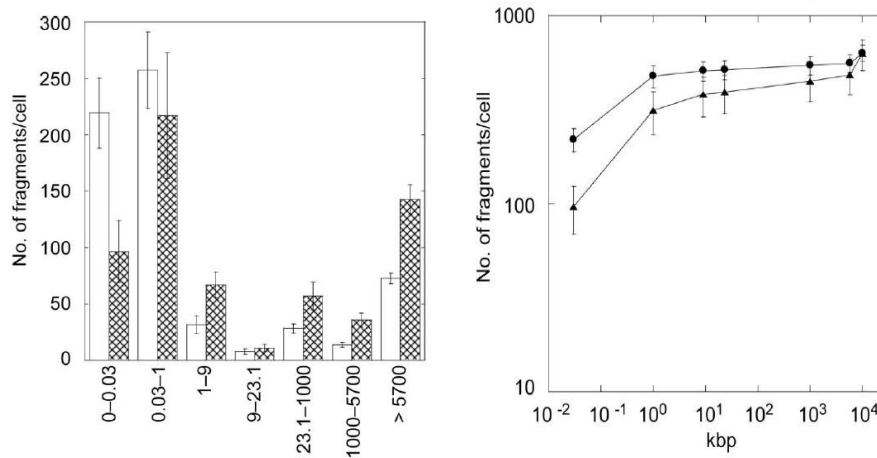


Figure 2.19: Comparison between DNA fragmentation spectra induced by irradiation with 442 keV/mm carbon and iron ions with a dose of 5 Gy. Left panel: Histogram of the fragment distribution (empty bins for carbon ions and filled bins for iron ions). Right panel: Cumulative fragment distributions (solid circles for carbon ions and solid triangles for iron ions); the lines are a guide to the eye. Error bars are standard deviations.

limit of the smallest size range is generally much larger than 1 kbp.

Obviously, the main issue with a code is its reliability in the representation of all the relevant processes that lead to the formation of DSBs. In our previous work, the validation of the PARTRAC code by comparison with available experimental data was our main concern. The satisfactory agreement led to the conclusion that the code can be reliably used to determine the fragmentation even outside the experimentally accessible range for various ions and LETs.

In principle, it has to be expected that the model structure is reflected in the calculated fragment distribution, in particular in the fragment size interval 10 to 40 kbp. In this respect, it is likely that the dip observed in the fragment distributions of Figs. 2.17 to 2.19 corresponding to the bin for the interval 9-23 kbp is correlated to the model structure. In fact, the 18-kbp linear chromatin fiber sticks could lead to a decrease of the number of fragments in that interval. Since the chromatin structure at that length scale is not yet known in detail, it is likely that these sticks cause an underestimation of the number of fragments in that bin and then an enhanced dip. Improved knowledge of the chromatin structure will have to be taken into account in the PARTRAC code in the future.

Carbon ions play relevant roles in hadrontherapy with ions heavier than protons [171], and both carbon and iron ions are important for radiation protection in space [6]. Although the second issue can be considered to be important only in perspective because it is related to the problems arising in long-term

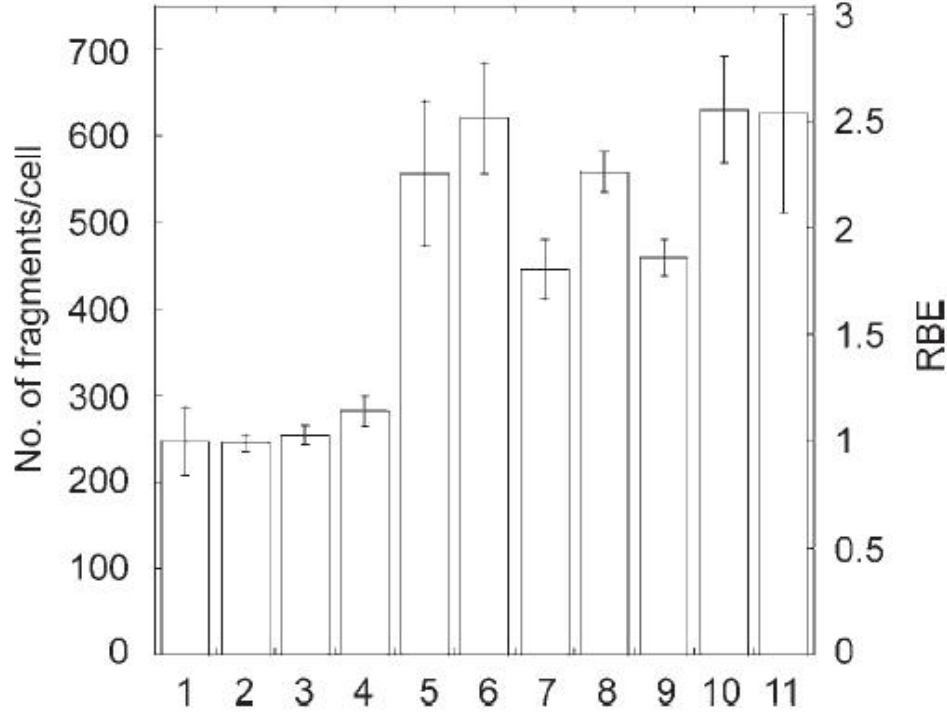


Figure 2.20: Histogram of the total number of fragments produced by the 11 radiation qualities considered in this work after an irradiation with 5 Gy. The numbers in the x axis identify the radiation according to the progressive numbering introduced in the list above. The scale on the left y axis gives the absolute fragment numbers, while the scale on the right y axis gives the RBE for fragment production. Error bars are standard deviations for the fragment numbers.

manned space missions, it has been the subject of recent work [29].

It links the basic research subject of the biological effects of heavy ions with a possible practical application in the future. Here we have presented results for monoenergetic ion beams. This is the condition usually met during *in vitro* studies, where the whole cell population is traversed by ions of the same energy. There will be also a score of secondary hadrons produced by nuclear reactions, which is particularly important for heavy-ion beams. The situation is clearly different if we consider the traversal of the human body. Due to the stochastic nature of energy depositions, even an initially monoenergetic beam gradually degrades and spreads in energy with depth, and therefore the cells will be hit, beyond the secondary hadrons, by primary ions with different energies. This feature is even purposely enhanced when use is made of a spread-out Bragg

peak. However, the production of very small DNA fragments has a simple additive property (unless the doses delivered are very high), since most of these fragments, which are the result of energy depositions within the nanometer scale, are due to correlated events from the same track.

The additive property will not extend to the late cellular effects, since there is no evidence that the repair capability, or more generally the damage processing, depends only on the damage clustering at the smallest scale. This implies that a precise and detailed determination of DSB distribution is only the first step in the construction of the relationship between track structure and cellular effects. The other, more difficult, step would be a better knowledge of the relationship between the DSB distribution and the kinetics of damage processing (See Chapter 3 for details).

2.3.3 Small Fragments analysis

In order to compare the simulation results obtained with the PARTRAC code, simulations have been performed in the framework of the results on DNA fragmentation obtained and published by Hoglund and Stenerlow [93][38].

In this case low-passage confluent cultures of cells (normal human skin fibroblasts) have been irradiated with high doses of Nitrogens nucleus (140 Grays) of different LETs (between 80 to 225 keV/ μm).

Experimental data very useful for comparisons (very good in all cases) with the DNA mass distributions obtained by the PARTRAC outputs. The results are showed in Fig. 2.21 for the case of Nitrogen ions at 175 keV/ μm . The results

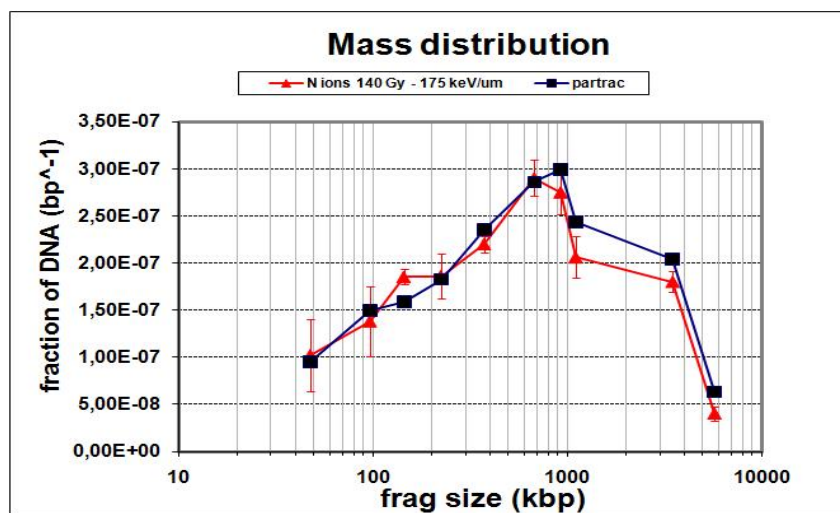


Figure 2.21: Mass distribution of DNA fragments after Ni irradiation

shown in Fig. 2.21 demonstrated the excellent agreement of the experimental data and the simulation results for this particular experimental set-up. From the experimental data, the fragment number distributions can be obtained from the mass distribution through the use of the mean fragment size of each size range using the formula:

$$n_f^{exp} = \frac{x_i G \delta M_i}{M_i} \quad (2.11)$$

where

- x_i are the experimental results
- $G = 6.425 * 10^9$ bp
- δM_i is the size range width
- M_i is the mean size range

This formula implicitly assume a uniform distribution of number of fragments within a certain size range. This represents a good approximation for high size range (> 100 kbp), whereas under a certain threshold this assumption can be challenged by the presence of resonance due to very small fragments of DNA produced by high LET irradiation. The results (the simulation data are directly obtained from the PARTRAC output) are showed in the next Figure. The results showed in Fig. 2.22 clearly demonstrated that this procedure to

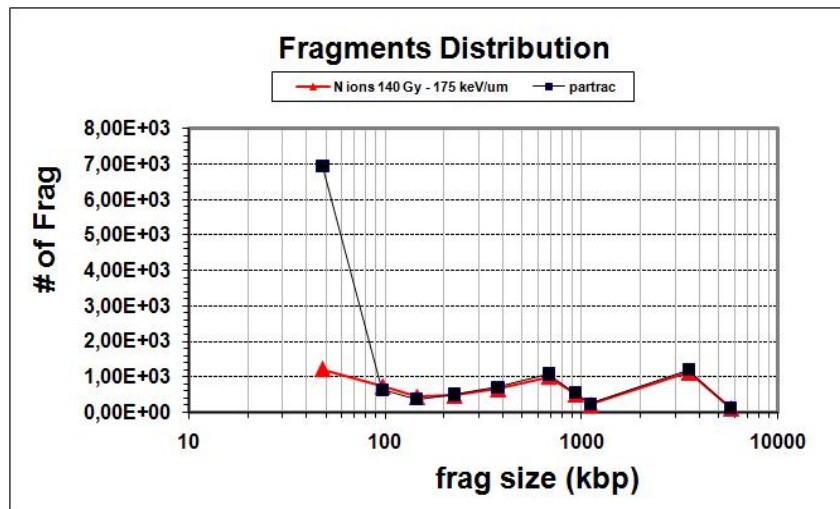


Figure 2.22: Fragments distribution after

obtain the number of fragments is a very reasonable for intermediate and large fragment sizes, but it could introduce large errors for the smallest fragments

due to peaks in the fragmentation spectra generated by DNA winding around histones and chromatin sub-structures. The total DSB yield is experimentally underestimated, due to the large underestimation of the small fragments number: in the paper [29] the experimental DSB Yield resulted to be 46, whereas the one obtained with the simulation (which takes account of the resonance of the very small fragments) resulted to be 81.

Finally, from these results it is clear that the DSB spectrum depends on the track structure, which in turn is not uniquely determined by the LET of the radiation: radiations with similar (high) LET can have very different track structures, if, e.g., they are made of ions of quite different charges. This indicates that each radiation quality should in principle be studied separately. As an example for iron ion beam, the higher energy of the lower-LET beam causes a larger radius of the tracks, and this in turn causes a smaller interaction with the lowest levels of the DNA spatial organization.

2.4 Internal Exposure

As we have seen in the previous section, the DNA damage at subcellular level was studied using the Monte Carlo code PARTRAC (PARTicle TRACks). The code can simulate the transport of photons, electrons, protons and ions in liquid water.

Starting from the existing code, some routines were added to study the behavior of internal emitters.

In particular we focused on the low energy β emitters, since the problem related with these nuclides is that the range of the β - produced is small compared to the dimensions of the biological target: for this reason if the nuclide is confined in the cytoplasm of the target cell (interphase fibroblast cell) conventional dosimetry tends to overestimate dose to the nucleus; on the other hand, if the nuclide is concentrated in the nuclei of the cells, the risk of underestimation of dose using conventional dosimetry exists [53].

In order to simulate the behavior of internal emitters we made some changes to the PARTRAC code. These variations were carried out only within *etrac* module (see Section 2.2.1 *Structure of the code*) that simulates the physical process of electron transport in matter, while all the other modules remained unchanged. The changes made on the program *etrac* are listed below [34].

- Changes in the shape of the sources used and their location.
- Resolution of problems arising from the splitting the target regions and subsequent analysis of the interactions in the region of interest.
- Implementation of internal emitters.
- Changes in the structure of the input file .esf

- Adding a program to calculate the number of DSB per chromosome.

2.4.1 Changes in the shape of the sources used and their location

The first changes were made on possible sources and their properties.

Usually the simulations had always been done through the use of an external source made of a thin disk, located under the layer of mylar, with z axis parallel to simulate typical experimental conditions (see Fig. 2.6). To simulate the behavior of internal emitters the main modification to the code was to bring the source within the cell. To reach our purpose we made a cylindrical shaped source, with the tracks of electrons starting from random directions from the whole volume of the cylinder. In the second stage we brought the emitting cylinder inside the cell, in order to simulate a radionuclide that does not penetrate into the nucleus but is distributed uniformly in cytoplasm itself (see Figure 2.23). In the Figure 2.23 it is possible to view the locations of starting position of the electrons (crosses found in the figures represent the traces of generated electrons with an energy of 300 eV, and each track is substantially constituted from a single cross). Our plan was to try to simulate 2 different emitters: Tritium (3H) and Nickel(${}^{63}Ni$). In order to simulate the emission of Tritium and Nickel, a proper energetic distribution of the beta particles was implemented.

Physical properties of the internal emitters: Tritium

- ${}^3H \longrightarrow {}^3He + e^+ + \nu_e$
- $T_{1/2} = 12.33years$
- $T_{1/2Biol} = 10days$
- $E_{max} = 18.63keV (Range = 5.2\mu m)$
- $E_{aver} = 5.7keV (Range = 0.42\mu m)$

Physical properties of the internal emitters: Nickel

- ${}^{63}Ni \longrightarrow {}^{63}Cu + e^+ + \nu_e$
- $T_{1/2} = 100years$
- $T_{1/2Biol} = 500days$
- $E_{max} = 66keV (Range = 20\mu m)$
- $E_{aver} = 17keV (Range = 5\mu m)$

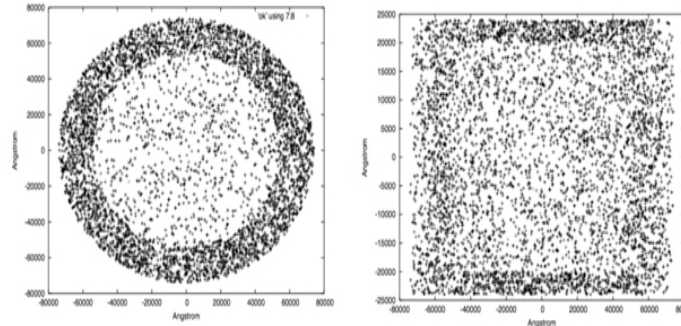


Figure 2.23: Beta emission induced by internal source placed in the cytoplasm region of the cell

In the next figures, the energy distributions of the 2 beta emitters are shown (as they are implemented in PARTRAC). With this new internal irradiation set up, the source can be any point inside the cell (variation depends on the ratio between nucleus and cytoplasm concentration). The new geometrical parameters were:

- Nucleus ($r=7.5 \mu\text{m}$, $h=5 \mu\text{m}$)
- Cytoplasm ($r=12.5 \mu\text{m}$, $h= 15\mu\text{m}$)
- Mylar ($r=25 \mu\text{m}$, $h=1 \mu\text{m}$)

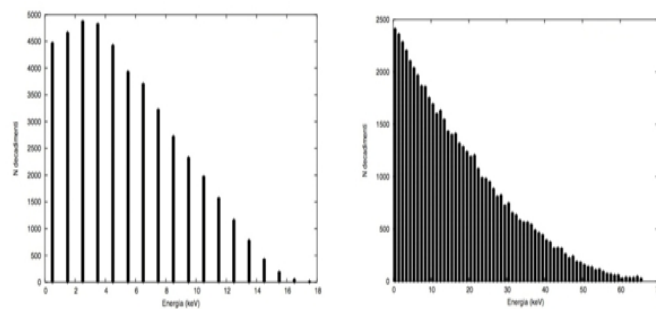


Figure 2.24: Energy distribution of the the Tritium and Nickel source

2.4.2 Results

After analyzing the energy deposition in the nucleus, the distribution of DNA damage induced by different concentrations of the radionuclides examined was

studied. As mentioned above, the nuclide considered are ${}^3\text{H}$ (the electrons emitted due to the β -decay have an average energy of 5.7 KeV and an average range of $0.42\ \mu\text{m}$) and $(63)\text{Ni}$ (whose electrons have an average energy of 17 keV and average range of $5\ \mu\text{m}$) (see Fig. 2.24).

First of all, the dose dependence on the concentration of the internal emitters inside the nucleus is linear, as expected. In case of ${}^3\text{H}$ the dose in the nucleus, coming from the tracks generated outside this region, is 15% of the average dose to the cell; in case of $\text{Ni} - 63$ the dose in the nucleus is 64% of the average dose to the cell (see Fig. 2.26). These results underline that the overestimation of the dose in the nucleus is higher for ${}^3\text{H}$ than for $\text{Ni} - 63$. Afterwards the DSB distributions in function of the concentration of the nuclides in the cell and of the dose were analyzed; the number of DSB in every interval of fragments was obtained as a function of the average dose to the cell (for different concentrations) (see Fig. 2.25). Thanks to the data obtained in the simulations it was possible to calculate the number of complex lesions (which have a high probability to induce lethal damage to the cells) per Gray (around 0.5/1) and the number of DSB per Gy. This value turned out to be of 50 (this value is obviously dependent on the quality of radiation; for γ -rays this value is near to 40).

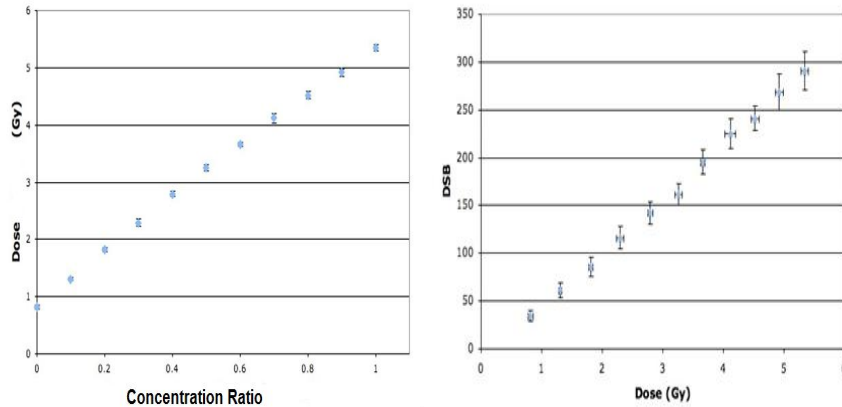


Figure 2.25: Left: Dose in the cell nucleus as a function of the ratio between the concentrations of nucleus and cytoplasm of the cell. Each point of the figure is obtained by averaging over ten simulations. The error bars are standard deviations. Right: Number of double breaks as a function of the dose in the nucleus per dose uniformly equal to 0.53 Gy. Each point of the figure is up from an average at least ten simulations. The error bars are standard deviations.

To further characterize the effects of internal emitters inside the cell, the distributions of DSB per chromosome were also studied for different radionuclide distributions in the cell.

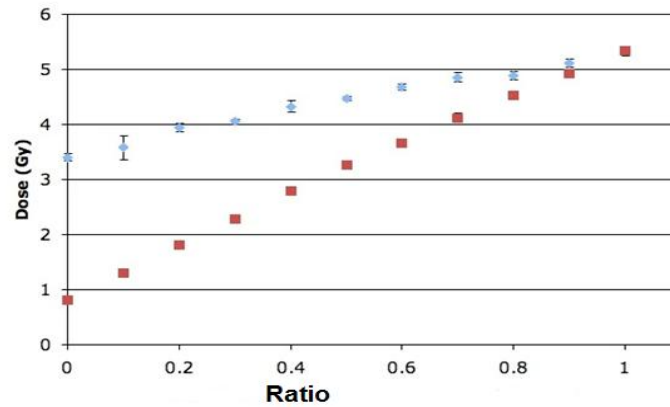


Figure 2.26: Dose in the nucleus as a function of the ratio between the concentrations of nucleus and cytoplasm with a mean dose to the cell of 5,34 Gy. Each point on the figure is obtained from an average of ten simulations. The error bars are standard deviations. The blue points are the nickel, red tritium. The values at ratio 0 represents the dose difference due to the different range of Tritium and Nickel electrons when the emitter are confined in the cytoplasm (average range ($0.42 \mu\text{m} / 5 \mu\text{m}$))

In the next Table and Figure the comparison between the number of DSBs per chromosome (for a total dose of 5.64 Grays), in three different irradiation *scenarios* are presented:

- Non Uniform distribution of nuclide inside the cell (Blue Bars)
- Uniform distribution of nuclide between the cell nucleus and cytoplasm (Red bars)
- Theoretical calculation of the number of DSBs per chromosome based on the chromosome length and a number of DSB equals to 50 per Gray (Yellow bars).

The results obtained show the possible overestimation or underestimation of the risk (particularly for tritium intake) due to the different distributions of the low energy emitters inside the cell.

# Chromosome	DSB (non unif)	DSB (unif)	Estimated DSB (Unif)
1	4.00 ± 2.16	35.25 ± 4.03	34.453
2	22.25 ± 5.91	8.75 ± 1.71	33.405
3	25.25 ± 3.77	25.75 ± 6.18	28.034
4	21.50 ± 7.59	27.25 ± 3.30	26.593
5	27.75 ± 5.44	23.00 ± 6.48	25.414
6	22.75 ± 5.06	22.75 ± 4.27	23.973
7	18.75 ± 4.99	19.75 ± 4.19	22.401
8	28.25 ± 6.40	23.75 ± 7.67	20.305
9	30.50 ± 3.51	21.50 ± 3.00	18.995
10	25.50 ± 4.93	23.00 ± 2.58	18.864
11	9.25 ± 1.26	20.75 ± 2.50	18.864
12	19.50 ± 3.12	18.00 ± 2.94	18.733
13	8.50 ± 2.52	15.00 ± 4.08	14.934
14	18.50 ± 3.70	13.75 ± 4.42	14.279
15	4.25 ± 0.96	12.00 ± 3.74	13.886
16	12.50 ± 4.12	13.75 ± 4.57	12.838
17	12.50 ± 4.04	13.25 ± 5.38	12.052
18	1.75 ± 1.26	13.75 ± 1.50	11.135
19	15.25 ± 4.27	10.75 ± 4.27	8.777
20	10.75 ± 3.69	8.00 ± 1.63	9.432
21	7.00 ± 2.71	5.50 ± 1.91	6.550
22	1.50 ± 1.73	5.25 ± 3.40	7.336
23	17.25 ± 5.25	21.25 ± 1.71	21.484
24	8.75 ± 2.75	36.50 ± 3.70	34.453
25	17.50 ± 1.29	34.50 ± 7.14	33.405
26	18.50 ± 4.43	23.50 ± 4.20	28.034
27	17.25 ± 6.70	24.00 ± 6.98	26.593
28	15.50 ± 4.51	26.25 ± 5.74	25.414
29	24.00 ± 4.97	23.25 ± 1.71	23.973
30	7.25 ± 2.06	19.75 ± 2.06	22.401
31	10.25 ± 4.03	20.50 ± 3.41	20.305
32	12.50 ± 2.65	18.00 ± 5.10	18.995
33	13.50 ± 2.38	14.00 ± 4.83	18.864
34	24.00 ± 0.82	20.75 ± 1.71	18.864
35	16.25 ± 3.86	17.25 ± 5.56	18.733
36	8.25 ± 2.75	11.75 ± 3.50	14.934
37	16.00 ± 7.57	15.25 ± 4.64	14.279
38	2.50 ± 2.38	13.75 ± 3.77	13.886
39	3.75 ± 1.89	14.75 ± 1.71	12.838
40	12.00 ± 4.69	9.50 ± 2.64	12.052
41	5.00 ± 2.83	11.00 ± 5.72	11.135
42	14.25 ± 2.22	10.25 ± 2.22	8.777
43	8.50 ± 5.80	10.00 ± 2.45	9.432
44	13.25 ± 5.56	8.00 ± 3.37	6.550
45	0.75 ± 0.96	7.00 ± 1.41	7.336
46	18.25 ± 5.06	20.5 ± 9.04	21.484

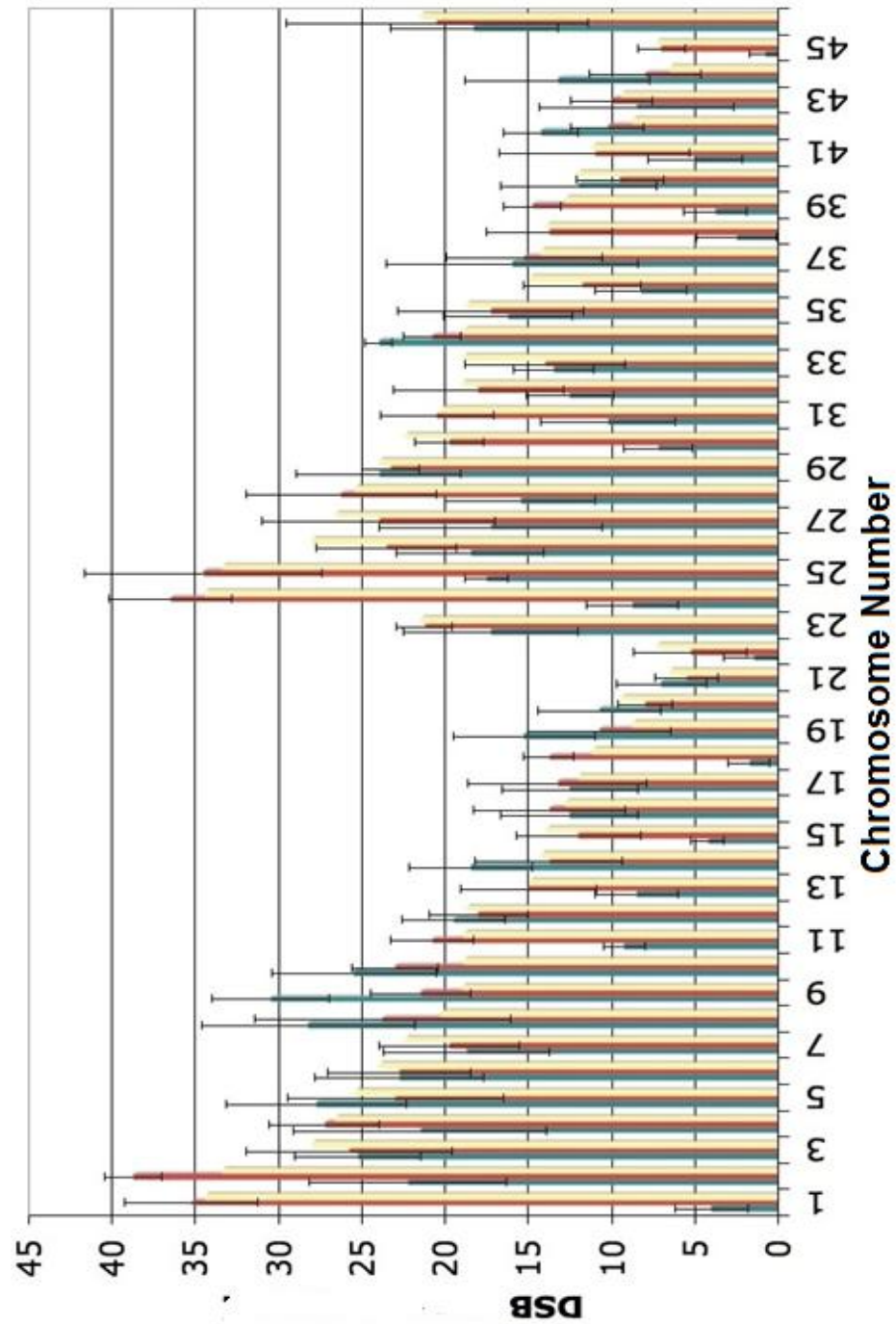


Figure 2.27: Correspondence between the number of fragments induced by radionuclide uniform distribution and the prediction based on chromosome lengths

Chapter 3

The evolution of DNA damage: protein recruitment at the damage site

As shown in the previous chapter, the physical methods for DSB quantification typically require the use of doses bigger than few Gray for a reliable evaluation of the DNA induced damage. Furthermore, the physical methods for the DSB detection require a DNA molecule free of histones and other proteins, usually obtained by high temperature lysis condition that can elicit a temperature-induced damage response (such as the labile sites, i.e. breaks in the DNA strands induced by the high temperature level reached during the experimental procedure). For these reasons, a different experimental technique is needed in order to investigate the radiation induced DNA damage for small doses of radiation (typically in the order of fractions of Gy)

3.1 Radiation Induced γ X2AX

The first response of a mammalian cell after the induction of a Double Strand Break by radiation is the recruitment of a large number of protein to the site of the damage [179] [54] [47] [48]. Sensor proteins are thought to detect the presence of a DSB, and then recruit transducer proteins which provide the signals to enzymes to repair the break. Depending on the severity of the damage and the cell cycle status of the damaged cell, sensor proteins, also modified by transducers, will induce either cell cycle delay for repair, programmed cell death or senescence [50]. The group of protein can be visualized as small spots into the cellular nucleus thanks to a proper staining with specific antibodies of the protein investigated (see Section 3.2.1 [59] [60]). A large number of different protein [40] can be recruited at the DSB position and possibly can form an ionizing radiation induced foci (IRIF) at - or in the vicinity of - the actual site of DSB [152].

In higher eukaryotic cells, DSBs in chromatin promptly initiate the phosphorylation of the histone H2A (a component of the core nucleosome around which the DNA is packaged) variant, H2AX, at Serine 139 to generate γ H2AX [63]. H2AX is one of the most conserved H2A-variants, and it is present in chromatin at levels that vary between 2% and 25% of the H2A pool, depending on the cell line and tissue examined (e.g. around 10% for normal mammalian cells). Overall, serine phosphorylations are the most abundant (approximately 86% of all phosphorylation sites in HeLa cells), followed by threonine (12%) and tyrosine phosphorylations (2%). There is now the evidence that changes in chromatin conformation is required for the correct development of the DNA repair processes. Modification of chromatin structure is important for all pathways utilized by the cell to repair DSBs [51] [41].

Particularly homologous recombination repair (HRR), the only error-free pathway, requires extensive chromatin modification to facilitate its essential steps: initial processing of DNA ends, search for homology, invasion into the intact homologous double helix, formation of a Holiday junction, DNA synthesis with the associated branch migration and final resolution of the Holiday junction. [79]

Thus, both the mechanisms of induction and repair of a double strand break can be investigated with this experiential technique. In the Figure 3.1 it is shown the different level of organization of the DNA and the key role of the histone in the structure of the chromatin fiber.

The phosphorylation process The key process underlying the induction of the RIF is the phosphorylation of histones protein by kinases (or dephosphorylation by phosphatases) which provides docking sites for interaction partners or triggers conformational changes that alter a protein's enzymatic activity or its interactions with other proteins or DNA [87]. It is important to stress that these altered enzymatic and or interaction properties may transmit signals in various ways. In this scenario, the phosposrylation of the H2AX acts as sensor of the DSB, and it is necessary for the recruitment of the other proteins involved in the Dna Damage Response [66].

Generally speaking, the phosphorylation status can determine the subcellular localization of a protein, controlling nuclear import (or export) in Janus kinase/signal transducer and activator of transcription (Jak/ Stat) and nuclear factor kB (NF-kB) pathways, see Section 4.2 for details) [68].

Phosphorylation dephosphorylation has been considered as a fundamental on off switch for protein function. Biochemical approaches, such as immunoblotting with phosphospecific antibodies, are routinely used for monitoring (previously identified) phosphorylation sites, and many studies based on this technique have yielded valuable mechanistic insight.

Physical Characteristics of a focus The induction of γ H2AX is not limited only in the vicinity of the DSB, but spread to a large chromatin re-

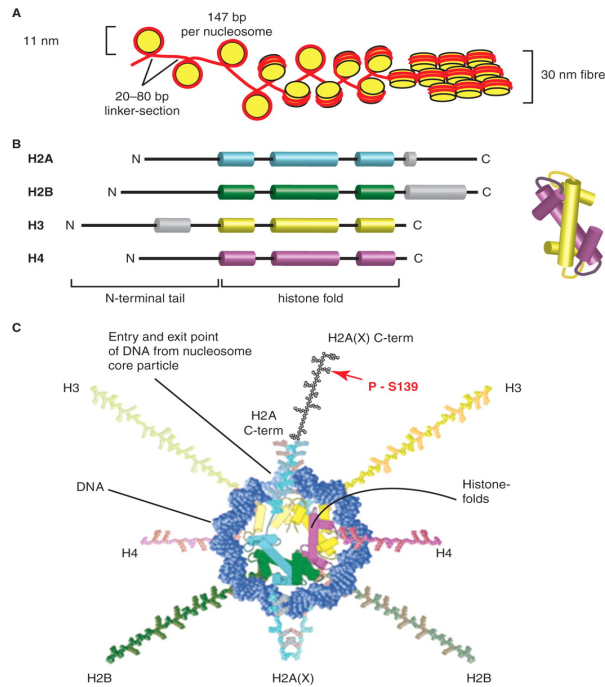


Figure 3.1: Localization and structure of the γ H2AX histone and its phosphorylation. [79]

gion surrounding the DSB. From blotting analysis, it has been evaluated that around 0.03% of the H2AX variant is phosphorylated per DSB [63]. Considering that H2AX represent the 10% (in chromatin) of the total histone, it has been estimated that the modification can take up to 2Mbp comprising around 2000 molecules of gamma H2AX [64]. On the other hand, from immunofluorescence analysis there has been the indication that region up to 30 Mbp can be modified, implying that not every contiguous HA2X molecule is phosphorylated.

As it will be show later in this chapter, from our immunofluorescence analysis, a single *focus* takes a linear dimension of (on average) tenth of microns, but these data depend strongly on the type of irradiation, the dose used, and the time at which the phosphorylated histone is stained. Our work, as illustrated in this chapter, was basically aimed to understand:

- How does radiation quality (qualitatively) influence the size and shape of the foci?
- How does radiation qualities influence the phosphorylation-dephosphorylation processes?
- How does radiation qualities influence the kinetics of foci formation (with

high LET, low LET and mixed field irradiation)?

3.2 Radiation Induced foci as a Function of radiation quality

The number of Double Strand Breaks induced after irradiation could be (very) roughly estimated (at least for low doses) counting the number of induced foci [58]. However, because the induction of foci is a biochemical process involving both formation and loss of foci [65] there is never an exact correspondence between the number of DBSs and the γ H2AX, even for X-Rays irradiation.

As deeply illustrated in the previous chapter, high-LET particles deposit energy along their trajectory and therefore present interesting opportunities for studying the spatial organization of RIF, but the increase of the LET of the incoming radiation can lead the formation of closely spaced complex DSBs [61] [62], and, in this scenario, the recruitment of the repair proteins to the nearby DBSs can be inhibited [51] [57]. Since high-LET particles induce more complex DSB, the investigation of the damage that last after 24 hours after irradiation (see Section 3.3.2) has been performed through the analysis of the persistent foci. In this framework severe lesions seem to induce more robust RIF formation.

In this study, performed in collaboration with the radiobiology group at the CCRCB (Queen's University of Belfast), we investigated the induction and the disappearance of the γ -H2AX as a function of the radiation quality (X-Rays, Alpha particles and Antiprotons irradiation). After some preliminary investigation concerning the size and the shape of the different foci, the main objective of the work was to quantify (experientially and theoretically) the different kinetics of the phenomena and the different residual amount of foci after 24 hours of irradiation.

3.2.1 Low LET irradiation: X-Rays

The source used to irradiated the biological sample was an X-ray cabinet (XRAD 225kV) from PXI industries (see Fig. 3.2). The source has an adjustable sample shelf from 15cm to 63cm from the center of the source, with a maximum Output Voltage of 225Kv and a Maximum current of 45 mA. In our irradiation the voltage of the machine was 225 kV, and the dose rate was 0.67 Gy/mina at 50 cm from the X-Ray tube. During this experiment we evaluate the kinetics of the repair process measuring the rate of formation and loss of γ H2AX foci after X-Rays irradiation. We adopted a primary tumor cell line, the invasive breast ductal carcinoma MCF-7. At least 150 cells per glass slide were analyzed from three independent experiments per dose or time point (examples are showed in Fig. 3.3). In particular we counted the number of foci per cell at 10 min, 30 min, 1 hour, 3 hours, 5 hours and 24 hours after



Figure 3.2: The X-Rays cabinet XRAD 225

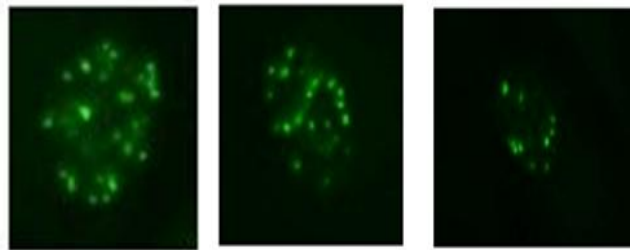


Figure 3.3: Example of foci induced after 0.5 Gy of X-Rays irradiation

irradiation. The results are shown in Fig. 3.4.

Experimental Protocol

1. Fixation

Remove culture medium and wash gently once with chilled PBS.
Add 2 ml/dish of ice-cold fixative(50%MeOH - 50% Acetone) and incubate at 4 °C for 8 min.
Wash three times with chilled PBS and store in PBS at 4°C.

2. Permealization

Add 2 ml/dish of Permealization Buffer(0.5% TritonX-100 in PBS) and incubate for 20 min at 4 °C.

Pour off Permealization Buffer and wash with chilled PBS.

3. Blocking

Discard PBS and add 2 ml/dish of Blocking Buffer (0.2% milk, 5% horse serum, 0.1% TritonX-100 in PBS)

Incubate for 1h at 4 °C.

4. Antibody Reaction

Drain the dishes and add Primary Antibody (anti- γ -H2AX monoclonal antibody). 1:10000 in Blocking Buffer, 900 microliters/well at room temperature for 1 h.

Wash with Washing Buffer (0.1% TritonX-100 in PBS).

Drain and add Secondary Antibody (GAM488). 1:1000 in Blocking Buffer, 900 microliters/well at 4 degrees Celsius for 1 h in the dark.

Wash with Washing Buffer.

Stain with DAPI. 1:20000 in PBS, 2ml/ well at room temperature for 3 min in the dark.

Wash with chilled PBS.

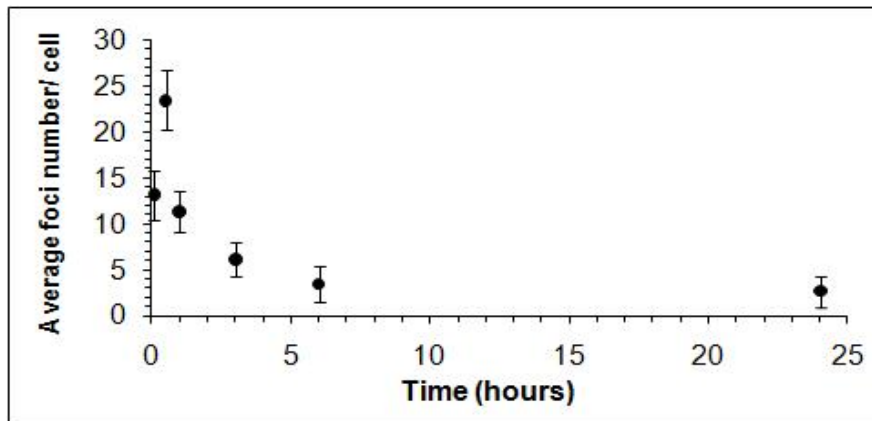


Figure 3.4: Average foci number per cell after 1 Gray of irradiation with X-rays

The results shown in Fig 3.4 represent the average number of foci per cell as a function of time from 0 to 24 hours. The maximum number of foci was

reached after 30 minutes from irradiation and the value was around 25 foci/cell, with a persistent number of foci of 2.3 (statistically above the background level)

3.2.2 High LET irradiation: Alpha particles

With high LET irradiation there is an increasing probability that there is a clustered damage. Concerning radiation induced DSB and foci induction, there are (at least) 2 different levels of clusterization:

1) DSB clusterization: This is the possibility of formation of cluster of damage due to higher probability of close ionizations in the case of high LET incoming irradiation.

Since the dimension of a focus is 2 Mb in terms of genomic coordinates, and $0.1\text{-}0.3\ \mu\text{m}^2$ in terms of metric coordinates, this can mean that several clustered damage (i.e. the definition of a cluster lesion is the presence 2 or more DNA DSB within 50 base pairs) can rely within a single focus, so that the focus induced by high LET irradiation can belong to different ionization clusters.

2) foci clusterization: It is experimentally and theoretically demonstrated [50] that the cells exposed to high LET irradiation show different spatial distribution of foci inside the cell, mimicking the spatial distribution of the irradiation ionization pattern (sparsely distributed foci for gamma irradiation, tracks-like distributed for high-LET irradiation). In this scenario, different independent foci can overlap, producing a chain of foci.

The source used was an alpha source made of Americium 241 (Half-life: 432.2 years), with α energies, respectively, of 5.4431 and 5.4857 MeV and with the emission of two gammas of energies of 0.03 - 0.06 MeV. The total disintegration energy is equal to 5.63781 MeV and the activity of the source is 40 kBq. This type of source consists of a thin layer of $Am - 241$ deposited by vacuum sublimation onto a lightly oxidized stainless steel disc of overall diameter 25 mm and thickness 0.5 mm. The diameter of the active area is approximately 7 mm. Due to the small penetration depth the alpha source, a peculiar experimental set up was realized. In the next figure it is possible to see a representation of the experimental set up. The experimental samples were irradiated at a distance of around 3 mm from the source with an *ad hoc* support already built for microbeam irradiation (not shown in the Picture). The detailed description of the support is illustrated in the *Experimental Results Section*.

Physical Characterization of the Source

In order to characterize the emission and the fluence of the source at the biological target a physical characterization was performed. Due to the small region of the source (7 mm) it was crucial to investigate the region of irradiation and the edges to evaluate the reduction, in term of fluence, of the incoming particles. Since the foci staining shows the energy deposition following the direction of the track, it was necessary to define the region of irradiation with a beam perpendicular to the cells surface, with an homogeneous number of

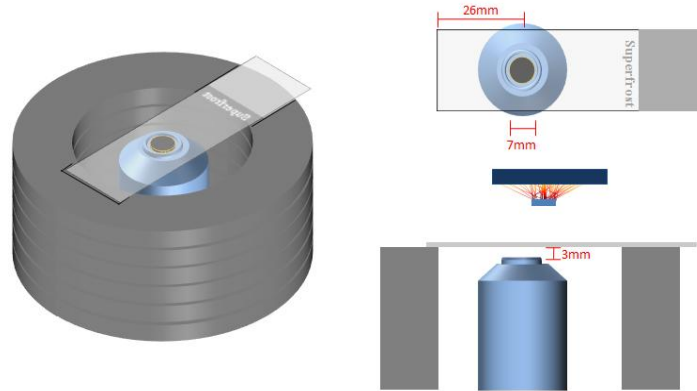


Figure 3.5: 3-Dimensional view of the Alpha Source and of its characterization

traversal per surface unit. We placed a CR-39 detector on the slide (as shown in Fig.3.6) in the same position where the cells should be irradiated and we measured the number of particle stopped by the detector as a function of the distance in order to investigate the change of particle fluence along the length of the biological samples (see Fig. 3.7a).

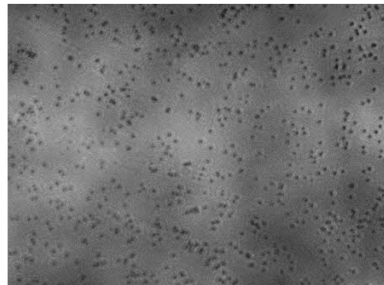


Figure 3.6: An example of a CR-39 field of dimension 150X70 μm after 2,5 Gy of alpha irradiation.

The number of particles which actually reach the center of the detector rapidly decreases, increasing with distance from the center of the source (due to geometric factors), with only a region of 1.5mm with an homogeneous distribution of particles. For this reason all the experiments were performed counting the foci only in cells placed directly above the source center, in a circle of 1.5 mm radius.

The number of alpha traversal was evaluated using a Poisson like distribution

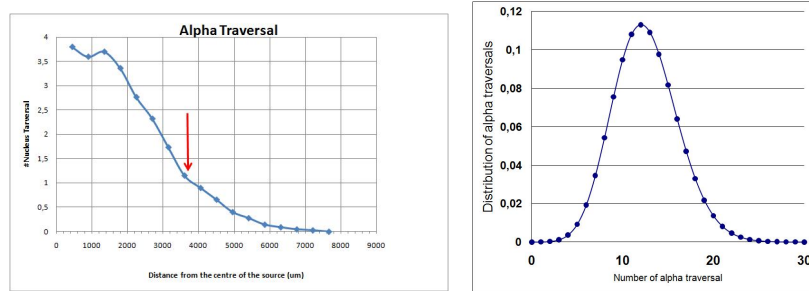


Figure 3.7: On the left panel: Measurements of the number of tracks per Gray as a function of the distance respect to center of the source. The arrow represents the edge of the source. On the right panel: Expected distribution of alpha traversals

for particles with $100 \text{ keV}/\mu\text{m}$ of LET, 1 Gy of Dose, and with a sensitive target with a diameter of $16 \mu\text{m}$. The distribution is shown in Fig 3.7b with a mean number of traversal equals to 12.53.

Alpha Tracks As mentioned above, due to the steep decreasing of the number of particle increasing the distance from the center of the source, we irradiated cells in a circle with a radius of 1.5 mm. However, thanks to this particular set up it was possible also to investigate the *foci chains* due to the tracks of the alpha particles. (see Figure 3.9)

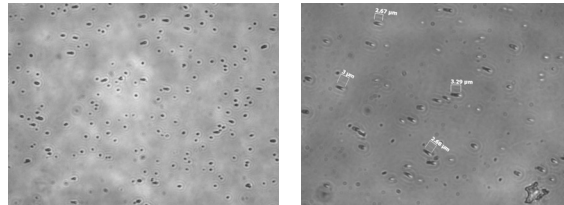


Figure 3.8: On the left panel: An example of the tracks detected with the CR-39 in a field at 5 mm from the surface area. On the right panel: estimation of the length of the alpha tracks at 5 mm from the center of the source area

Analyzing the data obtained at a long distance (8 mm) from the center of the source (See Fig. 3.8) it was possible to quantify an average length of few micron per tracks, according to what found in the literature [9]. With this particular set up it was the possibility to investigate the foci sizes for an incoming particle with an LET of around $100 \text{ keV}/\text{m}$. From the Fig. 3.9 it is clear that the foci sizes are bigger respect to the ones obtained with the X-Rays (Fig. 3.3) and are aligned along the alpha tracks.

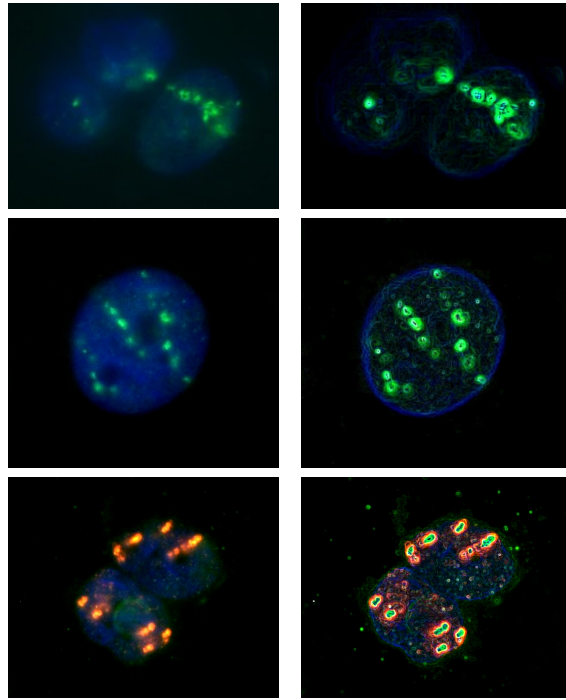


Figure 3.9: Example of foci induced in the region far from the source centre (> 7 mm). The alpha tracks are clearly visible

Biological Characterization of the Source

In order to obtain a biological characterization of the source we performed a survival curve for MCF-7 cells with the clonogenic assay for doses from 1 Gray to 10 Grays. A cell survival curve describes the relationship between the amount of absorbed dose and the fraction of cells that survive. Amongst the possible different types of cell deaths, with the clonogenic assay, a cell is considered dead when it loses its capacity to reproduce. Following a radiation exposition, a survivor that is able to proliferate indefinitely to produce a large colony is said to be *clonogenic*. The technique adopted for studying the survival fraction and the proliferation of cells *in vitro* is called *clonogenic assay*.

The clonogenic assay consists in preparing two samples with a known number of cells on two different dishes and to irradiate one of them. After a suitable period of incubation (up to two weeks) the colonies are scored using crystal violet, a protein dye with the characteristic deep purple color. The so called *plating efficiency* PE is calculated dividing the number of formed colonies by the total number of the initial cells. The surviving fraction for the cell survival

curve is given by the following formula:

$$\text{surviving fraction} = \frac{PE_{\text{irradiated}}}{PE_{\text{control}}}$$

and goes from 0 to 1. It is important to plate a convenient number of cells on the plate, in order to obtain an appropriate number of colonies. From the

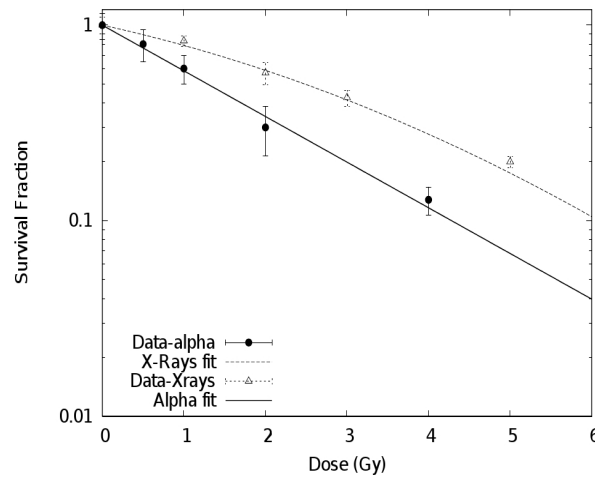


Figure 3.10: Survival curves for MCF-7 cells for alpha and X-rays irradiation

results shown in Fig. 3.10 the alpha particles result more effective. The dots represent the experimental data, while the lines represents the fit of a linear quadratic model. Nowadays, the *linear quadratic* is the most used model to describe the cell survival curve [25]. According to what proposed by Brenner et al, a possible interpretation is described by the following mechanisms:

1. Only double strand breaks (DSB) contribute to the cell total damage. Radiation produces DSBs proportionate to the dose.
2. These DSBs can be repaired with a rate constant $\lambda = \ln(2/T_{1/2})$ where $T_{1/2}$ is the repair half time.
3. In competition with DSBs repair, misrepair of pairs of DSBs produced from different radiation tracks can produce lethal lesions such as chromosomal aberrations, with a yield proportional to the square of the dose. Since the two radiation tracks can occur at different times, it is possible that the repair of the first DSBs takes place before the second radiation track.

4. Single radiation tracks can produce lethal lesions by several mechanisms, with a yield proportional to the dose.

The linear quadratic cell survival curve, drawn in Fig 3.10 , is represented by the following function:

$$S(D) = e^{-\alpha D - \beta D^2}$$

where α and β are two constants. As it is possible to see from the Figure 3.10, in the case of alpha irradiation the beta value has a value of around 0, resulting in a linear fit in the *log-log* graph, according to what found in the literature [40]. The *single track mechanism* - production of lethal lesions by a single track, typical of high LET irradiation - has a yield proportional to the dose. This is reflecting in a survival curve where only the α parameter is dominant.

Experimental Results

Following the same protocol adopted described in the Section 3.2.1 we counted the number of foci per at least 150 cells per time points (30 min, 1 hours, 3 hours, 6 hours, 24 hours) after 1 Gy of alpha irradiation. Due to low range of the alpha particles, peculiar dishes - already built for microbeam irradiation - were used. The beam was perpendicular respect to the cell surface. Furthermore the cells were attached to a thin membrane (optically transparent, and non-UV fluorescent), mounted on stainless steel support. The dishes were machined from medical-grade stainless steel. A 34 mm diameter thin membrane cell support (made from 1 μm thick Mylar) was sandwiched between the base and an annular piece that tensioned the membrane as it was located. A 0,5 mm thick silicon rubber gasket provided a water-tight seal. The membrane was the lowest part of the dish, which allowed unimpeded access to position the source close to any part of the underside of the membrane. [52]

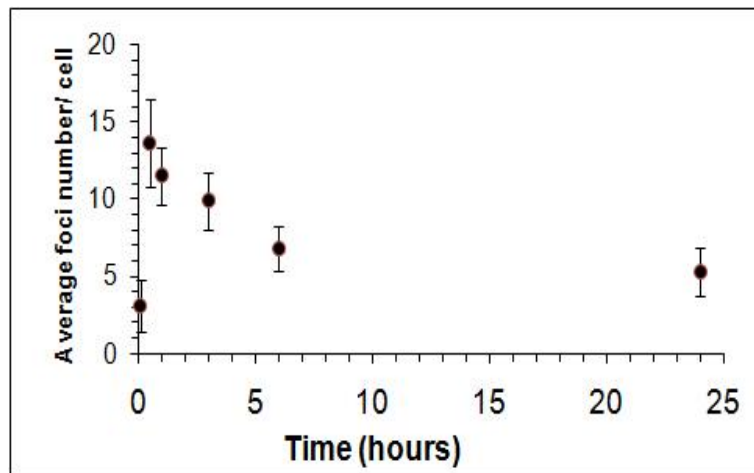


Figure 3.11: foci Induced after alpha irradiation

The number of foci at the maximum peak obtained in this experimental set-up was lower respect to X-Rays irradiation (around 12 foci per cell respect to the 25 foci found for X-Rays set-up). This is consistent with the hypothesis that, in this peculiar experimental set-up, the foci represent the number of the tracks instead of the number of DSB (see Section 3.2) Moreover, the kinetics of the foci induced by alpha particle was slower, with a pronounced shoulder of residual damage after several hours after irradiation that reaches a saturation level which has a double value respect to the value reached by the X-Rays radiation. In the next Figure the data from alpha irradiation and X-Rays irradiation are presented.

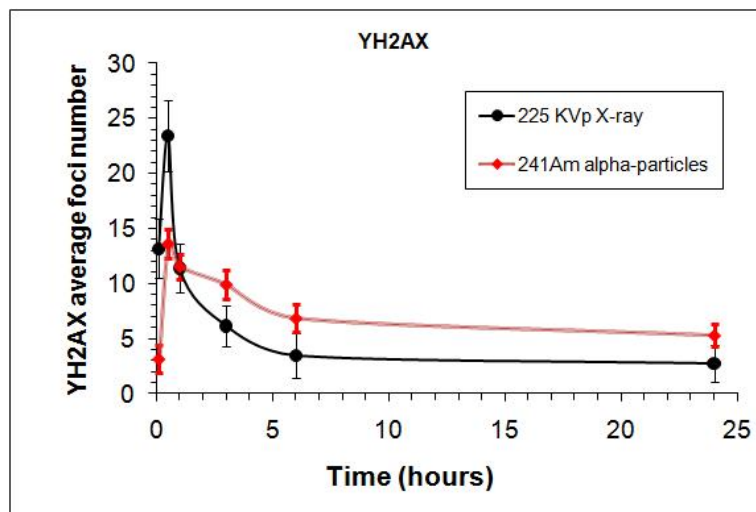


Figure 3.12: Survival curves for MCF-7 cells for alpha and X-rays irradiation

3.2.3 Example of mixed Field Irradiation: Antiprotons

Annihilation physics Antiprotons are interesting as a possible type of novel radiation therapy techniques. In fact, when fast antiprotons penetrate matter, protons and antiprotons have near identical stopping powers and thus the same radiobiological properties along the pattern in the tissues. Unlike protons, when antiprotons come to rest at the Bragg-peak, they annihilate, releasing almost 2 GeV per antiproton-proton annihilation. Most of this energy is carried away by energetic pions, but the Bragg-peak of the antiprotons is still locally augmented with around 20/30 MeV per antiproton [49]. Besides the higher physical dose, an increased relative biological effect also was observed [85], which can be explained by the fact that some of the secondary particles from the antiproton annihilation exhibit high-LET properties (see next Section for details). Another possible interesting use of this radiation type rely on the weakly interacting energetic pions emitted, which may provide a

real time tomography of the annihilation sites [55]. Gray and Kalogeropoulos first suggested radiation therapy with antiprotons in 1984 based on Monte Carlo calculation of a significant enhancement of physical dose in the Bragg-peak [85]. The total energy deposited locally by these particles has been estimated by Gray and Kalogeropoulos using Monte Carlo calculations to be 30 MeV per antiproton [85], which has been confirmed experimentally by Sullivan who used a continuous beam of antiprotons from the Low Energy Antiproton Ring (LEAR) at CERN and standard ionization chambers [143]. This energy represents an increase of the physical dose deposition in the Bragg-peak by roughly a factor of 2, when compared to protons of the same energy (and with the same range).

When fast anti protons penetrate matter, they have the same stopping power as protons, but when they come to rest, an annihilation may occur, that follows the following steps [49]:

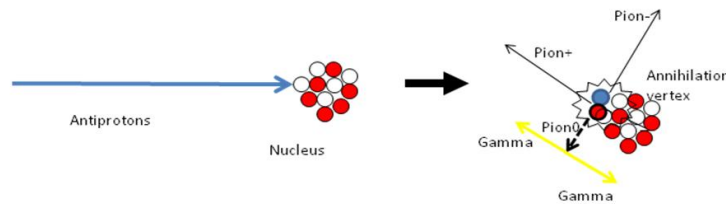


Figure 3.13: Schematic representation of the annihilation event

1. As the antiproton comes to rest, it will preferably be captured by a high-Z nucleus. For a polystyrene target 99% of the antiprotons will therefore annihilate on a carbon nucleus, whereas the rest (1%) will annihilate with a hydrogen nucleus. In the case of liquid water, the antiprotons more likely will annihilate on Oxygen ions [46].
2. When captured by the target atoms, the antiproton will immediately spiral towards the nucleus and annihilate on its surface.
3. This annihilation process releases 1.88 GeV corresponding to twice the rest-mass of the proton and the energy release is converted on average into 4 or 5 pions (circa 400 MeV each).

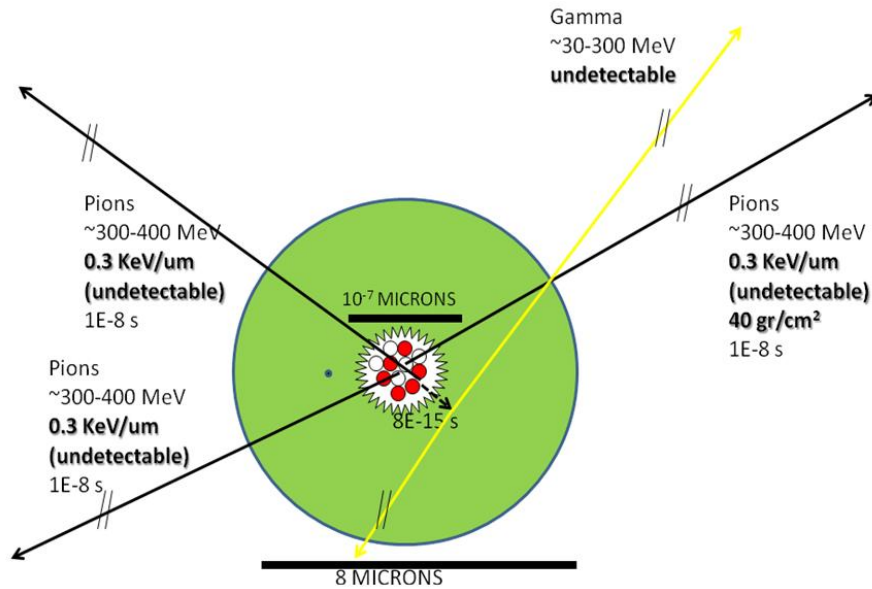


Figure 3.14: Schematic representation of the annihilation event

4. The pions created are π^+ and π^- particles, as well as π^0 . The π^0 meson is highly unstable and decays instantaneously into high energy gamma-rays with roughly energy of 70-300 MeV.
5. Due to the solid angle covered by the nucleus, 1 or 2 of the charged pions might penetrate the nucleus inducing an intra- nuclear cascade, causing the nucleus to break into fragments (see Fig. 3.13 and Fig. 3.14).
6. Charged fragments have a very short range in the target and will deposit their kinetic energy in the immediate vicinity of the annihilation vertex (see Fig. 3.15 for a Geant4 simulation). We expect that some of these fragments (e.g. $He - 4$ nucleus) will exhibit a high-LET and are responsible for an increase in biological effectiveness of antiproton annihilation compared to protons stopping in the target.
7. Antiprotons annihilating on particles heavier than protons will also produce neutrons which will have a larger range and will lead to a certain level of background radiation.

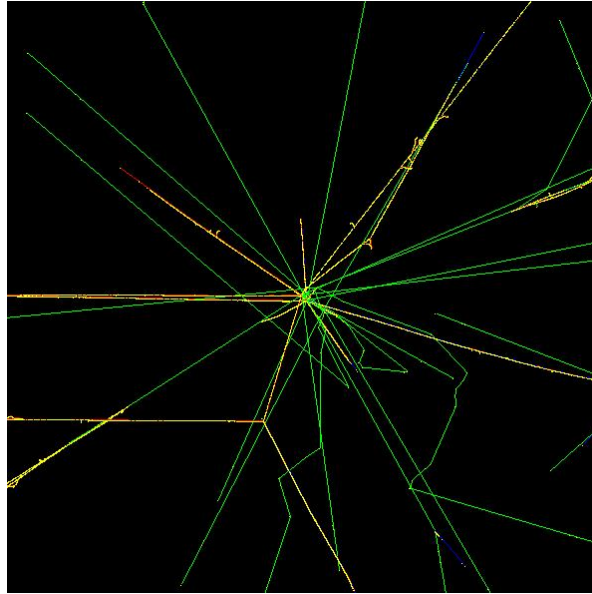


Figure 3.15: Example of an annihilation event simulated with Geant4

Experiments and simulations In order to investigate the possible augmentation of effectiveness of the antiproton beam at the annihilation site a series of experiments were performed at CERN within the framework of the ACE collaboration [175].

The main objective of the experiments was the quantification of the DNA damage at different depth along the Bragg peak, with immunofluorescence techniques able to detect the γ H2AX formation and thus the DNA damage induced. The irradiation were performed at CERN, with a beam of Antiprotons of 126 Mev and with the sample (flasks of monolayer of MCF-7 cells filled with media placed vertically) placed at the proper distance (3 cm for the Plateau measurements, at 10 cm for the Peak analysis) along the antiproton path in tank full of water. Between the tank and the sample a proper plastic degradator made of Polymethyl methacrylate (PMMA) 5 mm thick, able to induce a Spread Out Bragg Peak of around 1 cm at 10 cm from the beginning of the tank [56]. The dose delivered to the MCF-7 cells was 1 Gy at the plateau, and around 2 Gy at the peak, and the cells were fixed after 30 minutes after irradiation in order to score the highest number of foci before the loss due to the dephosphorylation process (see Figure 3.4 for an example of the foci kinetics). To correlate the different LET of the incoming antiproton irradiation and the spatial foci distribution we performed some in these experimental conditions. A series of simulation were performed with Geant4, a toolkit for the simulation of the passage of particles through matter able to follow the secondary particles produced in the annihilation events [176].

We built a proper geometry of the actual experiments, adopting the *QBBC Physics List* in order to better reproduce the annihilation physics for the 126 MeV antiprotons. The beam used was a 126 MeV pencil beam and the dose deposition was averaged on voxels with dimensions $100\ \mu\text{m} \times 100\ \mu\text{m} \times 100\ \mu\text{m}$ perpendicular to the beam axis.

The distribution of secondary particles from annihilation, as calculated with GEANT4, shows that mainly fragments such as pions, protons and some Helium ions contribute to the dose (results not shown). For the peculiar case of antiprotons irradiation performed at CERN in the framework of the ACE collaboration, it is peculiar the behavior of the foci induced formation at the different position along the SOBP (Spread Out Bragg Peak) [143].

The foci induced in the plateau of the dose distribution curve are sparsely-like distributed, whereas the foci induced in the peak region seem to be more clustered-like distributed. This lead also to different sizes of foci, as shown in the panel of Fig. 3. 17. Indeed the different properties of the energy deposition in the peak, led to different dimension of the foci.

In fact as it is possible to see from Figure 3.17 (left panel) the foci induced in the plateau region are relatively small, according to the relatively low LET of the incoming radiation (for comparison with the X-Rays irradiation see Fig.3.3), whereas the foci in the right panel of the figure show are bigger and clustered, according to the highest dose and to the higher LET of the secondary fragments produced at the annihilation site.

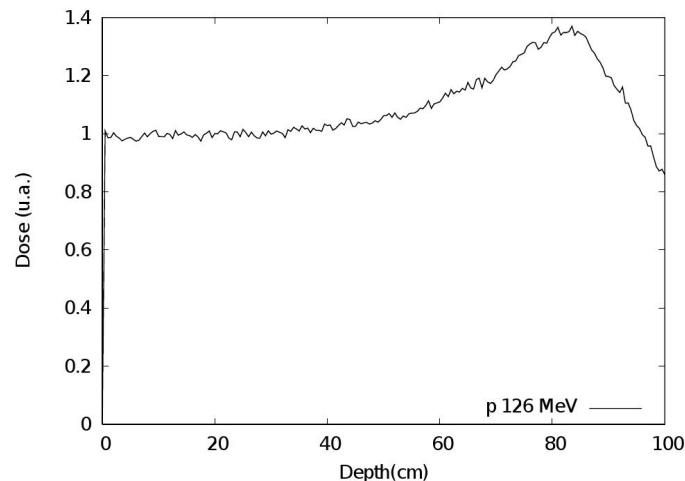


Figure 3.16: Dose-deposition curve simulated with Geant4

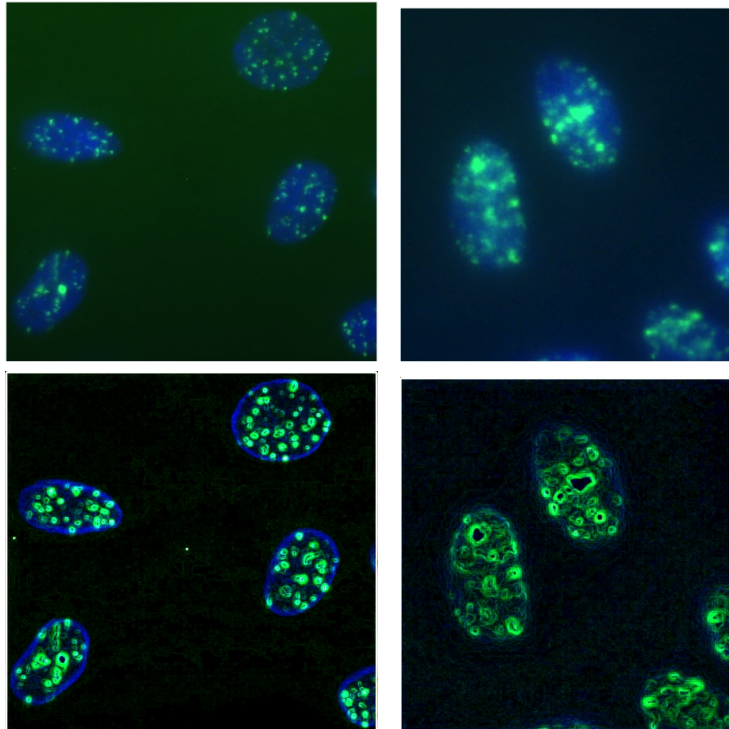


Figure 3.17: foci induced at the plateau (left) or at the Peak (right) by 126 MeV antiprotons (*Courtesy of Joy Kavanagh*)

3.3 Theoretical analysis

The number of foci observed experimentally depends on several factors [58]: cell type, time of fixation of the cells, radiation dose and quality. The dynamics of foci induction after irradiation follow a peak-bell shaped function, with the maximum at 30 minutes after irradiation. In particular it is not clear from the dynamics of foci phosphorylation/dephosphorylation, which could be the initial damage (SSB, DSB or complex lesions) able to elicit the formation of RIF. In fact the debate regarding the correspondence between the number of DSB and the number of foci is still on-going [79], [58], [65]. Starting from the experiential results obtained in Fig. 3.4 and 3.10, we developed an analytical model to try to describe the kinetics of the foci Phosphorylation and De-Phosphorylation, in order to get some insight on:

- The kinetics of foci formation.
- The kinetics of the de-phosphorylation process .
- The residual damage (foci which last also after 20 hours after irradiation).

and their dependence on radiation quality.

3.3.1 Model Definition

Several methods have been developed to try to model the kinetics of the foci formation and loss after irradiation for low LET irradiation. One of the first model developed was based on the mass-action chemical kinetics approach to describe the binding of repair enzymes to DSBs with several intermediate repair complexes leading to DNA rejoining (e.g. DNA-Pks, Ku70/80 dimeres etc), in the framework of the Non Homologous End-Joining [36].

The overall aim of this analysis is mainly to quantitative analyze the difference in the behavior of fci formation process in two cases of very low (i.e. Xrays) or high (i.e. alpha particles) LET irradiation.

Model Hypothesis

We hypothesized that the foci formation process is based on enzymatic reaction between phosphatases and their substrate, and that this behavior can be described by a Michaelis-Menten kinetics (1913) [167]. Michaelis-Menten kinetics approximately describes the kinetics of many enzymes, and is relevant to situations where very simple kinetics can be assumed, (i.e. there is no intermediate or product inhibition, and there is no allostericity or cooperativity). This first approximation modeling approach was adopted and described also by other research groups [87] [68]. In particular, in [167] Szallasi stated that "Among other thing, the Michaelis-Menten rate law can be used to reduce the number of variables which describe a typical enzymatic conversion process, such as phosphorylation[...]. This reduction is often useful when trying to understand the dynamics possibilities of a network using analytical and qualitative methods". With this approach the equation representing the phosphorylation process is :

$$f(x) = A * \left[\frac{x}{x + B} \right] \quad (3.1)$$

On the other hand, the foci loss (de-phosphorylation process) has been hypothesized to be an indicator the DSB repair processes. According to what already suggested by several research groups (for DNA damage repair measured with the techniques described in Chapter 2, see for a review [125] [122]), we modeled the foci disappearance following a double exponential decay (eq. 3.2).

$$g(x) = [C * e^{-D*x} + (1 - C)e^{-E*x}] \quad (3.2)$$

It is reasonable to assume that the components described by the exponential functions corresponds to 2 different classes of possible damage: the first

exponential can describe the relatively fast rejoined damage (not necessarily DSB), while the other component may correspond to more complex damage, which require more time to be rejoined (or may be even remain unrejoined, at last in the time-scale of the cell cycle).

The temporal behavior of the foci removal after irradiation can be described as:

Putting together the phosphorylation-dephosphorylation processes the number of foci at time t ($N(t)$) can be described by the following equation:

$$N(t) = A * \left[\frac{t}{t + B} \right] * [C * e^{-D*t} + (1 - C)e^{-E*t}] \quad (3.3)$$

As mentioned above, the first term represents the induction (Phosphorylation) of a single focus multiplied by a constant to take account of the actual number of foci (k) according (as a first approximation) to a Michaelis-Menten function. These foci disappearance is then described by the second exponential function. The meaning of the parameters is therefore the following:

- A represents the number of the initial damage (not necessarily DSB) and in part not even detectable. Some of them will be repaired quickly, whereas the others (more complex) will lead to the formation of persistent *foci*.
- B characterizes the *kinetics of the induction* of the foci induction, according with a Michaelis-Menten function.
- C represent a term that weighs the different contribution of the persistent and transient foci.
- D characterizes the *kinetics of the disappearance* of the persistent foci, according with an exponential function
- E characterizes the *kinetics of the disappearance* of these transient foci, according with an exponential function

We developed this global approach with the main objective of understanding and quantifying the possible difference in terms of dephosphorylation between the cells treated with the different radiation quality, and to quantify which could be the difference in terms of number and kinetics of the residual foci. Different behaviors of the parameters adopted could provide insights to the different repair kinetics induced by alpha or gamma irradiation.

3.3.2 Results

Kinetics of γ H2AX after X-Rays irradiation

We started the data analysis applying the model to the X-Rays irradiated cells, fitting the curve with the MINUIT program. The best fit to our experimental

data was made with *MINUIT*, a program developed in 1989 at CERN [177]. *MINUIT* is usually used to find the best values of a set of parameters, where "best" is in our case defined as those values which minimize the *chi square* on the basis of a given function fixed in the beginning by the user. This can be a general function with one or more unknown parameters; purpose of this program is to find these parameters on the basis of the experimental data. The plot of the function containing the parameters found was realized with *gnuplot* program.

In the Fig. 3.18 the results obtained with X-Rays irradiation are presented. The function represented in Fig. 3.18 is

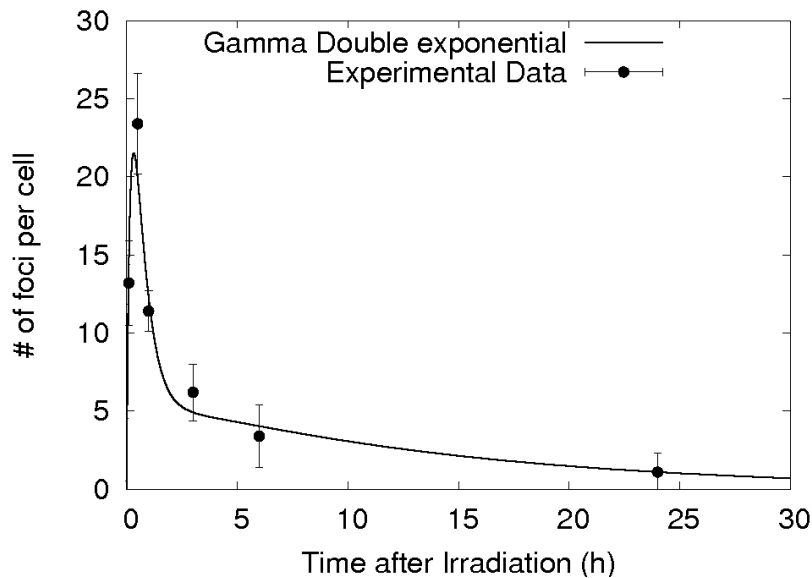


Figure 3.18: Kinetics of the radiation induced foci after 1 Gray of low LET irradiation

$$N(t) = 89.76 * \left[\frac{x}{x + 0.42} \right] * [(0.075 * e^{-0.0749*t} + (1 - 0.075)e^{-1.97*t}] \quad (3.4)$$

Figure 3.18 shows the good agreement between the experimental results and the theoretical model. This was expected, also due the high number of the parameters adopted and the number of experimental data points.

Nevertheless, some insights were obtained concerning the mechanisms of foci induction and processing.

The biphasic behavior is evident in this irradiation scenario: the curve is clearly different between the first 2 hours and the last 20. This can be easily illustrating looking at the values of the parameters in the model. In the first region, the foci behavior is dominated by the vast majority of lesions which are easily

removed. In the second region, there is a small number of persistent foci that decay with a small suppression, due to the difficulty in the rejoining process (small tail at long timing).

The interpretation is in agreement with what found in the literature, encouraging the interpretation of foci as a possible indicator/marker (though not in a 1-to-1 correspondence fashion) of DSBs. Particularly interesting was to apply the model also to the high LET irradiated cells, to quantify the different characteristics and the kinetics of the foci, as a function of the radiation quality.

Kinetics of γ H2AX after Alpha irradiation

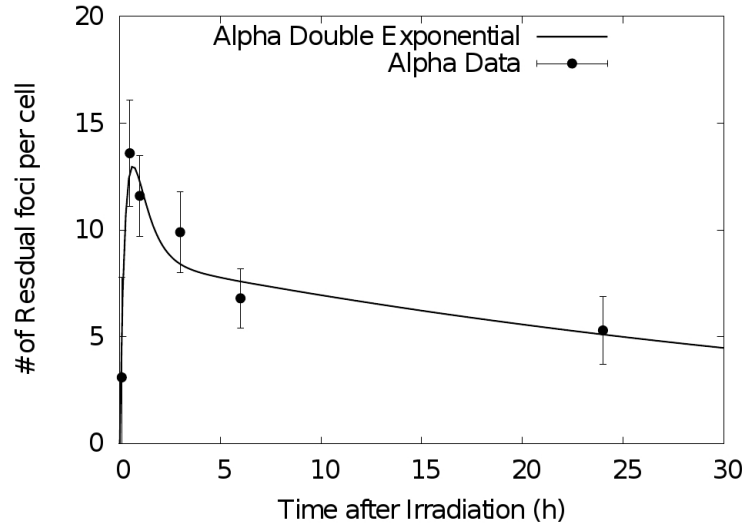


Figure 3.19: Kinetics of the radiation induced foci after 1 Gray of alpha particles (LET=90 keV/ μ m)

The function represented in Fig. 3.19

$$N(t) = 34.67 * \left[\frac{x}{x + 0.345} \right] * [(0.247 * e^{-0.022*t} + (1 - 0.247)e^{-1.446*t}] \quad (3.5)$$

Also in this case, the modeling results show a good agreement between the experimental results and the theoretical model.

The same considerations about the number of parameters vs the number of data points made for low LET are valid also in this case.

The biphasic behavior in this irradiation scenario is much less evident: in this case, after an initial increase, the curve is mostly dominated by slow decay, illustrative of a vast majority of lesions which persist also for a long time (longer and bigger tail). This interpretation of the results, in agreement with what found in the literature, indicated that the repair induced by high LET irradiation is persistent also at a longer time.

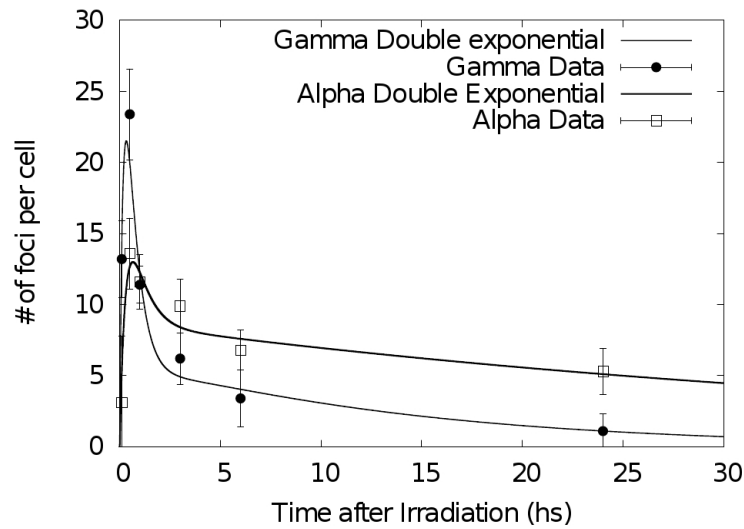


Figure 3.20: Experimental and theoretical results

The modeling results illustrates and quantify the strong difference of the 2 cases both in terms of the residual damage level and in terms of the kinetics. Analyzing in particular the decay kinetics it is possible to obtain an information regarding the different velocity of the repair for the 2 classes of damage, in particular the persistent one. The half-life decay for high LET radiation resulted to be significantly higher than for XRays irradiation (see (3.6) and (3.7)).

$$T_{1/2C}(X - rays) = \ln(2)/0.075hs^{-1} = 9hours \quad (3.6)$$

$$T_{1/2C}(Alpha) = \ln(2)/0.022hs^{-1} = 36hours \quad (3.7)$$

In Figure 3.21 the 2 different behaviors are illustrated, highlighting the residual damage This illustrates also the number of residual damage excepted

at 30 and 5 hours.

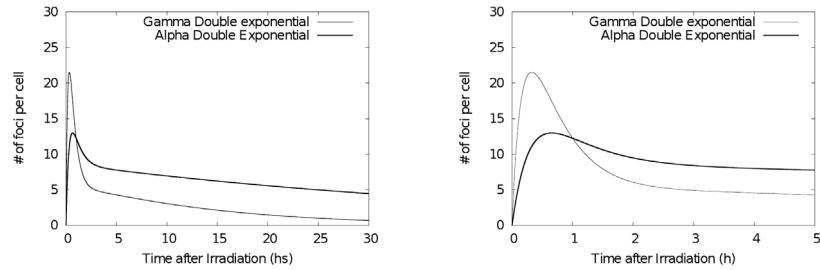


Figure 3.21: Kinetics of the residual damage

The analysis of the residual damage showed the different level reached by the 2 different radiation quality: in particular, the different residual is reached in a totally different timescale. [87] [36]. Recently, it has been suggested [50] that persistent RIF observed days following exposure to ionizing radiation could be nuclear marks of permanent rearrangement of the chromatin architecture. Such chromatin alterations may not always lead to growth arrest as cells have been shown to replicate these in progeny. According to previous finding obtained with PARTRAC [1] the estimated number of complex lesions induced by the alpha particles with that energy was about twice the number respect to the low LET lesions induced. This value seems to be roughly confirmed also in terms of the residual foci at 5 hours, according to the results shown in Fig.3.21 (right panel).

Chapter 4

The irradiated cell as a *perturbed system* in its environment

4.1 Bystander effect

During the last decade, a large number of experimental studies on the so-called “non-targeted effects“, in particular bystander effects, outlined that cellular communication plays a significant role in the pathways leading to radiobiological damage [25] [91] [150]. It is known that two main types of cellular communication (i.e. via gap junctions and/or molecular messengers diffusing in the extra-cellular environment, such as cytokines, NO etc.) play a major role [161] [104] [165] [17] [155] [162] [126] [73]. Therefore it is of utmost importance to better understand the underlying mechanisms of cell signaling, and how such mechanisms can be modulated by ionizing radiation in order to provide insights concerning the bystander effect mechanisms [114] [173] [169] [116] [102]. Although the major goal is to elucidate the *in vivo* scenario, in the meanwhile also *in vitro* studies can provide useful insights.

In recent literature [89] [103] [98], some possible bystander mechanisms have been presented focusing in particular on the process of induction of the bystander response in cells that have received signals from the irradiated ones [11].

The available information is still not sufficient to understand whether the Linear No Threshold approach for low dose risk has to be modified [131] [26]. However these studies suggested the possible need of a paradigm shift in (low-dose) radiobiology, where the DNA-centric vision needs to be integrated by a wider vision where cells constitute an organized population responding to external stimuli in a collective fashion, communicating by means of different molecular signals [109] [124] [133]. Further studies, in particular *in vivo* (or at

least in 3D tissues) and possibly combined with human epidemiological data, will be crucial to help solving such questions in the future.

Cellular communication is widely considered to be a necessary biological function for homeostasis, which is a complex and delicate orchestration of cell growth, cell differentiation and programmed cell death, as well as sequestration of germinal stem cells and pluripotent somatic stem cells [12].

The higher organisms utilize three main forms of cell communication: the *extra-*, *intra-* and *inter-*cellular communication [69]. Extra-cellular signals, in terms of secreted molecules (e.g., hormones, growth factors, cytokines, etc.), move in the extra-cellular space to trigger intra-cellular signals (e.g., Calcium ions, signal transduction enzymes, transcription factors, etc.). In turn, such signals affect not only gene transcription/translation, but also “gap junctional intercellular communication“ (GJIC), that is a different way of communication via ions and small molecules (generally not larger than 2000 Da) diffusing through the gap junctions, which are small channels directly connecting the cytoplasm of adjacent cells [119] [148] [160] [139] [168] [98] [20] [92].

Recently, the various forms of cellular communications started to be considered as fundamental pathways to the so-called “non-targeted effects“ (i.e., effects occurring in cells that were not hit by radiation, such as bystander effect, genomic instability, etc.) of ionizing radiation. [27] [134] [131].

It is now generally accepted that irradiated cells can release molecular signals that travel in the extracellular environment and interact with unirradiated cells, thus triggering in the latter ones a cascade of biochemical events that can finally lead to the formation of different damage types (e.g., DNA and chromosome damage, altered gene expression, cell oncogenic transformation, cell death, etc.) [15]

These phenomena have been observed not only in cell cultures but also *in vivo*. Recently, Mancuso and coworkers [127] observed a bystander-related tumour induction in the cerebellum of radiosensitive Patched-1 heterozygous mice following Xray exposure of the remainder of the body. Furthermore, the authors provided evidence supporting the role of GJIC in the transmission of bystander signals in the Central Nervous System [135].

All together, these findings challenge what is generally called “the central dogma of radiation biology“, according to which the effects of ionizing radiation are a direct consequence of DNA damage occurring in irradiated cells. While the first studies on non-targeted effects were necessarily phenomenological, various recent works provided very useful insights on the possible underlying mechanisms in terms of cellular communication. For instance, a work by Han et al. [89] showed a fundamental role of NO for bystander damage in human fibroblasts, following irradiation with very low doses (of the order of 1 cGy) of alpha particles and subsequent transfer of the conditioned culture medium to unexposed recipient cells.

Though many aspects of the biochemical pathways leading to non-targeted

effects are still not known, thus demanding for a strong need of mechanistic studies, times are now mature enough to develop (mechanistic) theoretical models, first starting from the most “under control“ scenarios (e.g., *in vitro* irradiation of cell monolayers) and then extending the work to more complex situations such as irradiation of 3D tissues and, as a final goal, *in vivo* exposure.

This kind of work demands for a tight and continuous interaction and feedback between modellers and experimentalists. On one hand available experimental data can be used as inputs for model development, whereas on the other hand the model outcomes can help to better interpret the data and can suggest new crucial experiments aimed at elucidating specific issues. Various modelling works dealing with non-targeted effects and their implications were developed in the last years [70].

Concerning the consequences of cellular communication and non-targeted effects in terms of low dose risk, it seems that times are not mature yet to abandon the Linear No Threshold approach recommended by ICRP. Indeed on one side it is a matter of fact that at very low doses/low dose rates the LNT might not hold, also depending on specific conditions such as radiation quality, dose rate, cell type, cell cycle stage, etc.

However, on the other hand it is still not clear whether the supra-linear behaviour observed for certain radiobiological endpoints (typically gene mutations, which are widely considered as initiating events for cancer, and cell neoplastic transformation) does imply that cancer risk is supra-linear, too. Indeed there exist experimental evidences suggesting that non-targeted effects might be protective, implying a sub-linear or even U-shaped risk response at low doses.

Further experimental and theoretical studies, in particular *in vivo* or at least in tissues conserving a 3D architecture, will be crucial to help solving such questions in the future, especially if these studies are combined with human epidemiological data to give rise to a significant impact on radiation protection.

In this framework, it is worthwhile to conclude mentioning a modelling work by *Jacob et al* [106], who analyzed lung cancer mortality in the period 1948/2002 for 6293 male workers of the Mayak Production Association, who were exposed to internal lung doses mainly due to plutonium inhalation. The analysis was carried out by means of the two-stage clonal expansion (TSCE) carcinogenesis model, according to either its original version or a modified version that takes into account possible detrimental and protective bystander effects on the rate of mutations and malignant transformation.

More specifically, bystander effects were assumed to influence a model parameter that is proportional to the product of the effective initiation and malignant conversion rates. Interestingly, the data were found to be incompatible with the model version including a detrimental bystander effect, whereas they were

fitted equally well by the version with a protective bystander effect and that without a bystander effect.

An analogous work on the possible role of genomic instability was carried out on the solid cancer mortality data in the Techa River cohort, which in the 1950s received protracted exposure due to the releases of radioactive materials from the Mayak plutonium complex. The extended cohort includes 29,849 people who resided along the Techa River between 1950 and 1960 [106], and were followed from 1950 to 1999; the analysis performed with the TSCE model showed that about 2.6% of the 1854 solid cancer deaths could be related to radiation. Similarly to the findings on a protective bystander effect for lung cancer mortality among the Mayak workers, it was found that the Techa River data could be described equally well by a model incorporating effects of genomic instability.

4.1.1 Bystander experimental techniques: The irradiated Conditioned Medium (ICM)

A large amount of data on bystander effects has been obtained with the so-called “ICM treatment“ . This technique consists in replacing the culture medium of non-irradiated cells with medium taken from cell cultures previously exposed to radiation.

The main finding of these studies indicated that such treatment can reduce survival of unexposed cells (See also Section 4.3.4). This suggests that, as a result of a radiation insult, certain cell types can release factors in the medium, which therefore becomes potentially cytotoxic [123] [121] [151] [99].

No significant dose-dependence was observed in the range 0.5-10 Gy. A significant increase of cell killing with the number of irradiated cells was observed: medium taken from cultures of 300,000 keratinocytes induced a response close to that of cells directly irradiated with 5 Gy. By transferring the medium at different post-irradiation times, the ICM toxicity was found to increase rapidly in the first few hours post-irradiation [131].

Only a slow increase was observed in the range from 3 to 60 h. The time-response and the fact that an increased number of irradiated cells can lead to an increase in the medium toxicity were interpreted as an indication that irradiated cells can release into the medium a factor able to influence survival of unexposed cells. In a subsequent work the authors hypothesized the secretion of a signalling molecule, rather than a factor toxic per se. Indeed the latter might be expected to provide a linear dose-response rather than a saturation-type effect [134].

Furthermore, on the basis of heating/freezing tests, this signal was supposed to be protein-like: interleukin-8 was considered an “attractive candidate“. This protein, which is involved in inflammatory responses (see Section 4.2), has

also been shown to be involved in a bystander increase of sister chromatid exchanges (SCEs) observed after conventional irradiation of human fibroblasts with very low doses of alpha particles [2] [142].

4.2 Cell Communication: general features

Cells possess complex systems-including receptors, kinases, phosphatases, GTP-binding proteins and several other molecules-that enable them to send or respond to signals to or from other cells. There exist three main forms of cell signalling: paracrine, synaptic and endocrine. Molecules secreted by a cell can be carried far apart to act on distant targets (synaptic and endocrine signalling), or can act locally by affecting the cells in the close environment (paracrine signalling).

By the same mechanisms, cells can send signals to other cells of the same type (autocrine signalling); it follows that they can send signals to themselves also. As can be defined from the currently available *in vitro* experiments, bystander effects are mainly a consequence of paracrine/autocrine signalling. In the literature there are several examples that can help in understanding these effects (for a review see [69]).

Intercellular communication through gap-junctions represents another way to co-ordinate the activities of neighbouring cells. These structures are specialised cell-cell junctions that can form between adjacent plasma membranes: gap-junctions directly connect the cytoplasm of neighbouring cells via narrow channels (around 2 nm in diameter). Intercellular communication via gap-junctions allows the exchange of small molecules (<2000 Da) such as Ca²⁺ and cAMP, but not macromolecules such as proteins and nucleic acids. Also compounds such as eicosanoids and lipid oxidative products can hardly diffuse through gap-junctions, due to the high lipophilicity of these compounds and to the presence of water in gap-junction channels.

A clear general frame emerges from the available data: the different forms of cell signalling triggered by oxidative stress (ionising radiation acts mainly through reactive oxygen species, ROS) are strictly correlated with cell proliferation and cell death. Communication between damaged and undamaged cells has been suggested to lead to a general increase in genomic instability [123] [121] [151] [144] [134].

More specifically, it has been shown that factors secreted by UV-irradiated cells can increase mutation rates in unirradiated cells up to 10-fold over five generations [11] [10]. Similar results have been obtained following irradiation with UVA rays in presence of psoralen, suggesting that the sensitizers may extend this response to long wavelengths. UV-irradiated skin fibroblasts can secrete at least two proteins, identified as interleukin-1 and the basic fibroblast growth factor. Moreover, also interleukin-8 and tumour necrosis factor alpha (TNF- α) have been shown to be secreted together with the already mentioned

eicosanoids as a consequence of inflammation processes.

4.3 Cell Communication perturbation: A systems radiation biology approach

In this section, we start the investigation of the basic mechanisms of the radiation-induced bystander effect by adopting an old cybernetic model into the framework of a systems radiation biology approach to investigate how radiation modulates and perturbs cell-to-cell communication.

Systems biology is characterized by emergent phenomena deriving from the complex interrelationship between the system elements. Typical emergent phenomena, e.g. carcinogenesis, involve intercellular communication and cannot be explained only in terms of the behavior of the basic elements composing the whole system. Intercellular signaling is an example of phenomena where the system behaviors cannot be described or explained as the result of the sum of each signal involved (reductionist vision).

Starting from the previous obtained results, in this work we focused on a single signal (IL-6) but within an integrated approach. In particular, with the aim of widening the investigation spectrum toward a systemic, holistic approach (taking into account the whole signal pathway), a revised Shannon-Weaver model was adopted as a starting modeling framework.

The paradigm shift illustrated before can be regarded as a different point of view in the radiation biology field, based on the response of a cell as a whole and as part of a complex/coordinated/networked system. This way cell behavior after ionising radiation is investigated not only in terms of DNA damage/repair, cell death, chromosome aberrations etc., but as a result of a perturbation in the homeostasis of cells in their tissue/organism environment. This can also be translated into a modification in the equilibrium of cell-to-cell signalling with a different regulation of specific signal molecules, triggered by radiation-induced stress. As a result non-targeted phenomena may occur, like bystander effects.

The way to try to understand the mechanisms underpinning bystander responses in a systems biology fashion ([22], [23], [80], [7], [167], [21], [182], [140], [14]) is the development of new models (both experimental and theoretical), with a strong interaction between experimentalists and modellers to design experiments in order to find the key parameters of the processes and to validate the model hypotheses.

The starting point is a model system with an experimental scenario initially “as controlled as possible” in order to minimize the number of assumptions and free parameters (see Section “Preliminary experiments for signaling investigation”).

4.3. Cell Communication perturbation: A systems radiation biology approach⁷⁹

However, the need to realize simple experiments, in order to have the “control“ of model system, can divert our attention from the real situation of cell communication in an organism. Indeed, the intercellular signalling processes between cells probed with *in vitro* experiments could be very different from intercellular signalling processes in organisms.

Starting from this theoretical framework we modelled interleukin-6 (IL-6) temporal behavior into the medium of normal cells both in the case of “sham irradiated“ and irradiated cells. The investigation of cytokine behavior was considered as a pilot experiment in order to formalize cell-to-cell communication via proteic soluble factors. The mechanisms of cytokine communication were important to establish a strong modelling framework of communication (validated by experimental data) that can be extended also to include other signalling molecules involved in the response of cells to radiation. These measurements were part of a more general strategy based on the following objectives:

- To develop a formalization of cell communication in order to have a different focus on the problem. This formalization (based on the first cybernetics studies applied to telecommunication problems [159]) allowed us to better frame the problem of *in vitro* cell-to-cell communication. It was possible to define typical quantities characterizing communications (e.g. robustness), which turned out to be useful in characterizing the signal transmission in biological systems. The following step, in order to explain the bystander effect mechanisms, was to quantify the role of radiation as a perturbative agent in the already identified mechanisms of signalling. This formalization was useful to model and quantify the mechanisms of single cell signaling (specifically IL-6 release) within a complex system, trying to overcome the cell-centric view towards a more systemic framework. This approach can be generalized towards a systematic investigation of the signaling mechanisms (i.e. perturbation of release and degradation processes induced by radiation) of the molecules possibly involved in bystander phenomena (e.g. IL-8, TNF-Alpha etc). Furthermore, this framework can be used to describe (and possibly quantify) different mechanisms of signal transmission. For instance for molecules like TGF-beta the key process does not reside only in a different rate of emission of the signals, but also in different mechanisms of activation of the signal itself that can occur in the media surrounding the cells, or in the “channel“ in the Shannon Weaver Model framework (see section “Communication model: a general formalization“).
- To develop a modelling approach that is able to reproduce and predict the mechanisms regulating the transmission of the signals and their modulation by radiation. In this model cytokines are formally treated as a

population. The temporal behaviour of this population is described by the standard balance differential equation, a non-homogeneous linear differential equation with variable coefficients .

- To design and carry out experiments to test hypotheses and to quantify the key parameters of the model, both for non-irradiated and irradiated cells (see Section 4.3.4).

4.3.1 Communication model: A general formalization

An approach to reach a comprehensive theory of cellular communication and its modulation by radiation can start from a properly redesigned Shannon-Weaver model [159], where the extracellular communication regulated by the release of soluble factors can be represented as follows.

A source (cell), possibly triggered by a physical or chemical stress, sends a message to one or more reachable destinations (recipient cells). The message must be codified properly by an encoder, transmitted through a channel (i.e. culture medium), and then decodified by the receiver through a proper decoder (see Fig. 4.1).

For the case of cytokine signaling, after the “stress“ triggers the source, the cell machinery starts transcribing the signals- for instance, for IL-6 molecules, molecules, via the activation of the nuclear factor NF-kB [39]-and releasing them in the extracellular environment.

The cytokines diffuse in the medium where they may degrade due to the interaction with free proteases (both specific and generic). If a signal reaches a cell during the diffusion (in the case of autocrine signaling, the receiver is the same emitting cell), it may be captured by specific receptors and possibly transduced (e.g. phosphorylating a protein) and lead to various possible consequences such as signal amplification and/or the induction of damage (bystander effect).

Radiation may perturb any step of the model, modulating the expression and consequently the emission/ release of the elements involved in signaling (e.g. signal molecules, degradation molecules and “receiver“ molecules). It is important to point out that every mechanism implemented in the model probably comes from modulated gene expression and transcription and ultimately from the DNA.

Following Shannon’s approach, there are already two ways that have been developed to model cell communication via soluble factors: one with a stochastic approach investigating the “local“ mechanisms and one with a deterministic approach investigating the time dependence of global quantities [72]. The stochastic approach is based on Monte Carlo simulations of single cytokine histories [70]. A code has been developed to build a properly rescaled geometry

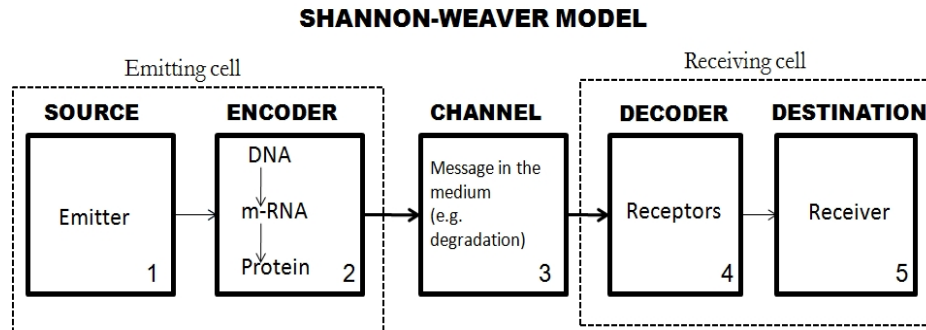


Figure 4.1: Shannon-Weaver model applied to cellular communication *via* proteic signalling

of the *in vitro* experiments (a grid of cells) where each cell releases signaling molecules (cytokines) with a given rate. Signals move in the culture medium according to pure diffusion, and whenever a signal falls below a certain distance from a cell receptor area, it is removed from the medium. For each cytokine removed from the medium, there is a small probability that the cell stops releasing cytokines; this means that the release rate averaged over all cells (“population release rate”) decreases with time.

The deterministic approach is based on differential equations in which cytokines are treated as a population. The temporal behavior of this population can be described by the standard balance differential equation, a non-homogeneous linear differential equation with variable coefficients [22]

4.3.2 Cytokine role in the bystander signalling

Cytokines are soluble polypeptides produced by a wide variety of cell types either constitutively or after induction [12] [136]. They are of outmost importance for signalling between cells and tissues and there is increasing evidence that they constitute a humoral component of the response of cells and tissues to radiation exposure [135]. In the context of radiotherapy, many studies have demonstrated the importance of such molecules in the genesis and perpetuation of radiation induced complications, in particular lung fibrosis, oral mucositis, intestine damage, brain injury [111]. More recently, radiobiology studies at low doses have demonstrated that the effects observable in cells that are in the vicinity of irradiated cells (bystander cells) are also due to the early release of several extracellular mediators, among which cytokines are likely to play a key role [164] [2].

These evidences have moved the radiobiologist’s attention toward the study of

cytokine release and/or its modulation after ionising radiation exposure with a dramatic increase in studies directed toward the analysis of these molecules in the medium of irradiated cells, aiming to understand the mechanisms responsible of the effects observed in bystander cells (bystander effects) [117] [33] [72]. In this section, we investigated mainly Interleukin-8 (IL-8) and Interleukin-6 (IL-6), two of the candidate bystander signals identified up to now [111] [160] [32] [149] [113], in the medium of normal and tumoural cells.

Before starting any possible quantification and modeling of cell signaling via cytokine, we define some experiments to answer some of the questions underlying all the signalling mechanisms:

- Is there a linear response after the stimulus?
- Are there any feedback mechanism underlying the cell response?
- Are there any local mechanisms regulating the release of the signals?
- How do the experimental conditions affect the signal release?

To answer these question we designed and performed several series of preliminary experiments to evaluate the cell response in the *standard condition*, without the perturbation of radiation. The aim was to evaluate the influence that different experimental conditions have on the presence/release of these molecules in the medium, and also with the purpose of obtaining quantitative and qualitative information to be included in mathematical models of cytokine release.

The effects of irradiation on the cytokine release over the time were evaluated after different doses of gamma rays. Due to the large uncertainties affecting the knowledge of the basic mechanisms governing cytokine release, only a few theoretical models were developed until now [70].

4.3.3 Preliminary experiments for signaling investigation

Within the experimental framework of the irradiated conditioned medium, our work was aimed to understand the modulation in cell communication induced by radiation. In particular the idea was to clarify the experimental conditions that might influence the release of cytokines in the culture medium and give some basic input for building a model for cytokine (e.g., Interleukin-6, IL-6) regulation in the case of ‘asham irradiation’ and after ionising radiation exposure.

As a preliminary study, the influence of cell type, cell density, medium volume, medium storage temperature and other methodological aspects on IL-6 and Interleukin-8 (IL-8) release were investigated. In addition, the effects over the time of different doses of gamma irradiation on the clonogenic survival of

4.3. Cell Communication perturbation: A systems radiation biology approach⁸³

bystander cells and on the secretion of these cytokines were studied.

Materials and methods

Cell line Primary human AG01522 fibroblasts at low passage were kindly donated by Italian National Institute of Health (Rome, Italy). These cells were routinely maintained at low passage number in α -modified Eagles minimal essential medium containing ribonucleosides (aMEM) (GIBCO, Invitrogen Ltd, Paisley, UK) supplemented with 18% foetal bovine serum and 100 units/ml penicillin/streptomycin at 37 Celsius degrees in an atmosphere of 5% CO₂.

Human glioblastoma T98G cells were purchased from the European Collection of Cell Cultures (Porton Down, Salisbury, UK) and cultured in Royal Park Memorial Institute (RPMI) medium supplemented with 10% foetal bovine serum, 100 units/ml penicillin/streptomycin, 2 mM L-glutamine and 0.01% Sodium pyruvate at 37°C in an atmosphere of 5% CO₂.

Stock cultures were maintained in exponential growth as monolayer in 75-cm² Corning plastic tissue-culture flasks. If not specified, all chemicals and plastics were purchased from Sigma-Aldrich (St Louis, MO, USA).

Medium collection Cells were trypsinized from totally confluent cultures and seeded on Corning plastics at the specified densities 20-22 h before medium collection and counted the day of assay to confirm actual cell numbers. The seeding medium was completely replaced with fixed volumes of freshly made complete medium before collection started.

The time of medium replacing was considered as time 0 for all our experiments. In the case of experiments with irradiation, medium was changed before irradiation. This experimental protocol for medium conditioning was kept identical for both clonogenic survival and ELISA measurements. Medium was collected, filtered with 0.22 mm pores Polytetrafluoroethylene (PTFE) filters and samples were kept at -20 degrees until the Enzyme Linked Immunosorbent Assay (ELISA) if not differently specified. For each measurement at least two dedicated flasks were prepared. When high concentrations of cytokines were expected (high cell densities or low medium volumes), medium samples were diluted 1:2 and 1:3 with fresh medium.

Preliminary screening of the cytokine Small ELISA tests using few points from a sample have allowed us to study qualitatively the presence of a certain cytokine in the cellular system. In general, these experiments were realized using two points from the same culture, one at short and the other at long times. From the intensity of the color of each well, it was possible to estimate where a certain molecule is situated and where there was no relevant expression.

At this preliminary stage, also the presence of cytokine in the cellular nucleus and cytoplasm was investigated, after a proper nuclear extraction procedure (See Section 4.4. for details)

All the results are summarized in the following table:

	Medium	Cytoplasm	Nucleus
IL-6	High expression, in particular at long times (see the following Section)		
IL-8	Low expression at very short time, equal expression at longer time (see the following Section)	Much higher concentration than the medium	Higher concentration than the cytoplasm
IL-1 β	No expression at short and long times	Clear expression, higher concentration at long times	Clear expression, higher concentration at long times
TNF α	Absent in the medium	Weak expression, constant in time	Weak expression, constant in time

Since the amount of nuclear material available from a nuclear extraction process was very small, some tests were not done in that compartment. Although taken from the analysis of few points, these results constitute a good estimation of the cytokines present in our cellular system. These results can be useful for a preliminary screening of the cytokine released by this cell line. It is clear from the analysis of the media collected from the flasks that, in this experimental scenario, IL-6 and IL-8 represent 2 possible candidates for the bystander signaling mechanisms.

Influence of storage temperature. Filtered supernatants were stored at 37 Celsius degrees for 1, 3, 5, 7 and 20 h and IL-6 levels were subsequently measured by ELISA; three independent measurements were performed.

Influence of aggregates removal modalities To evaluate the influence of aggregates and particles removing modalities on IL-6 concentration, culture medium samples were collected and filtered through 0.22 mm-PTFE filters or 0.22 mm-surfactant-free cellulose acetate (SFCA) filters or spinning at 125 g for 10 min prior to ELISA quantification.

As illustrated by bar graphs in Figure 4.3, these modalities had no significant influences on the IL-6 quantified by ELISA.

4.3. Cell Communication perturbation: A systems radiation biology approach⁸⁵

To evaluate the stability of the samples, aliquots of supernatants were stored at -20 Celsius degrees and the IL-6 levels determined by ELISA after 1, 2, 4, 5 and 10 freeze-thaw cycles. For each cycle, samples were thawed slowly at room temperature, left to stand for one hour, and then returned to -20 Celsius degrees.

Influence of cell number. Three different densities of AG01522 cells were plated in 25 cm^2 flasks and the amount of medium tailored to maintain constant the *ratio number of cells/ volume of medium* at 9600 cells/ml. In detail, 375,000 cells were incubated with 39 ml of medium, 250,000 cells with 26 ml and 125,000 with 13 ml. For each time investigated the medium from two flasks was tested.

Influence of medium volume. A total of 125,000 cells were plated in 25 cm^2 flasks to which different volumes of medium were added: 6.5 ml, 13 ml and 26 ml to obtain as ratio *number of cells/ volume of medium* 19,200 cells/ml, 9600 cells/ml and 4800 cells/ml respectively. For each time investigated the medium from two flasks was tested.

Influence of cell density. The same amount of medium (13 ml) was used to incubate 125,000 cells, 250,000 cells and 375,000 cells. Consequently, the ratio *number of cells/ volume of medium* was 9600 cells/ ml, 19200 cells/ml and 28,800 cells/ml, respectively. For each time investigated the medium from two flasks was tested.

Irradiation Exponentially growing human fibroblasts (AG01522) and glioblastoma cells (T98G) were irradiated with Cobalt-60 gamma rays (dose rate 0.83 Gy/min, Policlinico San Matteo, Pavia, Italy). A 5-mm thick plastic sheet was placed below the flask surface to allow dose build-up. Flasks containing cells were carried in an incubator-like container preserving a constant temperature of 37 degrees. Irradiations were performed at room temperature.

Clonogenic assay In T25 flasks, 200000 cells were plated 20 h before irradiation. To reproduce the same experimental conditions of the ELISA measurements, the medium was changed before gamma irradiation. After irradiation the flasks were placed in the incubator for 5 or 20 h. Afterwards the medium was collected, filtered and placed in T25 flasks where 150 non-irradiated parental cells were seeded 12 h before. One week later the medium was replaced with fresh medium and after another week the resulting colonies

were fixed and stained with gentian violet to determine colony forming ability. Colonies with more than 50 cells were scored as survivors. The mean colony counts were multiplied for the plating efficiency of the sham irradiated colony count from the same experiment.

Enzyme Linked Immunosorbent Assay IL-6, IL-8, TNF- α and IL-1 β concentrations in cell culture supernatants were determined with solid phase sandwich ELISA by means of immunoassay kits (Diaclone, Besançon Cedex, France) and the protein levels were calibrated on a microplate reader (DV990win6, GDV, Rome, Italy) at 450 nm wave length. For IL-6 the sensitivity was 2.0 pg/ml, whereas for IL-8, TNF- α and IL-1 β it was 525 pg/ml. All standards, controls and samples were run in duplicate. The assays were performed as described by the manufacturer. The concentration of the cytokine was determined with a dedicated software (DV990win6, GDV, Rome, Italy) plotting the absorbance of the standards against the standard concentration to derive the unknown sample concentrations. Comparisons between groups were made by the Student's t-test. A p value of 0.05 was considered significant.

Clonogenic survival

To prove that our studies were done under conditions that induce bystander effects, we evaluated the clonogenic survival of parental nonirradiated cells incubated with medium collected and filtered from cells irradiated with 0.25 or 0.5 Gy of γ rays.

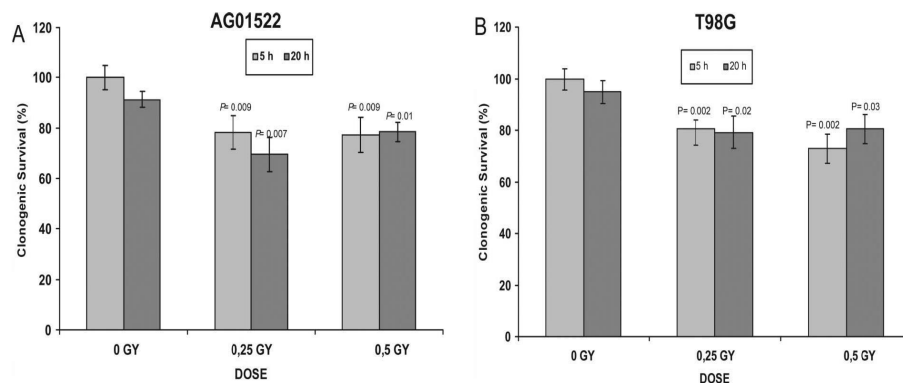


Figure 4.2: Clonogenic survival in AG01522 (A) and T98G (B) unirradiated cells after transferring medium from parental cells exposed to different doses of gamma rays. Data are represented as mean of three independent experiments and error bars indicate the standard error of the mean (SEM).

4.3. Cell Communication perturbation: A systems radiation biology approach⁸⁷

Our results demonstrate that medium collected 5 or 20 h after gamma exposure of T98G or AG01522 cells was able to reduce clonogenic survival [108] of bystander parental cells (Figure 4.2).

The proportion of clonogenic inactivation was rather constant in these two cell lines, at about 20% for medium conditioned for either 5 hours or 20 h after irradiation. We also tested that medium irradiated in the absence of cells, either complete medium either medium without serum, had no effect on clonogenic survival when transferred to unirradiated cells (results not shown).

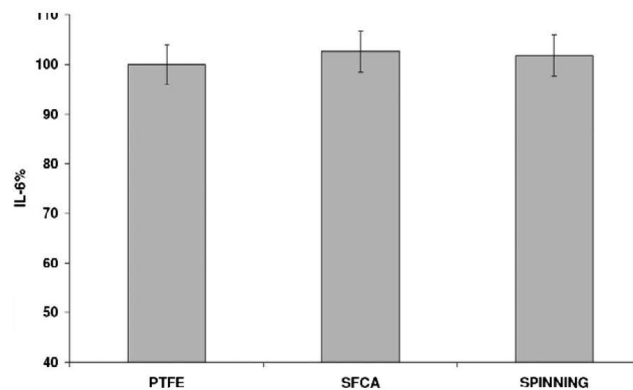


Figure 4.3: Comparison of three different modalities of aggregate removal commonly used in bystander effect studies: Polyetrafluoroethylene (Teflon, PTFE) filters, surfactant-free cellulose acetate (SFCA) filters and 1000 rpm spinning. 100% IL-6 refers to the concentration of IL-6 measured after filtration with PTFE. Medium was incubated with 5000 cells/cm² for 5 hours prior collection. Data represent the mean of duplicate measurements of one experiment. Error bars represent intra-assay errors.

Storage stability

To examine whether IL-6 released by AG01522 cells is degraded by proteases present in the conditioned medium, cytokine concentrations were measured in supernatants collected, filtered and maintained either in incubator at 37 and 4 Celsius degrees for 1 h, 3 h, 5 h, 7 h and 20 h in comparison with supernatants processed immediately after collection (time 0) for ELISA measurements.

Figure 4.4 illustrates the percentage of recovery compared to time 0 of the samples kept at 37 Celsius degrees (mean of three independent experiments) and 4 Celsius degrees. These results indicate that IL-6 released in the medium by human fibroblasts was not degraded during the time interval investigated. These values are also comparable with the ones measured with the samples kept at -20 Celsius degrees (data not shown).

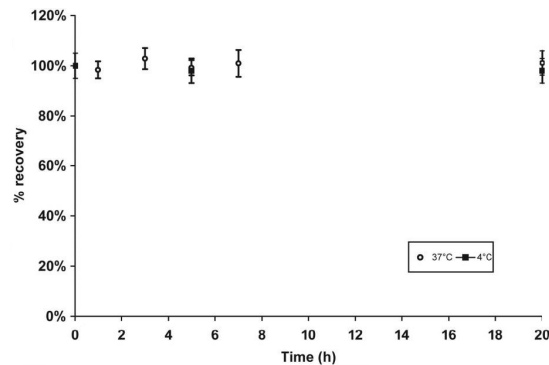


Figure 4.4: Percentage of IL-6 measured in medium samples considering 100% the amount of IL-6 measured at time zero. Medium was collected after 5 hours of incubation with human fibroblasts (AG01522), filtered and maintained either in incubator at 37 Celsius degrees or in refrigerator at 4 Celsius degrees. Data represent the mean of three independent measurements. Error bars represent the standard error of the mean (SEM).

Freeze-thaw stability

To determine whether IL-6 was stable to repeated freezing and thawing, we used AG01522 conditioned medium samples. Their IL-6 concentrations were determined by ELISA after 1, 2, 4, 5 and 10 freeze-thaw cycles compared to samples that had not been thawed prior to assay. Our results proved that IL-6 is stable to repeated freezing and thawing, since variations as small as 4% were observed (data not shown).

Influence of seeding parameters

In order to evaluate whether the number of cells has any influence on the release kinetics of IL-6 (and to evaluate the possible presence of non-local and non-linear mechanism in the signal release), 3 different amounts of AG01522 cells were plated in 25 cm^2 flasks whereas the amount of medium was tailored to maintain constant the ratio *number of cells/ volume of medium* at 9600 cells/ml. We observed that the number of cells does not affect the amount of IL-6 released in the medium when the amount of medium per cell is maintained constant.

In a second series of experiments, the number of cells was kept constant (5000 cells/ cm^2) whereas the amount of volume was doubled (19,200 cells/ml)

4.3. Cell Communication perturbation: A systems radiation biology approach⁸⁹

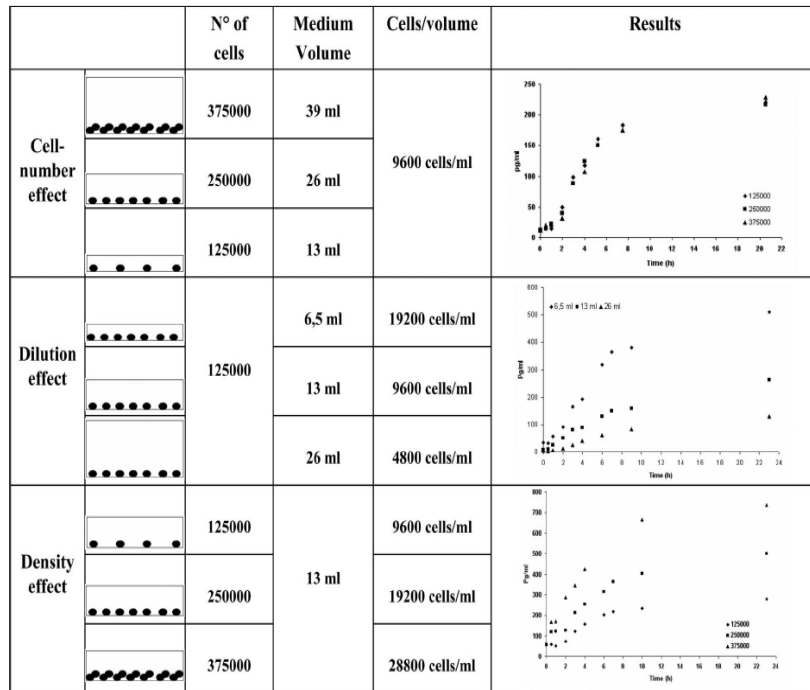


Figure 4.5: Summary of the experimental conditions tested for IL-6 release by human fibroblasts (AG01522) in the medium and the respective IL-6 concentrations measured.

or halved (4800 cells/ml) compared to our standard conditions (9600 cells/ml). In these conditions, the concentration of IL-6 resulted to be halved and doubled respectively suggesting that each cell releases the same amount of cytokines whatever is the amount of the medium.

In the third group of experiments the same amount of medium (13 ml) was kept to incubate 125,000 cells, 250,000 cells and 375,000 cells. Consequently, the ratio *number of cells/ volume of medium* was 9600 cells/ml, 19,200 cells/ml and 28,800 cells/ml, respectively. Figure 4.5 summaries these experiments with the respective ELISA measurements, whereas Figure 4.9 illustrates the mean quantity of IL-6, expressed as pg/cell, which was released by each fibroblast in the experiments of Figure 4.5

Furthermore, the release rate induced per cell by the fibroblasts was evaluate for sparse or confluent cell culture, with the results represented in the Figure 4.6. A small difference in release occurs after 20 hours form the change of the medium

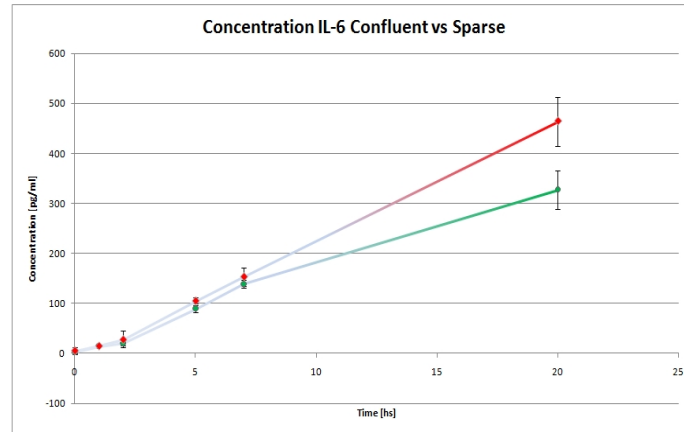


Figure 4.6: Concentration of IL-6 cytokine in the medium of confluent (red dots) vs sparse (green dots) cells. The data are normalized per the total amount of cells. In case of confluent cells (Gap Junctions open), the AG1522 fibroblasts seem to release an (slight) higher amount of cytokine

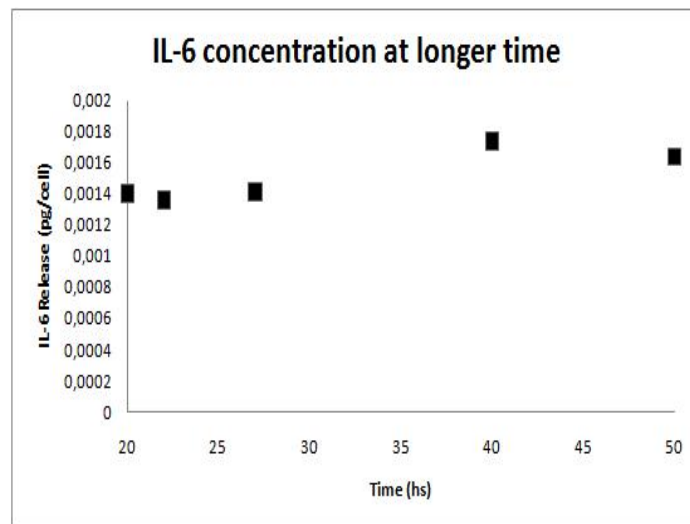


Figure 4.7: Concentration of IL-6 cytokine in the medium of cells for timing up to 50 hours. The data are normalized per the total amount of cells. The plateau level reached by IL-6 concentration at 20 hours was maintained up to 50 hours

4.3. Cell Communication perturbation: A systems radiation biology approach⁹¹

From the summary shown in Figure 4.5 the cytokine concentration reaches a maximum value (*plateau*) after 20 hours from the change of the medium. To test the stability of the plateau experiments were quantified the cytokine accumulation in the medium (normalized by the total number of cells) up to 50 hours. No strong difference was found during this time interval (Fig. 4.7).

Effects of cell type (fibroblasts versus glioblastoma cells)

In order to evaluate if the medium volume does have any influence on the release of IL-6 also in tumor cells, we repeated the *dilution effect* experiment with T98G glioblastoma cells which are characterized by a high and heterogeneous cytokine profile.

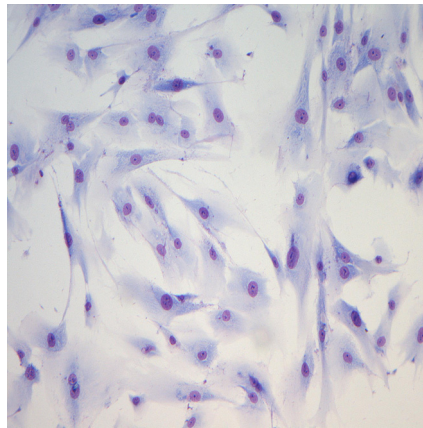


Figure 4.8: FibroblastAG1522

In Figure 4.10a it is clear that even in T98G cells the quantity of IL-6 released by a single cell is independent of the amount of medium culture. To conclude the methodological study, the quantity of IL-8 released by single T98G cells cultured was quantified with three different amounts of medium (Figure 4.10b). The cytokine was detectable in the medium at least 4 h after the change of the medium (time 0) and subsequently its concentration raised linearly over the entire time interval considered (up to 24 h). The dependence of IL-8 release on the quantity of medium, (i.e., more is the dilution more cytokines are released by the cells), is clearly shown in Figure 4.10b, where the quantities of cytokine released per cell over 24 h are graphically represented. Also for HL60 a small preliminary study has been conducted, revealing a modulated expression of IL-8 (Fig. 4.11). No modulation for IL-6 occurred.

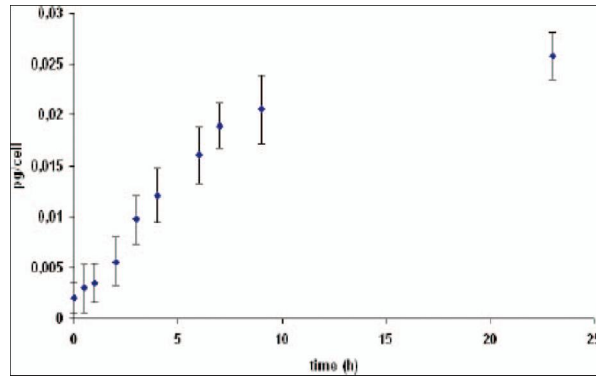


Figure 4.9: Quantity (Pg) of IL-6 released per cell by human fibroblasts AG01522 in the different cell culture conditions summarized in Figure 3. Data are represented as mean of nine independent experiments and error bars indicate the standard error of the mean (SEM).

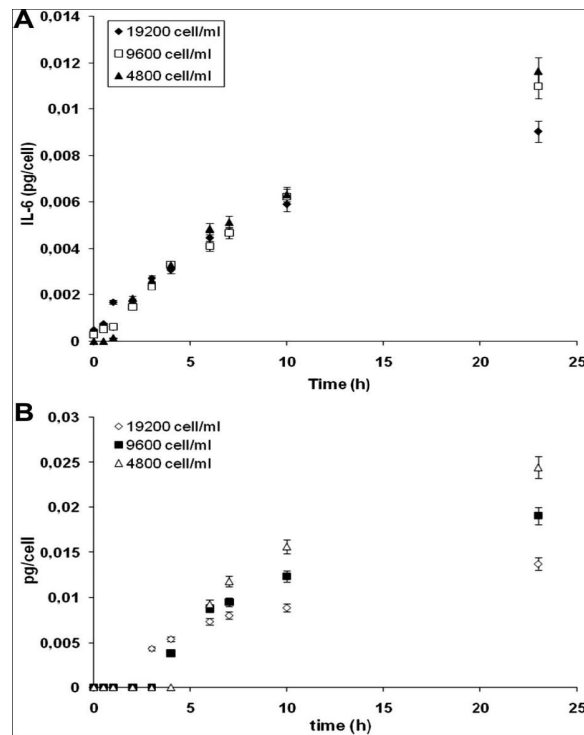


Figure 4.10: Human glioblastoma T98G cell. (A) Quantity of IL-6 released by single cell in the presence of different amounts of medium. (B) Quantity of IL-8 released by single cell in the presence of different amounts of medium. Data are represented as mean of three measurements and error bars indicate the standard error of the mean (SEM).

H]

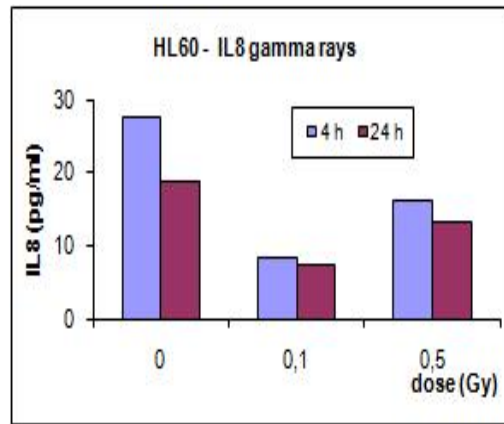


Figure 4.11: HL60 cells. Preliminary quantification of IL-8 cytokine in the medium of HL60 cells. IL-6 was not present (results not shown).

Effects of irradiation

IL-6 concentrations in the medium of irradiated cells were measured by ELISA over 20 h after exposure to 0.1, 0.25, 0.5 and 1 Gy gamma rays in comparison with control conditions (sham irradiation, 0 Gy). In Figure 4.12, the concentrations are represented as a function of time, where time 0 corresponds to irradiation and the medium was changed 2 h before.

Fibroblasts exposed to 0.25 Gy released the highest quantity of IL-6, whereas exposure to 1 Gy and 0.5 Gy seemed to reduce the production of this cytokine. The most interesting results were observed 20 h after irradiation, when the difference between sham and 0.25 Gy is statistically significant ($p=0.043$) as highlighted in the small panel of the Figure. In parallel, the same measurements were performed seeding a doubled density of cells (10,000 cells/cm²) with the same volume of medium: also in these conditions an exposure to 0.25 Gy determined an increase of IL-6 in the medium culture, especially for the longest time considered (20 h) (data not shown).

As a comparison with IL-6, the concentrations of IL-8 were evaluated in the same medium samples collected during the above experiments. As illustrated in Figure 4.13, IL-8 showed a different dose and time dependence, compared to IL-6. Indeed the exposure determined an increase of the cytokine release which reached the maximum at 5 and 8 h after irradiation, whereas after 20 h no differences were observed for all the doses tested.

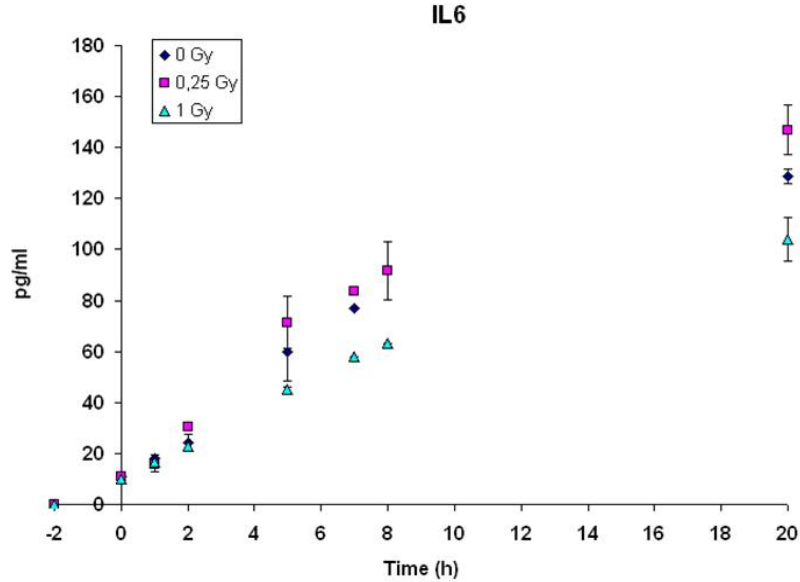


Figure 4.12: Concentration (pg/ml) of IL-6 in the medium of gamma irradiated fibroblasts (10,000 cells/cm²). Medium was changed 2 hours before irradiation (time 0). Data are represented as mean of three independent measurements.

4.3.4 How do the experimental condition affect the cytokine release?

In summary, the significant reduction in clonogenic survival of AG01522 and T98G cells observed after medium transfer suggests that within 20 h after irradiation these cells secrete factors into the culture medium that are capable of affecting the reproductivity ability of unirradiated parental cells. Results similar to these were collected also with other cell lines [149] determining an increase of studies performed with medium transfer technique.

This technique necessarily involves the removal of aggregates from the collected medium prior transferring, mainly by filtration through sterile systems. In a recent paper by the chemist Newman [44], the author warns the radiobiologists on the possibility that filters may bind protein aqueous factors, affecting their bystander studies. In our study we observed no differences in IL-6 quantification by ELISA comparing two different sterile filters (PTFE and SFCA) and spinning. However, if not tested before, PTFE filters should be recommended as a filtration modality for medium transfer technique in bystander effect studies. In particular, we addressed to the analysis of IL-6 and IL-8 release in the medium: first without perturbing agents (i.e., exposure to ionising radiation) but modifying cell density or medium volume, or ratio *ratio number of cells/volume of medium* or cell type. Since it is known that the cellular response to

4.3. Cell Communication perturbation: A systems radiation biology approach⁹⁵

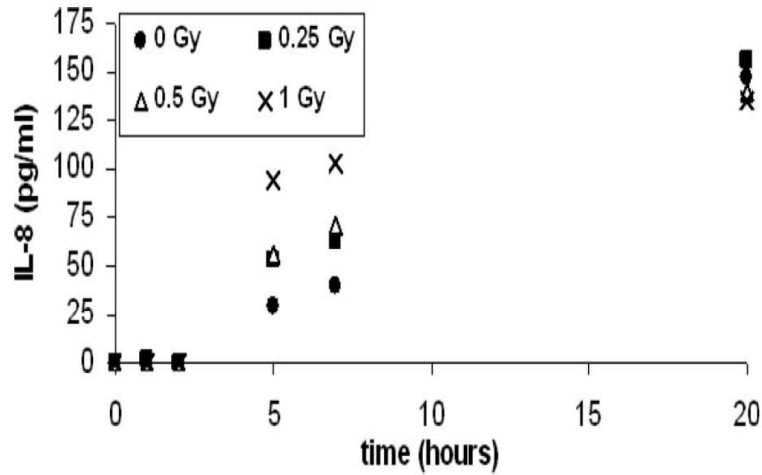


Figure 4.13: Concentration (pg/ml) of IL-8 in the medium of gamma irradiated fibroblasts (10,000 cells/cm²). Medium was changed 2 hours before irradiation (time 0). Data are represented as mean of three independent measurements.

any stimulus is influenced by the differentiation status, the configuration and the distribution of cytokine receptors and the current status of cell signalling (see last Section of this Chapter for further details), we kept these variables constant by using cells in the exponential growth phase exclusively, obtained from totally confluent flasks. Moreover all sets of measurements started at the point of medium change (i.e., with the same environmental conditions).

Analysing the release of IL-6 and IL-8 in the medium over 22 h, we observed that both the cytokines studied had a sort of response to the stimulus *change of the medium* since when new complete medium (not containing IL-6 nor IL-8) was placed in the flasks, the curve describing the concentration had an immediate (for IL-6) or delayed (for IL-8) steep slope which slowly bend after 7-8 h and maintain the plateau level up to 50 hours.

The achievement of a plateau level of these cytokines 8 hours after the change of the medium might be explained by several mechanisms. Indeed, to prevent overstimulation, a complex network of regulatory mechanisms to modulate cytokine-mediated signals exists. Besides the protein internalisation by membrane receptors, one of the ways to regulate the availability of cytokines is proteolysis mediated by enzymes whose release might be induced by the cytokine itself .

We evaluated whether the medium collected after incubation with human fibroblasts contains soluble substances, likely free proteases, released by the cells themselves that degraded IL-6 independently by the presence of the cells. These data would be practically important for two reasons. First of all, the

presence of proteases activity would stress the importance of sample storage before cytokine quantification to avoid cytokine loss, particularly in experiments where alterations in concentration of few percentages are under study. In addition, these data might be translated as parameters for modelling of cytokine release kinetics since whenever we are modelling anything mathematically we would be wise to remember that a mathematical model is only as good as the assumptions on which it is based.

Subsequently, we moved our attention to the modulation of IL-6 and IL-8 release after exposure to relatively low doses (0.25, 0.5 and 1 Gy) of gamma rays where we observed that these two cytokines are differently modulated by radiation. In particular, in our conditions, the release of IL-6 was significantly increased by gamma radiation at long time intervals (i.e., 20 h) after 0.25 Gy exposure, whereas 0.5 Gy and 1 Gy did not cause significant alterations in the release of this cytokine. On the other hand, the release of IL-8 after gamma exposure showed differences compared to control as soon as the concentration was detectable by the assay (i.e., 5 h after irradiation) and persisted for few hours.

Besides the differences on the timing of effect appearance, IL-8 had also a different dose-effect relationship with the highest effect observed at 1 Gy exposure.

4.3.5 How does the cytokine release affect the cell behavior?

Although such alterations in IL-8 and IL-6 concentrations do not appear to be dramatic compared to control levels, the relatively small but abrupt modulation of cytokines in culture medium can have functional consequences on bystander cells (See Fig 4.14). In a first set of experiments, we evaluated whether the changes in IL8 release observed 5 h after exposure were able to affect the proliferation capacity of AG1522 cells and consequently might be related to the decrease in clonogenic activity we observed in bystander cell cultured with conditioned medium (Figure 4.2) We cultured fibroblasts with the amounts of IL-8 measured 5 h after 1 Gy and 0 Gy exposure and we evaluated their proliferation activity.

Preliminary results (Fig. 4.14) showed a significant decrease in the proliferation activity of the cells cultured with the amount of IL-8 measured after 1Gy exposure concentration compared to the 0 Gy levels. The fact that even small differences in IL-8 concentrations in the culture medium are able to affect the proliferation activity might indicate that this cytokine is involved in the observed decrease in clonogenic survival of recipient (bystander) cells although more studies are needed to investigate the underlying mechanisms.

In addition, our results suggest that gamma irradiation affects the production of both IL-6 and IL-8, also influencing the post-transcriptional mechanisms (for instance via active Transforming growth factor β internalization). These

4.3. Cell Communication perturbation: A systems radiation biology approach 97

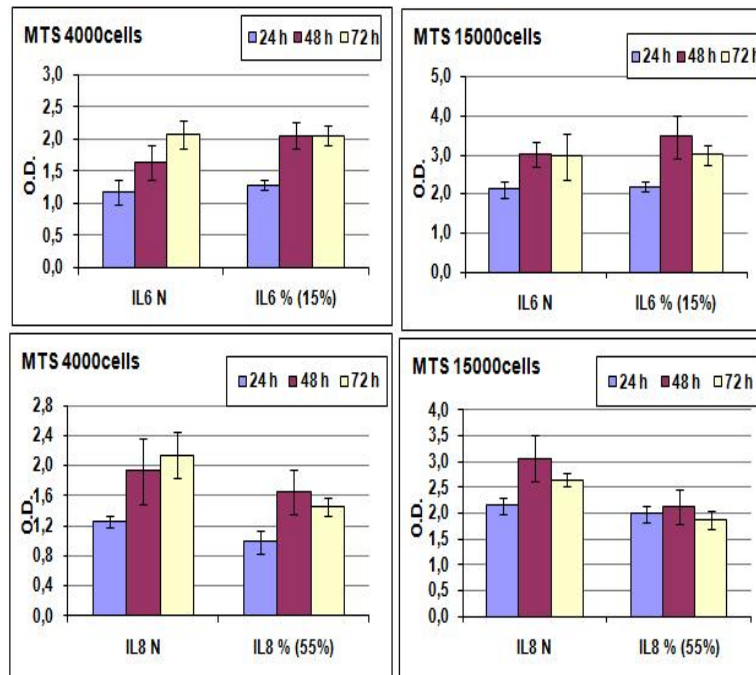


Figure 4.14: Proliferation activity of the fibroblasts cultured with a media in which a certain amount of cytokine (IL-6 and IL-8) has been added, in order to obtain a functional analysis of the signal investigated. The amount of IL-6 does not seem to influence the cell activity (in terms of cells proliferation) while IL-8 decreases the proliferation of the cells at long time (48 and 72 hours)

mechanisms may include the cytokine itself, acting in a negative feedback autocrine loop or, alternatively, paracrine inhibitory factors, among which are other cytokines triggered by or derived from the cytokine process itself. Also activation/degradation of the signals should be taken in consideration. For example, latency appears to be a critical step in the control of TGF- β activity, as enhanced TGF- β expression does not always correlate with increased levels of active TGF- β and the presence or absence (i.e., without serum supplement) of this growth factor in the culture media might dramatically affect the type and timing of signals released.

In parallel with the cytokine negative feedback control, there is usually a down-regulation of the corresponding receptors (see last Section of this Chapter).

4.3.6 Theoretical analysis (I): the stochastic approach

To investigate the bystander effect mechanisms, we first developed a Monte Carlo code specifically aimed to the reproduction of bystander effects observed *in vitro* after microbeam irradiation of a few cells selected over a population of sparsely seeded cells [70].

More recently, we focused on the mechanisms of signal release (from both irradiated cell cultures and unexposed cultures), motion and depletion/degradation, where the term “depletion“ refers to internalization by specific cell membrane receptors, whereas degradation refers to the interaction with enzymes (e.g., proteases) that disrupt the molecular signals themselves.

The Monte Carlo code was developed reproducing the geometry of *in vitro* experiments, and simulating the processes of signal release, diffusion and depletion/degradation in a 3D environment (see Fig. 4.15); the code was applied to the specific case where the signals are cytokines and the cells are human fibroblasts, and the simulation outcomes were compared with ad hoc experiments carried out in our research group. This approach deals with local mechanisms

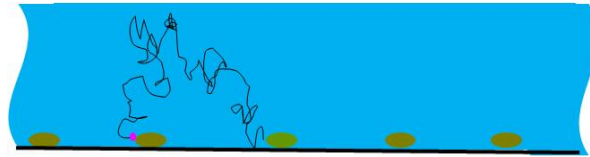


Figure 4.15: Scheme of the diffusion process reproduced in the Monte Carlo code

concerning single cells, since the history of each single cytokine is followed. Main objective of the model is to quantify the cytokine release rate and the mechanisms regulating the signal transmission (such as depletion and degradation) for both unexposed and exposed cell cultures, with focus on low doses. Each single fibroblast was represented as a “box“ of dimensions $80 \times 20 \times 10 \mu m^3$. A 2D matrix was built with 1 mm side, characterized by a homogeneous distribution of 121 fibroblasts (11 per side), to reproduce an experimental surface density of $10,000 \text{ cells}/cm^2$ (see Fig. 4.16). This cell matrix was located at the bottom of a container of 5 mm height, that is the real height of the culture medium in the flask used in the experiments. To simulate cytokine release, it was assumed that each cell is able to release a certain number of cytokines, left as a free parameter. The starting position of each cytokine was randomly selected from the surface of one of the sides of the box representing the cell (excluding the box base, which is attached to the dish). After release, each molecule was transported step-by-step using a free diffusion model (Brownian

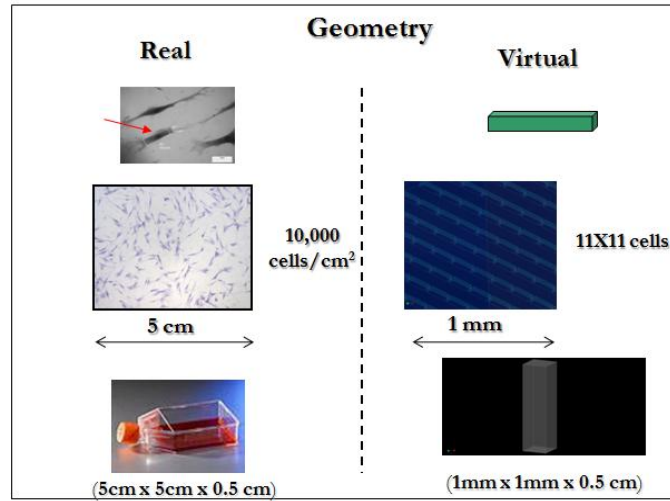


Figure 4.16: Simulated geometry adopted in the Monte Carlo simulation

motion) with a mean square displacement of

$$\langle r^2 \rangle = 6Dt \quad (4.1)$$

where D is the diffusion coefficient and t is the time. The free diffusion model represents the “static” limit, where the flask containing the cells is kept still. A diffusion coefficient of $10^8 \text{ nm}^2/\text{s}$ and a time step of 0.1 s were adopted, corresponding to a random-walk length of $7.7 \mu\text{m}$. When a cytokine hits the walls of the cell container, it is assumed to undergo specular reflexion. This way the simulation can be considered as representative of a randomly-chosen section of the experimental environment, which is much larger ($5 \times 5 \text{ cm}^2$). On average, for each molecule “leaving” the simulation volume, another one will “enter” it. The code also simulates the presence of specific cytokine receptors on the cell surface. When a cytokine “reaches” a cell, if the cytokine is located in the vicinity of a receptor, that cytokine is considered as internalized, and it is “removed” from the simulation. More specifically, we assumed that each cytokine in the vicinity of a cell has a probability P to be internalized via a membrane receptor. A value $P = 0.01$ was chosen, consistent with the fact that cytokine-specific receptors cover about 1% of the cell surface. Furthermore, each cytokine internalization was assumed to have a probability P to make the cell stop releasing cytokines, to take into account a feedback mechanism. The number of cytokines present in the simulated culture medium was sampled every second from time 0 to 72,000 s, that is 20 h. An example of simulation outcome is reported in Fig. 4.17, where experimental data on IL-6 are also reported for comparison.

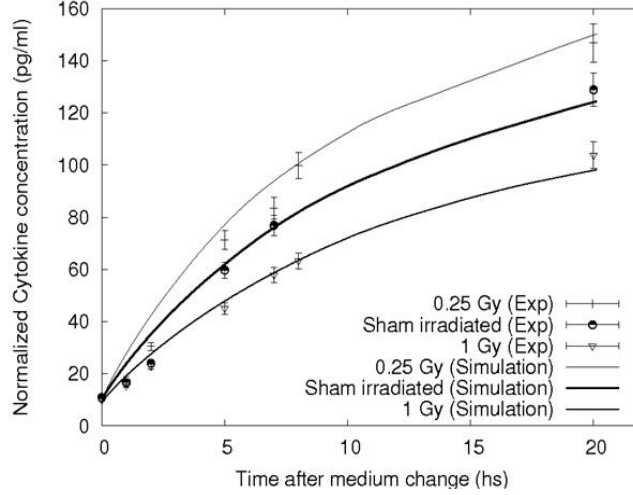


Figure 4.17: Comparison between simulation results and experimental data on 250,000 fibroblasts in the case of sham irradiation and g dose of 0.25 Gy and 1 Gy.

4.3.7 Theoretical analysis (II): the analytical approach

The general aim of this approach was to evaluate how radiation modulates cell response and, more specifically, the emission of signal molecules [128]. In the mathematical framework used here, this means that the functional forms of the signal release rate must be evaluated for both non-irradiated cells and cells irradiated with low doses of γ rays.

As a pilot study to test our method, we described the features of one of the possible signal molecules (IL-6) involved in cell communication. In this case, the “state“ of the system can be described by a differential equation (standard balance equation):

$$\frac{dQ(t)}{dt} = k_1(t) - k_2(t)Q(t) \quad (4.2)$$

where $Q(t)$ is the concentration of IL-6 molecule in the medium, $k_1(t)$ is the “net release rate“ function (i.e., the release rate of the whole population implicitly taking into account the effects of the local interaction mechanisms, such as autocrine signaling), and $k_2(t)$ represents the time-dependent “decay rate“ of the cytokine, which results from the interaction between the cytokine and the protease enzymes present in the medium. Therefore, $k_2(t)Q(t)$ represents the rate of reduction of the concentration in the medium. The net release rate $k_1(t)$ can be assumed as the product between the net cytokine release rate per cell $k_3(t)$ and the total number of cells $N(t)$:

$$k_1(t) = k_3(t)N(t) = k_3(t)N_0e^{\theta t} \quad (4.3)$$

where $N(t) = N_0e^{\theta t}$ if cells are in exponential growth, N_0 is number of cells at time 0, and θ is the growth rate ($0.045h^{-1}$ in the case of the AG01522 fibroblasts used in our experiments). By substituting $k_1(t)$ in Eq.4.2 we obtain

$$\frac{dQ(t)}{dt} = k_3(t)N_0e^{\theta t} - k_2(t)Q(t) \quad (4.4)$$

In general, it is possible to solve Eq. 4.4 analytically (unless the functional forms of the cytokine release rate per cell $k_3(t)$ and of the decay rate $k_2(t)$, that appear under integration are too complex). The solution is

$$Q(t) = e^{-\int k_2(t)Q(t)dt} (C_{int} + \int (k_3(t)N_0e^{\theta t})e^{\int k_2(t)Q(t)dt} dt) \quad (4.5)$$

That is the general solution of the balance Eq. 4.2 providing the cytokine concentration as a function of time. $Q(t)$ and $k_2(t)$ can be obtained with ELISA experiments (see the section 4.3). In particular,

$$Q(t) = e^{-\int k_2(t)Q(t)dt} C_{int} + e^{-\int k_2(t)Q(t)dt} \left(\int (k_3(t)N_0e^{\theta t})e^{\int k_2(t)Q(t)dt} dt \right) \quad (4.6)$$

and C_{int} is equal to 0 if, as an initial condition, we take $Q(0)$ equal to 0. As mentioned at the beginning of this section, the main aim was to evaluate $k_3(t)$, which represents the rate of release of Il-6 as a function of time for sham-irradiated and low-dose-irradiated cells:

$$k_3(t) = \frac{1}{Q_0e^{\theta t}e^{\int k_2(t)dt}} (Q'(t)(e^{\int k_2(t)Q(t)dt}) + Q(t)(e^{\int k_2(t)Q(t)dt})') \quad (4.7)$$

where the primed quantities represent time derivatives. In the next sections we will see the procedure to obtain the analytical description of $k_3(t)$ in the case of shamirradiated and low-dose-irradiated cells.

Measurement of the cytokine decay To evaluate the removal of signal molecules in the medium due to interactions with free proteases, a tailored experimental procedure was adopted. To investigate the release of proteases, medium was collected from three different seeded flasks at 3, 7 and 20 h after the irradiation (or, in the case of sham-irradiated cells, after the change of the medium). The medium was then filtered with 0.22-mm PTFE filters and kept in the incubator at 37 Celsius degrees. One flask was prepared for each cytokine measurement (1, 3, 5, 7 and 20 h). An aliquot of the medium was collected from each of these samples and kept at -20 Celsius degrees until ELISA was performed.

Results for sham irradiated cells

IL-6 molecule concentration $Q(t)$ The total amount of cytokine present in the medium for sham-irradiated cells was measured in the experiments. $Q(t)$ was fitted to ELISA experimental data using a sigmoid described by a Gompertz law (the Gompertz function was chosen because this was the sigmoid with the best agreement with the experimental data):

$$Q(t) = e^{\frac{\alpha}{\beta}(1-e^{\beta t})} - 1 \quad (4.8)$$

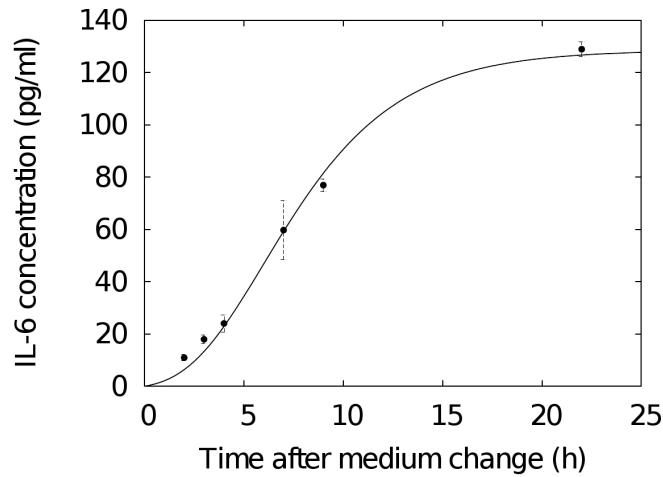


Figure 4.18: IL-6 concentration in the medium of sham-irradiated fibroblasts as a function of time $[Q(t)]$. Points are experimental data; the solid line represents the best fit of Eq. (4.8). Errors are standard deviations of the means of three independent experiments

with α equals to 1.2508 and β equals to 0.2569. The result is shown in the Figure 4.18.

Cytokine decay rate $k_2(t)$ The $k_2(t)$ function described removal due to the possible presence of protease enzymes. No decay was observed if IL-6 is added to fresh medium (see Fig. 4.4). This means that if any cytokine removal occurs, it is likely due to the release of these enzymes by the cells.

We measured the cytokine concentration in the medium after removal of the cells in medium collected after 3, 7 and 23 h of cell culture.

The data in Fig. 4.19 provided the best-fit values of the decay constant rates k_2 - using the formula $Q(t) = e^{-k_2 t}$ - corresponding to the medium

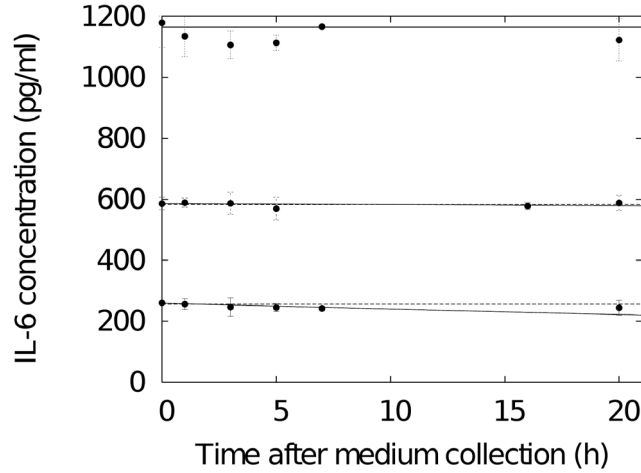


Figure 4.19: IL-6 concentration in medium without cells after 3 (lower line), 7 (central line) and 20 (upper line) h of culture with cells (at 37 Celsius degrees) as a function of time after medium collection. Points are experimental data; the solid lines are best fits assuming an exponential decay.

collected at 3, 7 and 23 h.

The decay rate values are all compatible with 0. No significant change in $k_2(t)$ was observed for different times of medium collection. The observed absence of decay allows us to assume that $k_2(t)$ equals to 0 at all times. As a consequence, the associated *in vitro* half-life becomes $T_{1/2} = (\ln 2)/k_2$ equals to infinity, whereas preliminary studies showed that the IL-6 half-life *in vivo* was a few hours [4]. Once the decay rate values and the cytokine concentration as a function of time are quantified, the functional form of the release rate of cytokines is obtained by deriving both sides of Eq. (4.7) with respect to time, giving

$$k_3(t) = \frac{1}{N_0 e^{\theta t}} (Q'(t)) \quad (4.9)$$

Figure 4.20 represents Eq. (4.9) multiplied by a factor ($1.56 * 10^8$ ml/pg) to obtain the release rate in terms of the average number of released molecules per cell per hour.

This factor takes into account the amount of medium (6.5 ml) and the IL-6 mass (assumed as 25 kDa).

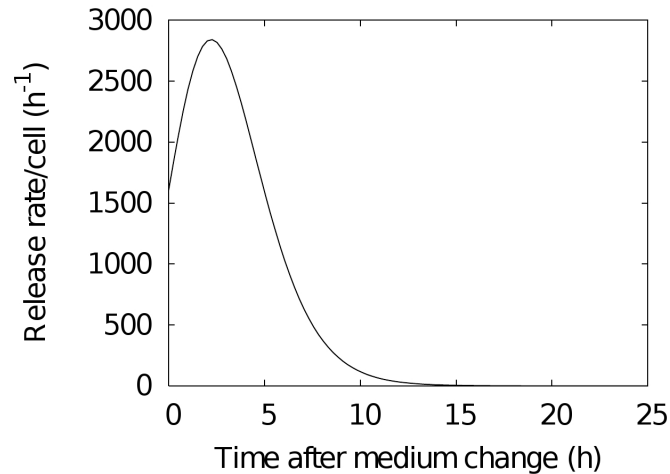


Figure 4.20: Calculated IL-6 molecule release rate per cell [in molecules/(cell h²¹)] as a function of time after medium change [based on function $k_3(t)$ in Eq. (4.9); see text for details]. In the absence of decay, the release rate is the derivative of the total concentration properly rescaled for the total number of cells. The maximum release rate is reached at 2 h after the medium change.

The release rate reaches its maximum at approximately 2 h, and it decreases with increasing time: the population releasing rate assumes the highest value right after the stress (medium change in this case) and then decreases with time. This particular functional form of the release rate is in agreement with Monte Carlo assumptions adopted in models already developed.

Results for irradiated cells

In the case of irradiated cells, the parameters of the population functional form $Q_R(t)$ are different from the previous ones. Using the same previous formalism, it is possible to obtain the functional form of the cytokine population in the case of fibroblasts irradiated with a low dose (0.25 Gy) of γ rays.

The total amount of cytokine present in the medium of irradiated cells was obtained from the experiments, and the effect of radiation was studied as a perturbation of the control case (sham-irradiated cells). The functional form of the cytokine population $Q_R(t)$ is represented by the sum of the sigmoid $Q(t)$

for sham irradiated cells (Eq. 4.9) and a Gompertz function representing the perturbation due to radiation.

Since the irradiation was performed 2 h after the medium change (considered time 0 in our analysis), the sigmoid function that represents the perturbation is added only for times longer than 2 h.

This new function has been fitted with MINUIT program and gives the following result:

$$Q_{TOT}(t) = \begin{cases} Q_{TOT}(t), & \text{if } t < 2 \\ Q(t) + Q_R = Q(t) + e^{\frac{\alpha_R}{\beta_R}(1-e^{\beta_R t})} - 1, & \text{if } t > 2 \end{cases} \quad (4.10)$$

In our experiments, 2 h corresponds at the time of γ irradiation.

The results shown in Fig. 4.21 were obtained with α equals to 1.1426 and

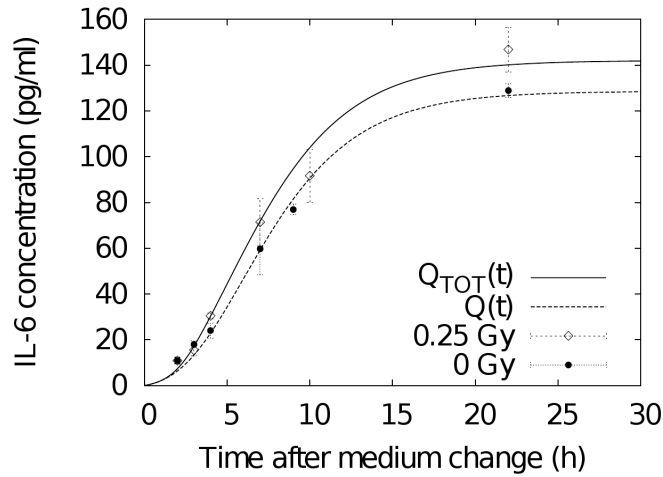


Figure 4.21: IL-6 concentration in the medium of c-irradiated fibroblasts [thin line, function $Q_{TOT}(t)$ in Eq. (4.10)] and for sham-irradiated cells [thick line, function $Q(t)$ in Eq. (4.8)]. The points are experimental data; the solid line represents the analytical function obtained with the fit (MINUIT algorithm) of the sum of two Gompertz curves [Eq. (4.10)], one representing the behavior due to the change of the medium, $Q(t)$, and one representing the perturbation induced by radiation, $Q_R(t)$. Experimental results and best-fit analysis are also shown for cells irradiated with 1 Gy of rays. Errors are standard deviations of the means of three independent experiment results.

β equals to 0.245. We also measured IL-6 release after 0.1 Gy and 1 Gy of γ irradiation. For 0.1 Gy, the release was not significantly different from the 0

Gy, whereas for 1 Gy we observed a significant reduction in the release rate (as shown in Fig. 4.21). At 1 Gy, several cells are expected to be severely damaged, consistent with that observed for this cell line by others for clonogenic inactivation [surviving fraction around 50% (68) and M. Tabocchini, personal communication].

The medium of cultured cells irradiated with 0.25 Gy γ rays was analyzed to evaluate the release rate of irradiated cells. To evaluate the dependence of the decay on the dose, doses 0.1 and 1 Gy were also investigated. The results are shown in Fig. 4.22. There was no experimental evidence of decay of the signal molecules in the medium, indicating that the release of free proteases does not appear to be relevant for the dose of interest (0.25 Gy) and does not appear to be modulated by radiation.

Once it has been quantified that the decay rate value is also equals to 0 after irradiation, the functional form of the release rate of cytokines is

$$k_{3(TOT)}(t) = \frac{1}{N_0 e^{\theta t}} (Q'_{TOT}(t)) \quad (4.11)$$

$$k_{3(TOT)}(t) = \begin{cases} \frac{1}{N_0 e^{\theta t}} (Q(t)) & \text{if } t < 2 \\ \frac{1}{N_0 e^{\theta t}} (Q'(t)) + \frac{1}{N_0 e^{\theta t}} (Q'_R(t)) & \text{if } t > 2 \end{cases} \quad (4.12)$$

The first term in eq. 4.12 represents the release rate due to the change of the medium, whereas the second one (4.12b) represents the release rate due to radiation (see Figs. 4.23 and 4.24). Figures 4.23 and 4.24 represent Eqs. (4.12) multiplied by $1.56 * 10^8$ ml/pg (as discussed above) to obtain the release rate in terms average number of molecules release in the medium per cell per hour.

Radiation induced perturbation of cell signaling: conclusive remarks

In summary, the main goal of this part of the work was to quantify the processes induced by ionizing radiation in cell-to-cell communication to explain the mechanisms of the bystander effect. To reach this objective, we redesigned an old general communication model to take into account the basic mechanisms of bio-communication via soluble factors. This formalization provided us with an interpretative framework for understanding the intercellular signaling and, in particular, for focusing on the study of cell-to-cell communication in a step-by-step approach. Using this model we separated the phenomenon of signal transmission into independent processes to investigate them separately. We designed experiments that allowed us to quantify (both experimentally and theoretically) a single mechanism per experiment (under certain hypotheses) and to evaluate the perturbative effect induced by a low dose of radiation on these mechanisms (as in typical bystander effect scenarios).

Our investigation was focused mainly on the study of the release rate of IL-6 (as an example of a possible signaling molecule) by fibroblasts and its modulation by radiation and the behavior of the channel (interaction with free

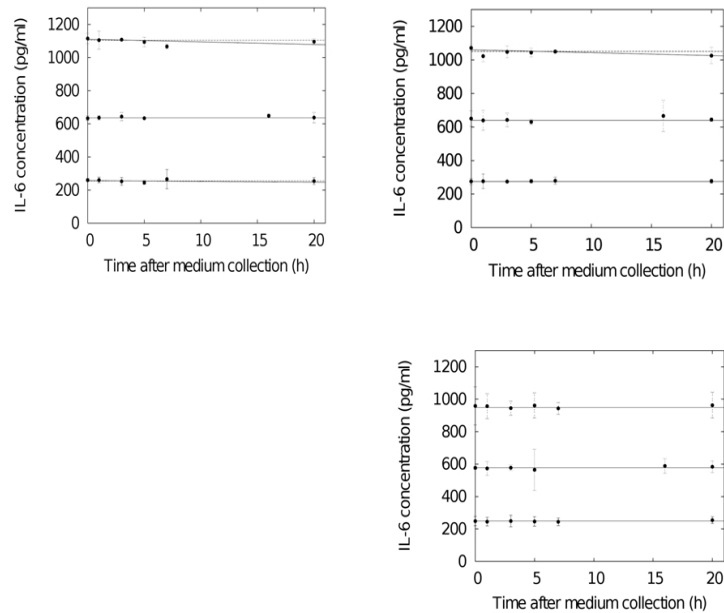


Figure 4.22: IL-6 concentration in medium without cells after 3 (lower line), 7 (central line) and 20 (upper line) h of culture with cells irradiated with different doses as a function of time after medium collection. The cells were irradiated with 0.1 (upper left panel), 0.25 (upper right panel), and 1 Gy (bottom left panel) of rays. Points are experimental data; the solid lines are best fits assuming an exponential decay.

proteases) in both cases. The information about the time characteristics of these signals and about the relative intensity of their overmodulation in response to low doses of radiation provided elements for an interpretation of the possible role of cytokines in inducing a bystander effect. The “net” release rate of IL-6 molecules in the control cells is a truncated bell-shaped function that reaches its maximum release value at 2 h and returns to near 0 at 10 h. In this experimental setup, each cell emits around one cytokine per second at the time of maximum release (according to the Monte Carlo results)

This behavior indicates that changing the medium (i.e., one of the fundamental techniques used in standard protocols for bystander studies) is an important trigger for cell signaling. It appears that, to re-establish and maintain homeostasis, cells emit large amounts of signals. For cells irradiated with a low dose of γ rays (0.25 Gy) (Fig. 4.24), the maximum release peaked at 3 h.

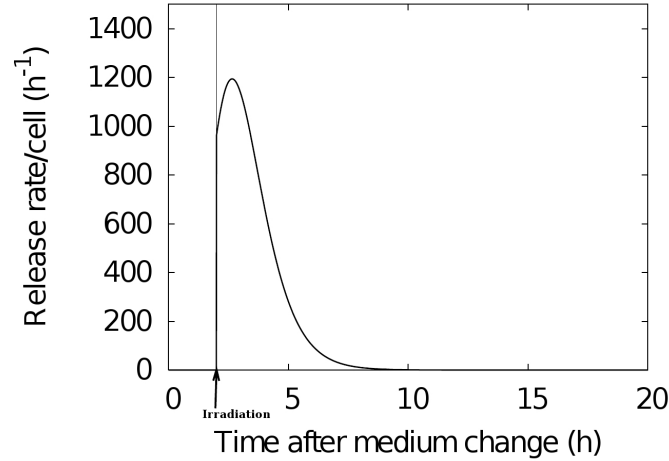


Figure 4.23: Calculated IL-6 molecule release rate per cell as a function of time after 0.25 Gy γ irradiation [based on equation 4.12; see text for details]. In absence of decay, the release rate/cell is the derivative of the total concentration divided by the total number of cells [Eq. (4.12)]. In this case the maximum release rate is reached after 3 h instead of the 2.5 h obtained in the case of sham irradiated cells.

The radiation-induced response is approximately one third of the response induced by the medium changes. The release rate due to radiation was about 0.3 cytokine/(s cell) (corresponding to a 30% increase over nonirradiated cells). The radiation-induced emission appears to confirm the role of these kinds of signaling molecules in low-dose response. The kinetics might raise for discussion the role of IL-6 alone in inducing some of the early biological effects seen in specific bystander experimental scenarios.

The IL-6 signal decay was evaluated to quantify the corresponding capacity of the channel in the case of irradiated and nonirradiated cells. No decay of IL-6 was observed *in vitro*, whereas an IL-6 *in vivo* half-life of a few hours is reported in the literature. The persistence of the signal in the medium appears to indicate a different role for this kind of signals *in vitro*, indicating also that it may be very difficult to extrapolate these experimental results for living organisms.

The role of radiation can be very important because it can also act in other subsystems of the signaling process, inducing different patterns of expression of membrane receptors [160] or modifying the state of the recipient cell. Generally speaking, the same message internalized by a “healthy“ cell or by a cell

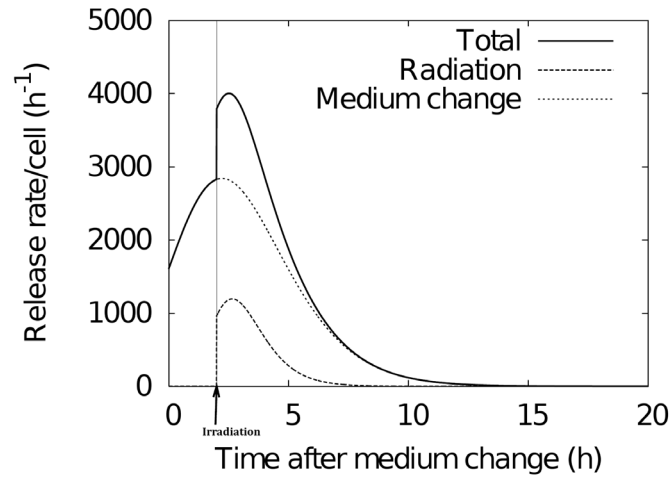


Figure 4.24: Calculated IL-6 molecule release rate per cell (solid line) due to the medium change (at t equals to 0) and irradiation (at $t = 2$ h) in case of low-dose cell irradiation [(based on function $k_{3(TOT)}$, Eq. (3.10)]. The contributions from the separate effect of medium change and radiation are also shown (dashed lines).

in a perturbed state can lead to different responses. These results show how the experimental conditions can perturb the system and in particular the signaling between cells. The perturbation induced by radiation (release rate of signal and its decay) appears to modulate the signaling already perturbed by the medium change.

The final goal of the investigation is the systematic quantification of the signaling perturbation for the major signals involved in bystander effect from the beginning of the process (release of the molecules) until their receipt by bystander cells to correlate these data with the broad bystander phenotype investigated experimentally. The proposed linear cause-effect model (e.g., an isolated and unique signal that is able to induce a single effect), although very useful to frame the theoretical and experimental work, is an oversimplified view of cell-to-cell signaling.

In case of a perturbation of the system, it appears evident that the radiation can act on any of the components of the model illustrated in Fig. 4.11, modulating its behavior. In this extended view, it is also clearer that the isolation of a single cause (i.e. of a unique signal) able to induce a certain effect can be achieved only if the characteristics and the status of the non-perturbed system are perfectly known. Indeed, because of the experimental condition (change

of the medium), the modulation of cell communication induced by radiation is part of a perturbed system that is reaching a steady state.

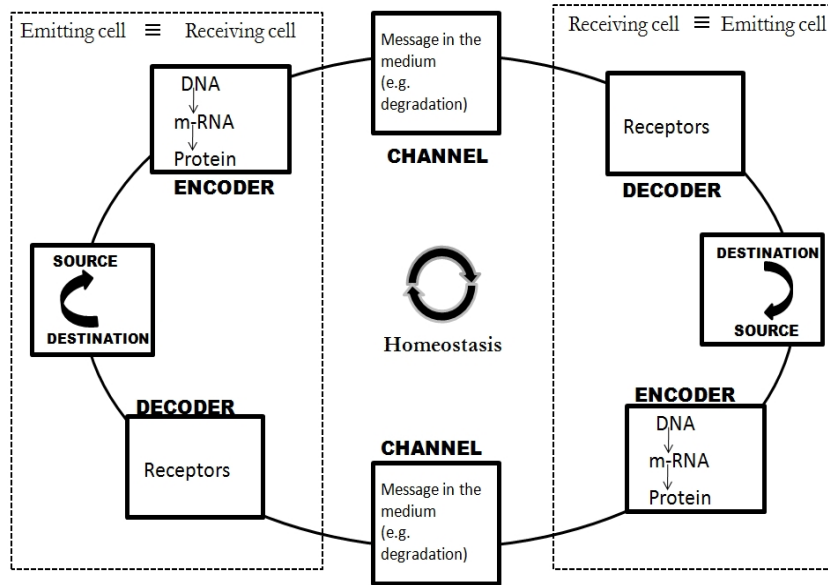


Figure 4.25: Circular view of the cell signalling

Therefore, an experimental investigation of the *in vitro* system results must include an investigation of the dynamics of a system that, at least for a short time, might still be dedicated to finding and maintaining physiological and metabolic homeostasis (see Fig. 4.25).

4.3.8 Cell signaling modulation induced by different radiation qualities

The investigation on cytokine release (through experimental and theoretical analysis), carried out as a function of the dose, indicated that the overall qualitative behavior after gamma irradiation seemed to be maintained for the whole cell population also for alpha irradiation. In particular the same dose dependence was observed for the 2 different radiation quality: over-expression stimulated by the lowest dose (0.1 Gy in this case), under-expression stimulated by higher doses (0.5 Gy in this case). See Figure 4.26 for the data.

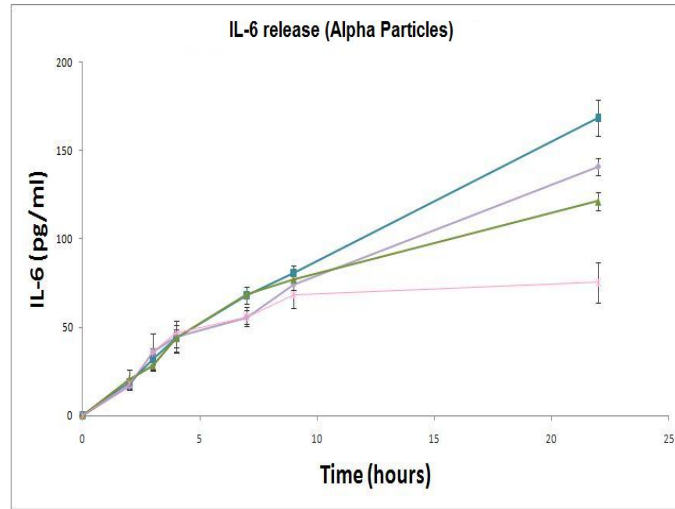


Figure 4.26: IL-6 release induced after alpha irradiation for AG01522 fibroblasts. The maximum release is reached after 0.1 Gy, followed by 0 Gy, 0.25 Gray and 0.5 Gy

The results on cytokine release were used to build a model (on the basis of the one shown in the previous section) aimed to the evaluation of the single cell response after exposure to the same dose, namely 0.1 Gy of gamma rays or α -particles. In order to make a comparison between the 2 different experiments, we present here also the release rate of the fibroblasts exposed to 0.1 Gy of gamma irradiation (see Fig. 4.27).

The results clearly show that there is no difference in the release respect to the control case. The comparison between the high/low LET process/perturbations was carried out taking into account the inhomogeneous pattern of energy deposition for alpha particles (at a first approximation with a Poisson-like distribution of the tracks in the cells). This analysis allowed us to evaluate the single cell response, that is different after the exposure to the same amount of dose deposited by different radiation types (high LET/low LET), with a stronger efficiency in cytokine release induced by high LET irradiation. Considering the whole cell as the sensitive target for the modulation of cytokine release, we calculate the number of alpha traversal for that surface area. In this experimental scenario, we trusted the average value of traversal as actually indicator of the received dose (as it will be shown later, this assumption could not be accepted in different scenario). For this reason, we used the model developed for the gamma irradiated cells also in this case, assuming that all the cells behave, in term of releasing cytokine, following the same analytical function. Therefore, starting from the total concentration of cytokine for 10 cGy of alpha irradiated cells (see Fig. 4.29),

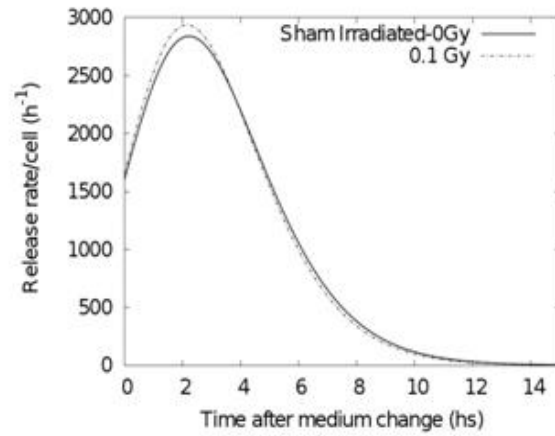


Figure 4.27: IL-6 release induced after 10 cGy of gamma irradiation compared to the unirradiated case

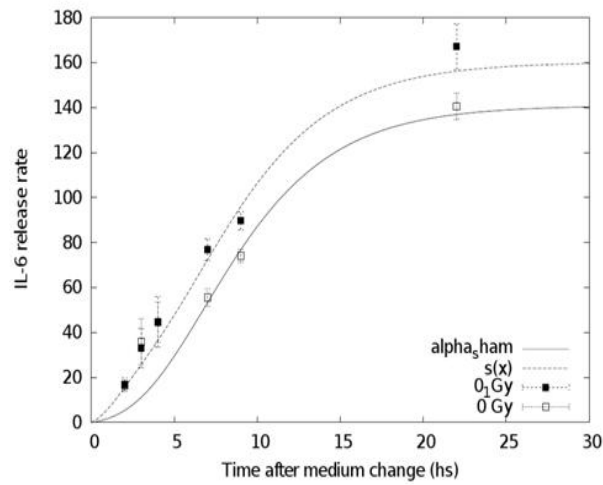


Figure 4.29: IL-6 accumulation in the media for cells sham irradiated and cells irradiated with 0.1 Gy of alpha particles.

we obtained the release rate per cell, shown in the Figure 4.30.

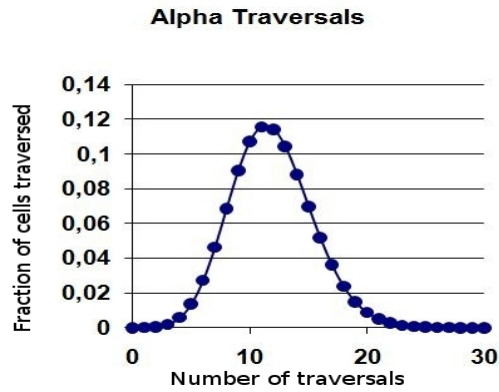


Figure 4.28: Number of alpha traversal per cell distributed following a Poisson distribution that takes into account the LET of the incoming particle, surface of the sensitive target and dose deposited

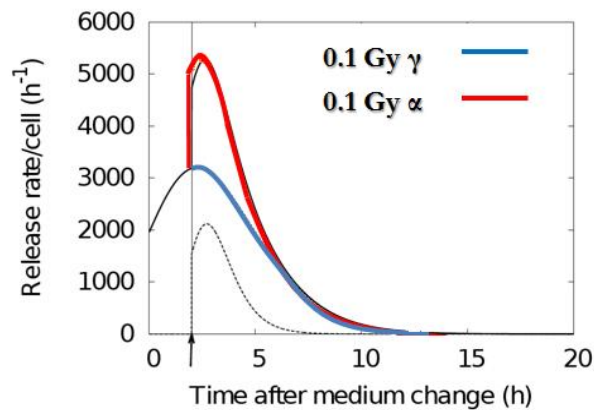


Figure 4.30: IL-6 Release rate per cell after 0.1 Gy of irradiation of gamma rays or alpha particles

with the clear indication of the different (higher) effectiveness of the alpha particle in the induction of the cytokine release respect to the same amount of dose of gamma rays.

Cell nucleus as a possible target for cytokine expression? If we now calculate the number of traversal induced by the same amount of radiation,

but considering only the cell nucleus as the sensitive target for the cytokine release, we obtain a distribution of alpha traversal as follows: In this situation

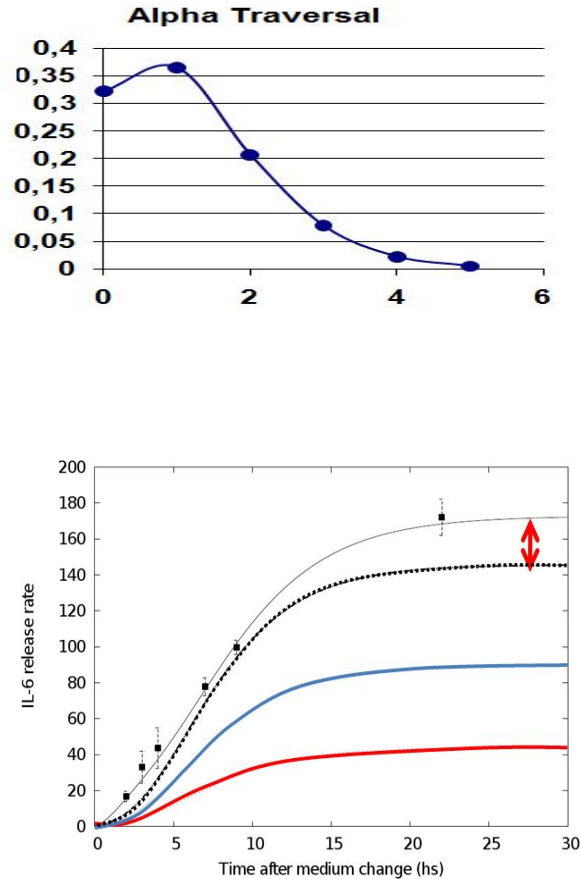


Figure 4.31: Upper panel. Number of traversal for 0.1 Gy of alpha particles in the *cells nucleus* scenario. Lower panel: Predicted amount of cytokine (dashed line) calculated with the contribution of the three subpopulations with the gamma parameters release. The solid line represents the actual amount of IL-6 for alpha irradiated cells

we clearly have (at least) 3 subpopulation of cells, each one receiving a different dose: around 32% receiving none traversal, around 36% one traversal (10 cGy), around 23% 2 traversal (20 cGy) and the remaining ones (less than 10%) more than 2 traversals. In this scenario it is difficult to extrapolate the release of the single cell, because there are too many degrees of freedom.

For this reason we try to understand the effectiveness of the alpha irradiation with a predictive model.

In particular we simulate the results obtained in Fig. 4.26 predicting the total amount of cytokine calculating the release induced by the 3 subpopulation in the gamma irradiation scenario. If the total amount of cytokine were bigger or equal respect the experiments with the alpha, this could mean a lower (or equal) effectiveness of the alpha particles, whereas otherwise this could lead to a bigger effectiveness. The results are shown in Figure 4.31.

In this situation the effectiveness of alpha seems to be confirmed also within the hypothesis of restriction of the sensitive area of cell nucleus.

4.3.9 IL-6 and IL-8: The role of oxidative stress

In vitro, we have previously shown that low doses (i.e. 0.25 Gy) of irradiation determine an increase of IL-6 release in the culture medium of irradiated AG01522 fibroblasts [70]. However, due to the long time interval (i.e. 20 hours) needed to observe an effect of IR on IL-6 release we hypothesized that the modulation of this cytokine might be a consequence of a more rapidly modulated signal. This hypothesis is also supported by the fact that several previous studies demonstrated biological effects in bystander cells also short time after irradiation, when cytokines are not yet modulated.

Recently, it has been demonstrated that NO in the alpha particle irradiated AG01522 cells acts as intercellular signaling molecule in the initiation of DNA damage in non-irradiated bystander cells [89]. The present study is aimed at investigating, by the use of low doses of specific scavengers, whether and to which extend two of the candidate molecules for the trigger of bystander signal formation, reactive oxygen species (ROS) and nitric oxide (NO), might be involved in the modulation of IL-6 signal in irradiated fibroblasts.

Preliminary to this study, we investigate the cytotoxicity of these compounds. The MTS measurements were performed on the AG01522 cells incubated for 20 hours with complete medium supplemented with different concentrations of DMSO (0.15, 0.5, 1, 2.5, 5 and 10%) or c-PTIO (5, 10, 15, 20, 25 and 30 μM) (Figure 4.32). The test was performed 20 hours after incubation with the compounds since this was the longest time interval planned for the subsequent experiments. The optical densities measured indicated that in our experimental conditions DMSO is cytotoxic for AG01522 cells when present in the medium with a ratio higher than 2.5%. Of importance, the presence of DMSO in the medium at the concentration of 0.5% (arrow in the graph), which is the one hypothesized for this study, did not affected the viability of AG01522 cells within 20 hours. On the other hand, the presence of c-PTIO at the concentration tested had negligible effects on the viability of AG01522 cells.

A set of experiments aiming to evaluate the effect of DMSO and c-PTIO on the release of IL-6 by AG01522 cells was performed. For this purpose several different concentrations of these compounds were added to the complete medium and the cytokine concentrations were determined by means of the ELISA assay 20 hours after incubation. As comparison, this study was re-

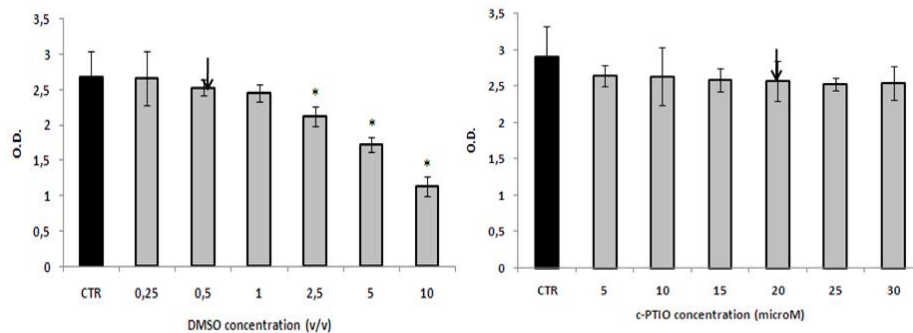


Figure 4.32: AG01522 cells vitality evaluated with MTS assay after 20 hours incubation with different concentrations of DMSO (left panel) and c-PTIO (right panel). The arrows indicate the concentrations used for the experiments with irradiation. *= statistically significant ($p < 0.05$) versus control (CTR)

peated after exposure to 0.25 Gy (Figure 4.33). The presence of both of the compounds in the culture medium determined a decrease in the release of IL-6, whereas their combination with 0.25 Gy gamma rays did not showed significant differences compared to sham irradiation. In detail, the DMSO induced a dramatic decrease of IL-6 in the medium of both sham and irradiated fibroblasts even at the lowest concentration tested (0.1%). The reference concentration of DMSO in the culture medium (i.e. 0.5%, arrow in the figure) induced approximately a 35% reduction of IL-6 compared to the control condition (0% DMSO).

Incubation of AG01522 cells in the presence of c-PTIO 10, 15 or 20 μM slightly modulated the release of IL-6 protein, whereas higher concentrations (25 and 30 μM) significantly ($p=0.028$ and $p=0.016$ respectively) impaired IL-6 secretion. Although not statistically significant ($p=0.1$), the presence of 20 μM of this scavenger caused a decrease of IL-6 in the medium (arrow in the figure).

Subsequently, the IL-6 release in presence of DMSO 0.5% or c-PTIO 20 μM was evaluated over 20 hours in comparison with control conditions. As shown from graph of Figure 4.34, both DMSO and c-PTIO decreased the release of IL-6 by fibroblasts when incubated longer than 5 hours. This decrease was statistically significant compared to control conditions when measured 20 hours after incubation ($p=0.04$ with c-PTIO and $p=0.009$ with DMSO).

Finally, the amount of IL-6 in the medium of irradiated (0.25 and 0.5 Gy, gamma rays) and sham irradiated AG01522 cells in presence of c-PTIO 20 μM , DMSO 0.5% was evaluated. As represented in the graphs of figure 4.35, the presence of these scavengers in the medium of irradiated cells did not affected the release of IL-6 in the culture medium, neither at short time nor at longer time after irradiation, compared to the sham irradiated condition (0 Gy). Based on the obtained data, ROS and NO might be the triggers for the

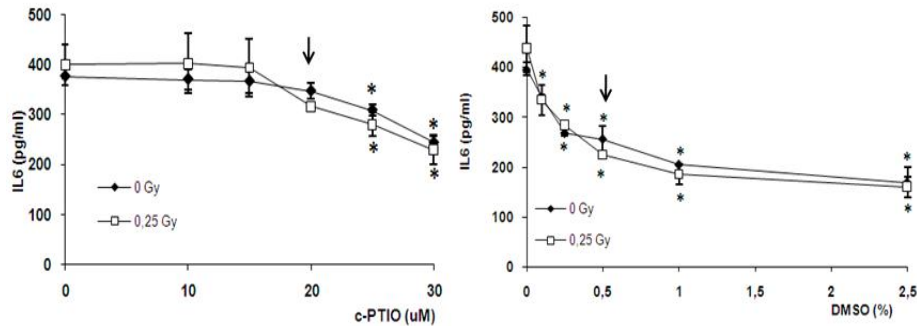


Figure 4.33: IL-6 release by AG1522 cells after 20h incubation with different concentrations of c-PTIO and DMSO, in sham or 0,25 Gy irradiated cells.

modulation of IL-6 release from human fibroblasts exposed to ionizing radiations. Indeed, it has already been observed that ROS, which are known to be formed after IR exposure, are capable of inducing the production of soluble mediators in a variety of cells. For example, it has been demonstrated that the production of IL-6 in human bronchial epithelial cells is increased via the oxidative stress induced by asbestos. NF-KB activation requires cytosol dissociation of the inhibitory subunit IKB from the NF-KB protein complex, and ROS have been postulated to be involved in these modifications and consequently in the activation of NF-kB nuclear transcription factor (see Section 4.5 for details). Then it has been demonstrated, by the evidence that antioxidants including DMSO can suppress the induction of IL-6, that intracellular ROS may be one of the signals acting as second messengers to produce IL-6. Another signal known to be rapidly generated after exposure to IR is NO. For example, Han and coworkers [89] have demonstrated that X-ray irradiation increases the activity of inducible nitric oxide synthase (iNOS) as early as 3 hours post irradiation. Several experimental studies performed *in vitro* showed that constitutive NO acts as intercellular signaling molecule in the initiation and propagation of bystander effects or in the generation of second messengers. In summary, the first part of the present study demonstrated that c-PTIO, and more strongly, DMSO, are potent inhibitors of IL-6 production in AG01522 cells, even in control conditions. DMSO is well known as a radical scavenger and it has been extensively used in the radiobiology field to suppresses the induction of lethal effects of ionizing radiation by means the scavenging action of short-lived active radicals such as OH and H radicals.

Concerning the release of IL-6, some studies reported inhibitory effects of ROS suppression on the release of IL-6 but although none discussed the effects of this scavenger on cytokine release in control conditions. For example, the detailed work of Yoshida [180] demonstrated that 0.5% of DMSO in the culture medium of human bronchial epithelial cells exposed to ROS is able to suppress

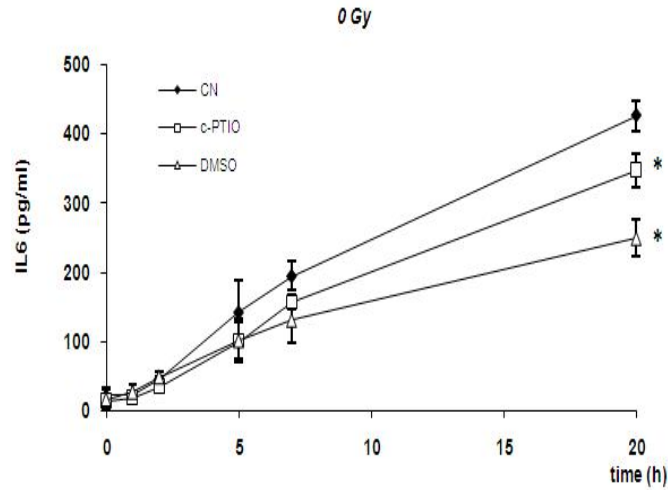


Figure 4.34: IL-6 release from AG01522 cells in presence of c-PTIO $20 \hat{I}_{4}^{\mu}\text{M}$, DMSO 5% v/v or in control (CN) conditions. * = difference statistically significant ($p < 0.05$) compared to control.

the stimulus to produce IL-6, however no observations were made on the effects of DMSO alone in the medium on the release of this cytokine. Recently, Kashino G and colleagues [172] demonstrated an effective suppression of bystander effects by DMSO treatment of irradiated cells

. In this study they checked for morphological changes after DMSO treatment for 1 hour and they observed that a concentration of 3% caused morphological changes. Therefore they used $< 1\%$ concentration of DMSO for their experiments. Subsequently they evaluated the effects of 0.5% and 1% of DMSO on the induction of micronuclei concluding that these two concentrations were not able to induce micronuclei. However with this study they concluded that at lower concentrations (i.e. 0.5%) DMSO acts as activating factor for a radioprotective signal, while at higher concentration DMSO acts as radical scavenger. According to the work of Valota A and coworkers [110] we calculated that the scavenging capacity of 0.5% of DMSO doubled the physiological scavenging capacity of the cells. As consequence of this and the results from our studies, we speculate that this concentration of DMSO is low enough to be not cytotoxic to the cells but is high enough to induce a cell response, probably a sort of stress response, which determines the alteration in cell signaling, which might be radioprotective for micronuclei induction as hypothesized by Kashino. These effects of DMSO on cell signaling, and probably on other cell functions, is extremely important when investigating small modulation of cytokine release, such as the one after low doses of ionizing radiation, otherwise it might happen that the effect under investigation is masked by the effect of DMSO, as in our

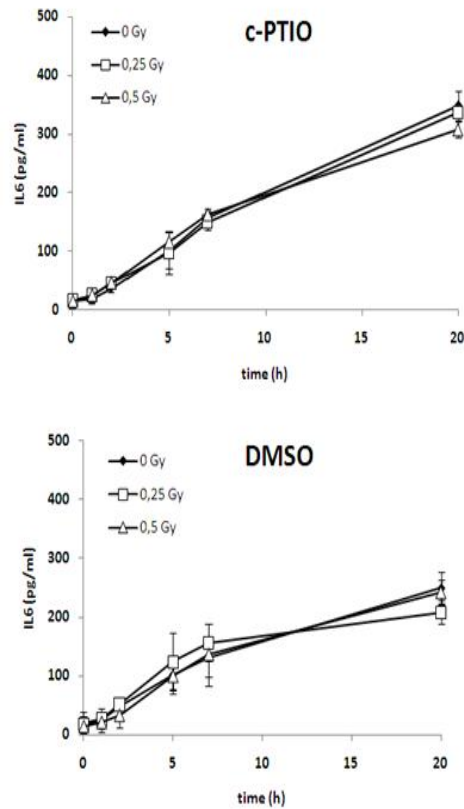


Figure 4.35: IL-6 release from irradiated (0.25 and 0.5 Gy, gamma rays) and sham irradiated (0 Gy) AG01522 cells in presence of either c-PTIO 20 \hat{I} $\frac{1}{4}$ M (upper panel) or DMSO 0.5% (lower panel)

case.

Same speculation comes for c-PTIO, although its effect on the normal cell homeostasis seems to be less evident, at least when considering IL-6 release.

4.4 Expression of NF- κ B

In the previous sections, examples of relationship between bystander effect and cellular communication were shown. As demonstrated before, a low dose of radiation can be responsible for an increase in the cytokines concentration. Once the information carried by the cytokines is transferred to a cell, two mechanisms are usually possible: effects on the cell (for example induction of bystander effect) or induction of a secondary signalling mechanism, which

results in the production of further cytokines.

Keeping in mind this process, our idea was to study more into details the mechanism of production of cytokine following a radiation exposure, in order to have a larger view of the system and to give a contribute to the general pathway of bystander effect. Based on our data regarding the expression of IL-6 and IL-8 (and their possible regulation induced by ROS and RNS), we wanted to analyze what exactly is responsible for the release of these cytokines and how this mechanism can be related to a radiation exposure. Being the cytokine a protein, its birth starts in the cellular nucleus (with the associated m-RNA), where a certain DNA sequence is transcribed. This information is contained in a gene and the process by means a specific code is used in the synthesis of a protein is called *gene expression* [178]. The copy of this information from DNA to mRNA is controlled by *transcription factor proteins* and one of them of particular importance in immune and inflammatory responses is the *Nuclear Factor- κ B* (NF- κ B). Since NF- κ B controls the gene expression and the synthesis of proteins that regulate the immune functions [147], this transcription factor is likely to be involved in the cytokine pathway.

In this part of the work we tried to give a contribution in the investigation of the bystander effect mechanisms by connecting the expression of NF- κ B transcription factor with an absorption of energy in the cells following a radiation exposure.

Nuclear Factor- κ B was first identified by Sen and Baltimore in 1986 as a regulator of the expression of the kappa light-chain gene in murine B lymphocytes [13]. Following its discovery, NF- κ B has been shown to exist in most cell types, and also the range of biological factors and environmental conditions known to induce NF- κ B activity has been demonstrated to be remarkably large and diverse.

The NF- κ B transcription factor activated form consists of two proteins, a *p65* (also called *relA*) subunit and a *p50* subunit (see Fig. 4.36). It has been discovered that other subunits, such as *rel*, *relB*, *v-rel* and *p52* [83], may also be part of activated NF- κ B and that different forms of NF- κ B may activate different sets of target genes [147] (see Fig. 4.37). When the cell system is not stimulated, NF- κ B complexes are sequestered in the cytoplasm in an inactive form via interaction with a class of inhibitory proteins called *I κ B*. Several *I κ B* proteins have been identified and the most important are *I κ B α* , *I κ B β* , *I κ B γ* , *I κ B ϵ* , *p100* and *p105*. These proteins have the important function of preventing the NF- κ B to enter in the nucleus. Different *I κ B* molecules preferentially inhibit distinct subsets of NF- κ B protein dimers [3].

Following the activation signal by external stimuli such as cytokines, the *I κ B* protein is phosphorylated by a class of proteins called *I κ B kinases* (*IKK*), for example *IKK α* and *IKK β* (see Fig. 4.36). These proteins are able to break the non-covalent interactions between NF- κ B and *I κ B*, allowing NF- κ B proteins to enter the nucleus and induce gene expression. The dissociated *I κ B* component will be degraded in the cytosol. The NF- κ B activation process is represented

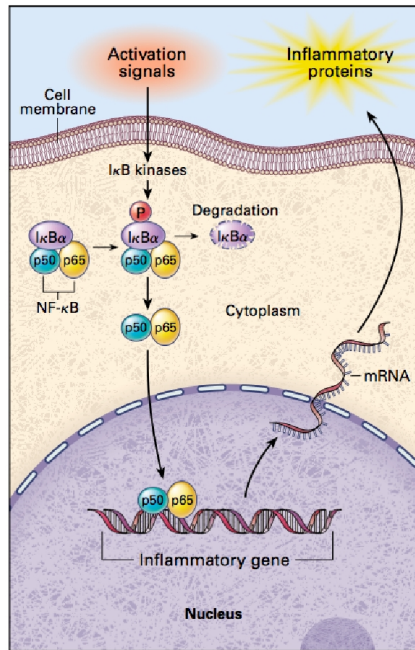


Figure 4.36: Schematic diagram of NF- κ B activation process. [3]

in Fig. 4.36, where a class of proteins has been chosen as components of the transcription factor. As the two components reach the nucleus, they bind to Dna and transcript the genes involved in the inflammatory proteins such as cytokines, enzymes, and adhesion molecules are present [3].

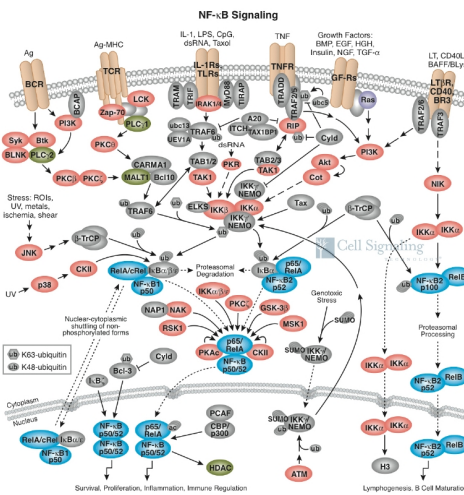


Figure 4.37: Complete pathway of the NF- κ B signalling. [130]

Although the mechanism of gene expression presented here is an over-simplification of the reality, it is worth keeping in mind that a lot of different proteins and inhibitors exist, and each of them has a particular function in the gene transcription. Fig. 4.38, updated to 2008, represents a good summary of the different proteins involved in the process.

4.4.1 Activation and role of NF- κ B

As already mentioned, NF- κ B acts as a central coordinator of immune and inflammatory responses. It has also been demonstrated that NF- κ B covers an important role in promoting basic cancer mechanisms [39] [129] [157] [100] [24] [147]. Its activation is induced by signals that in general represent states of infection or stress. An important characteristic of the NF- κ B pathway is that products of the genes that are regulated by NF- κ B also cause the inactivation of NF- κ B (Fig. 4.38) [95] [97] [112] [105].

TABLE 1. STIMULI THAT ACTIVATE NF- κ B.	TABLE 2. PROTEINS REGULATED BY NF- κ B.
Cytokines	Proinflammatory cytokines
Tumor necrosis factor α	Tumor necrosis factor α
Interleukin-1 β	Interleukin-1 β
Interleukin-17	Interleukin-2
Protein kinase C activators	Interleukin-6
Phorbol esters	Granulocyte-macrophage colony-stimulating factor
Platelet-activating factor	Macrophage colony-stimulating factor
Oxidants	Granulocyte colony-stimulating factor
Hydrogen peroxide	Chemokines
Ozone	Interleukin-8
Viruses	Macrophage inflammatory protein 1 α
Rhinovirus	Macrophage chemotactic protein 1
Influenzavirus	Gro- α , - β , and - γ
Epstein-Barr virus	Eotaxin
Cytomegalovirus	Inflammatory enzymes
Adenovirus	Inducible nitric oxide synthase
Immune stimuli	Inducible cyclooxygenase-2
Phytohemagglutinin	5-Lipoxygenase
Anti-CD3 antibodies (by means of T-lymphocyte activation)	Cytosolic phospholipase A ₂
Antigen	Adhesion molecules
Other	Intercellular adhesion molecule 1
Lipopolysaccharide	Vascular-cell adhesion molecule 1
Ultraviolet radiation	E-selectin
	Receptors
	Interleukin-2 receptor (α chain)
	T-cell receptor (β chain)

Figure 4.38: Activation and role of NF- κ B in protein regulation. [156]

Fig. 4.38 clearly shows the importance of this transcription factor in the protein synthesis. Since NF- κ B is responsible for such a large amount of signalling, small modifications in its expression can affect the whole cellular system. It is important to notice from Fig. 4.38 that, among all the possible stimuli, ultraviolet radiation can be responsible for NF- κ B activation [112]. The main purpose of this work consists in studying whether or not a low dose of ionizing radiation, low enough to do not cause relevant cellular damage, can be

included in the list of stimuli that inactivate NF-kB.

Several works have been already done about NF-kB modulation and ionizing radiation, in particular regarding its activation by reactive oxygen species ([132] [83] [84]). For example, increases in ROS have been postulated to be associated with increased active NF-kB. As firstly demonstrated by Schreck *et al.* in 1991 [157], direct addition of H_2O_2 to the culture medium could activate NF-kB in Jurkat cells. It is important to notice that this mechanism strongly depends on the cell-type considered and for this reason it is difficult to establish a general model valid also for our cell line (primary human fibroblasts).

NF-kB activation by γ -irradiation has been attributed also to the enhancement of $NO\cdot$ production. As shown in [120], this effect occurs at around 6-10 Gy, condition in which the DNA damage are dominant and the bystander effect is not relevant. Another interesting result at high doses has been found in [173], where it is reported that the NF-kB activation reaches a maximum at ~ 5 -20 Gy.

As demonstrated in [147], even lower doses are capable of inducing expression of NF-kB in 244B human lymphoblastoid cells. In this work, the expression of NF-kB is likely to be maximum after the 0.5 Gy exposure (see Fig. 4.39). This is an important result for the explanations of the bystander mechanisms

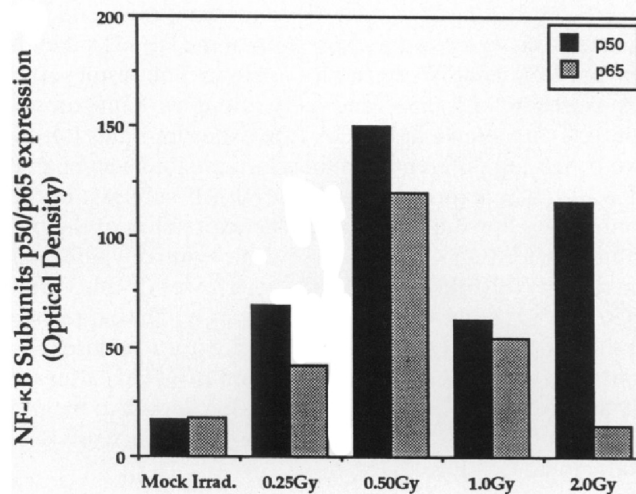


Figure 4.39: NF-kB expression at 1 h after radiation exposure. [147]

because it is stated that the effect on the activation of NF-kB seems to be more relevant also at relatively low doses.

Starting from the finding already present in the literature [28] [158] [86] [16] [82] [96] [42] [13] [132] [83] [84], the hypothesis for this investigation are:

1. if a clear relationship between low radiation dose and NF-kB expres-

sion will be demonstrated, the mechanism of bystander effect would be explained as a particular characterization of the gene transcription;

2. if the NF- κ B expression will not change with doses typical of bystander communication effects, the pathway of non-targeted effects would be different (and maybe more complex) and would involve other proteins, transcription factors or more generally molecules, following a pathway different respect the inflammatory one.

4.4.2 Experimental Detection of NF- κ B

Materials and methods

The number of cells required for this experiment has been calculated through preliminary test that outlined a number of 10^7 cells to be collected for the nuclear and cytoplasmic extraction in order to have reliable results.

The cells have been cultivated in T175 flasks, each of them contained $\sim 7 \times 10^6$ cells at 90% confluence. According to the number of cells indicated in the ELISA protocol for NF- κ B, each flask could be used for a single concentration measurement. In order to avoid misunderstandings, we define *value* as the result found following the analysis of a single flask and *point* as the average of three values, collected at the same time. Since each value describes a concentration at a certain moment after irradiation, this time is set by the start of nuclear extraction process.

Experimental protocol

1. After selecting the number of strips needed, equilibrate the plate and buffers at room temperature;
2. Add 100 μ L of *complete transcription factor buffer* (CTFB), previously prepared according to the manual, in A-D1; 80 μ L of CTFB, 10 μ L of *Competitor dsDNA* and 10 μ L of unknown sample in E-F1; 90 μ L of CTFB and 10 μ L of *Positive Control* in G-H well of the last used strip (for ex. G-H12); 90 μ L of CTFB and 10 μ L of sample¹ in all the other wells;
3. Use the cover provided to seal the plate and incubate overnight at 4°C;
4. Empty the wells and wash 5 times with 200 μ L of *1X Wash Buffer* previously prepared, then tap the plate on a paper towel to remove any residual Wash Buffer;
5. Prepare *NF- κ B (p65) Primary Antibody* and add 100 μ L of it to each well except A-B1;
6. Cover and incubate 1 hour at room temperature;

¹In this case the sample consists in nuclear or cytoplasmic material, depending on the area of investigation.

7. Repeat step 4;
8. Prepare *Diluted Secondary Antibody* and add 100 μL of it to each well except A-B1;
9. Repeat steps 6-7;
10. To each well being used add 100 μL of *Developing Solution* which has been equilibrated to room temperature;
11. Incubate the plate for 15 to 45 minutes at room temperature with gentle agitation protected from light, until the solution in the wells turns to dark blue;
12. Add 100 μL of *Stop Solution* per well being used;
13. Read absorbance at 450 nm with a microplate reader within 5 minutes of adding the *Stop Solution*.

The main differences between the procedure for NF-kB and cytokine consist in the use of intra-cellular material instead of the culture medium, a different primary antibody and diverse incubation processes. The microplate reader has the function of analyzing the intensity of the color and transfer this information into an absorption value, proportional to the concentration of NF-kB in the sample.

Regarding the samples adopted, according to the protocol each sample must be taken in duplicate. In this way the final result of a concentration is given by an average between two values, with a consequent increase of the accuracy of the results. For each condition studied, three independent experiments were performed.

In this experiment, we have cultivated 54 flasks, which, considering irradiated and sham-irradiated samples, result in a kinetics of 9 time-points with a statistic of three values each point. The temporal points after the irradiation have been chosen following the previous experiment about IL-6.

4.4.3 NK-kB activation: Experimental results

The flasks were irradiated 30 minutes after the change of the medium. One point has been collected before the irradiation, in order to control the starting level of NF-kB concentration. The other points regards short (1-8 hours) and long (~ 24 hours) times after irradiation. It is important to mention that the measurements have been done on nuclear samples, while the cytoplasm has not been used for this purpose (only the nuclear NF-kB is active, and so only the nuclear NF-KB can regulate the gene expression).

Fig. 4.40 represents the results we have found about the absorbance in the nucleus, (the absorbance is directly proportional to the concentration of the targeted molecule).

Because of the size of the flasks used for this experiment, the radiation facility

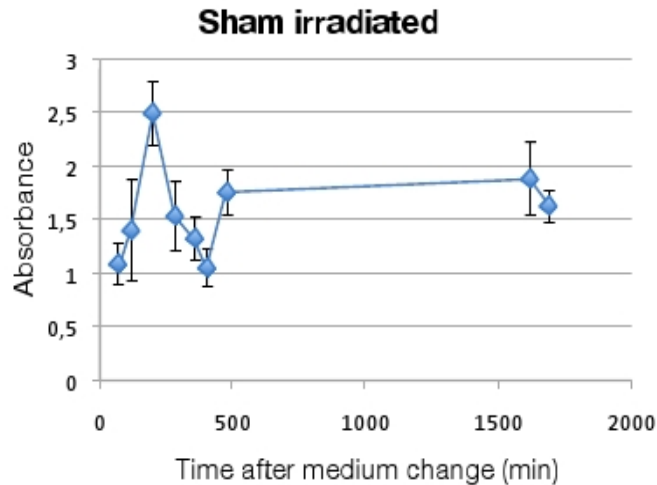


Figure 4.40: Results from ELISA test.

was only able to irradiate one flask at a time. Moreover, the time gap between the first and the last irradiation is relatively big (~ 30 min) because of the large number of samples. For these reasons, Fig. 4.41 does not show the irradiation instant. However, regarding the first flask the irradiation occurred ~ 90 min after the medium change.

The results are expressed as an average between three independent experiments. Errors are standard deviations of the three values. The solid lines are traced in order to highlight the oscillating nature of the result found. This is in agreement with recent works done both with an experimental [174] [137], [3], [156] and a theoretical approach [120] [101] [39]. It has been hypothesized, in particular, that the response of NF- κ B after the medium change consists in an increase in its nuclear concentration with a damped oscillatory trend.

From the results found in the literature, this might be the first result about the time variation of NF- κ B concentration with ELISA technique. The previous experimental works have been done mostly with *Western blot*, a procedure that uses gel electrophoresis to detect specific proteins. The advantage of ELISA respect this technique consists in a more precise output, as it provides directly a value of concentration (or absorbance) without the need to analyze with an external optical device.

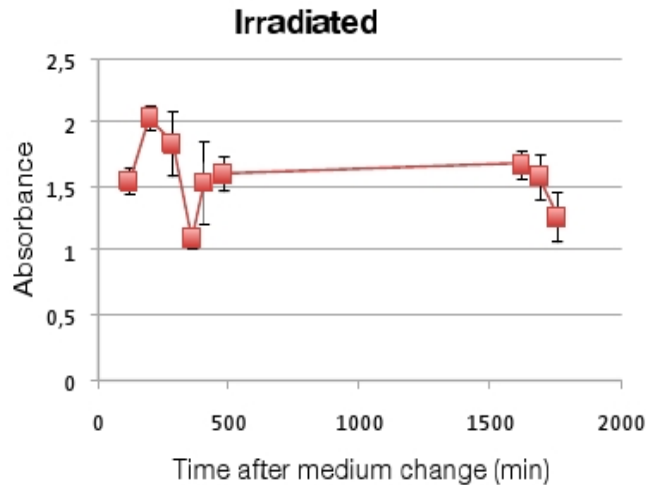


Figure 4.41: Results from ELISA test.

4.4.4 NF-kB and cytokine expression

To better understand the role of radiation on this experimental system, we investigated how the system has been perturbed following an exposition to 0.25 Gy of γ -rays, the previous graphs are shown together in Fig. 4.42

Whereas the temporal behavior of NF-kB concentration has been clearly shown from its oscillating nature, the role of a low dose exposition is not trivial. From the analysis of Fig. 4.42, it seems that the NF-kB in the irradiated cells is under-expressed respect to the case where no perturbation occurs. In particular, the amplitude of the first oscillation looks smaller, although the oscillatory period is likely to be similar.

If we now consider as true the hypothesis that the amplitude of the signal from irradiated cells is smaller, the radiation is likely to act as a destructive perturbation.

Comparing the experimental results with the expression of cytokines, we are able to connect an over expression of IL-6 [128] by a radiation exposure with a under expression of NF-kB in the same conditions. Indeed, a precise compatibility between the NF-kB oscillatory behavior and the cytokines release rate can be outlined by the parallel analysis of the graphs (Fig. 4.43).

The emission rate curve has been realized with the analytical model reported in Section 4.4.3 and derives from the expression of the cytokine release rate. From the comparison, the peak in the IL-6 emission rate, which represents the maximum slope of the curve in Fig. 4.40, seems to coincide with the

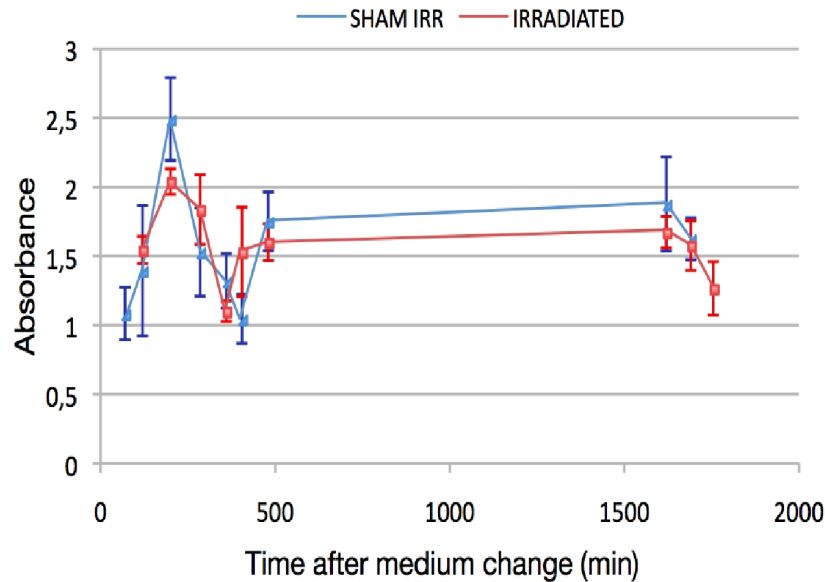


Figure 4.42: NF-kB absorbance values for sham irradiated and irradiated samples.

maximum of the first oscillation of NF-kB.

Now, analyzing our data on the basis of a theoretical model, we will try to quantify how a low dose radiation exposition has a role in the nuclear concentration of NF-kB.

In summary, the ELISA test for NF-kB has provided an important information about the dynamics of the activated transcription factor in a cell nucleus. In particular, an oscillatory trend seems to be confirmed both with non irradiated and with irradiated samples.

4.4.5 Theoretical analysis

Thanks to the high reliability of the data collected, our attention has shifted to the analysis of the mechanism of activation of NF-kB starting from a theoretical analysis of our results.

The negative feedback loop

In molecular biology, most intracellular signalling networks incorporate *feedback loops*, in which the output of a process acts back to regulate the process itself. Feedback loops are of great general importance in biology, and they regulate many chemical and physical processes in cells. They can be divided in two categories:

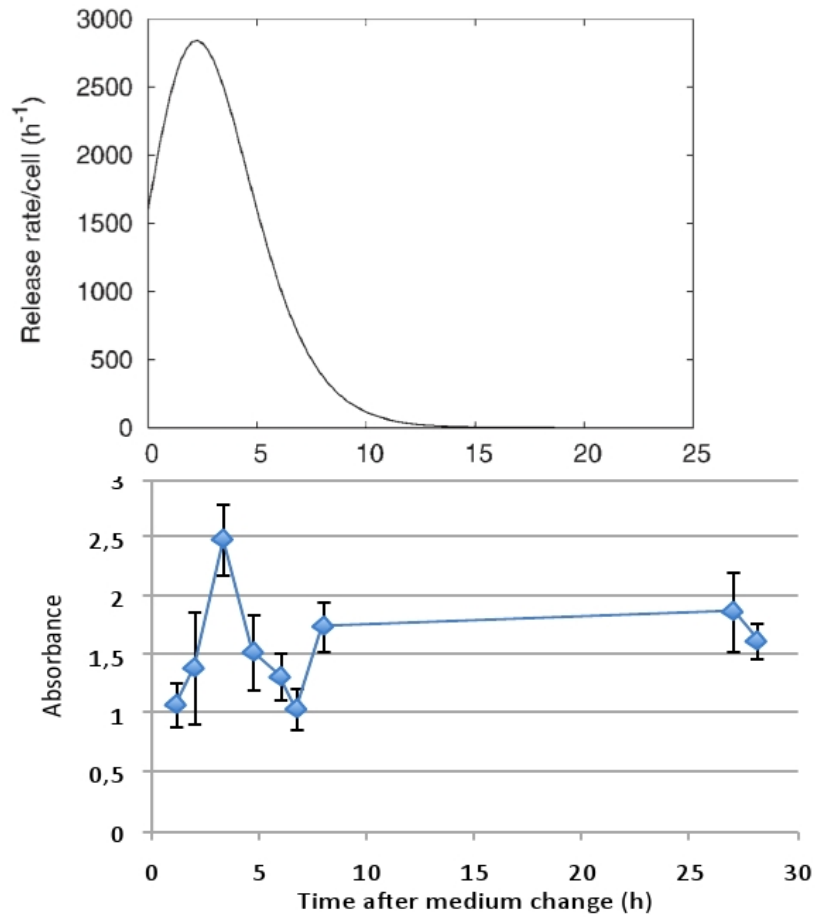


Figure 4.43: Comparison between IL-6 release rate/cell and our result for sham irradiated.

- *positive feedback*: the output stimulates its own production;
- *negative feedback*: the output inhibits its own production.

A simple representation of how this mechanism acts is depicted in Fig. 4.44 and Fig. 4.45. In this scheme, a stimulus activates protein A, which, in turn, activates protein B. Protein B then acts back to either increase or decrease the activity of A, depending on the loop that persists.

The expression of protein B can be represented in Fig. 4.46, which refers to E kinase protein. In the graphs, *SIGNAL* indicates the stimulus, which is kept for a certain amount of time. Differences between positive and negative feedback are clear from the trend of the curves: while in the first case the activity of E kinase increases when the signal is activated, in the negative

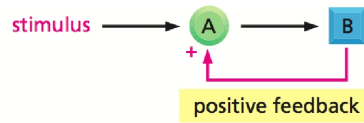


Figure 4.44: Positive and negative feedback in a biological system [12].

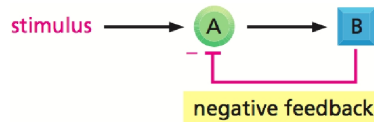


Figure 4.45: Positive and negative feedback in a biological system [12].

loop the system reaches a peak and then starts to oscillate, usually with an exponential decay.

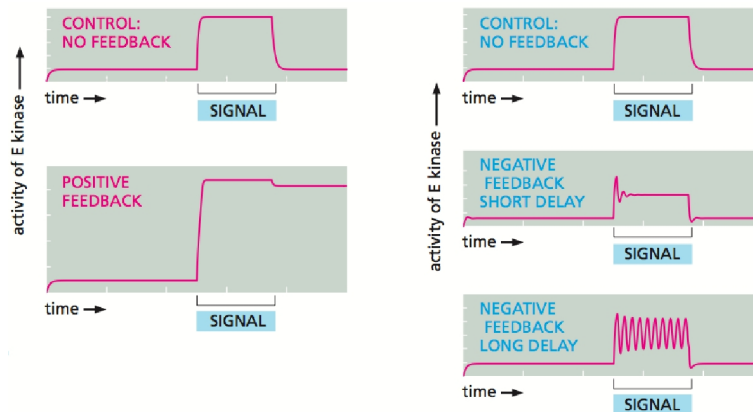


Figure 4.46: Effects of feedbacks on E kinase protein expression [12].

These mechanisms can last in time from milliseconds (for example in the case of an action potential) to many hours (cardiac oscillations). In this part of the research, we were interested in the process that controls the activation of NF- κ B transcription factor: the negative feedback loop.

The ability of NF- κ B to enter the cellular nucleus and regulate gene expression is controlled by chemical modifications of proteins from the I κ B family. The binding of NF- κ B to I κ B helps to localize NF- κ B in the cytoplasm. Upon activation of the NF- κ B signaling pathway by external stimuli such as TNF α or IL-1 β , the I κ B molecule degrades and NF- κ B is free to migrate to the nucleus. Here is the crucial point of the feedback: one of the genes activated by NF- κ B consists in the gene that encodes I κ B. Newly synthesized

I κ B binds to NF-kB and attenuates the pathway response to the activation stimulus, thereby creating a negative feedback loop within the NF-kB/I κ B signaling pathway. This pathway has been already investigated in the literature [3] [137] [39] [101] [120] [156] [163] [31] [181] [90].

Negative feedback amplifier

A negative feedback amplifier is an electronic device used to combine the output with the input when the two signals are opposite. In a voltage amplifier (Fig.4.47), the *open loop gain* A_{OL} is defined as the gain of the amplifier without feedback and the *feedback factor* β governs how much of the output signal is applied to the input [71] [5].

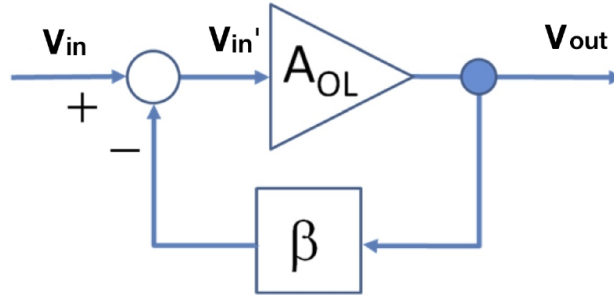


Figure 4.47: Ideal negative feedback circuit.

The open loop gain A_{OL} is defined by:

$$A_{OL} = \frac{V_{out}}{V'_{in}} \quad (4.13)$$

where V'_{in} is the input to the amplifier (in this case, equal to V_{in}), assuming no feedback, and V_{out} is the amplifier output. Since in a negative feedback loop the output is opposite to the input, a fraction βV_{out} of the output is subtracted from the input. In this case, the input to the amplifier is given by:

$$V'_{in} = V_{in} - \beta V_{out} \quad (4.14)$$

and the output becomes:

$$V_{out} = A_{OL} V'_{in} = A_{OL} (V_{in} - \beta V_{out}) \quad (4.15)$$

From the previous equation we obtain:

$$A_{fb} = \frac{V_{out}}{V_{in}} = \frac{A_{OL}}{1 + A_{OL}\beta} \quad (4.16)$$

where A_{fb} is the *closed loop gain*, or the gain of the amplifier with feedback. In this part, we have obtained from equation (4.16) an expression of the output

in a negative feedback amplifier. Since the NF-kB signal is regulated by a similar mechanism of loop [90], it is interested to study its response and connect it with the results of an electronic model.

Step response

Let's consider now a so called *second order control system* [90], that consists in a negative feedback loop with unity feedback ($\beta=1$) (Fig.4.47). In this configuration, the parameter s indicates the *frequency domain*, while the parameter t represents *time domain*.

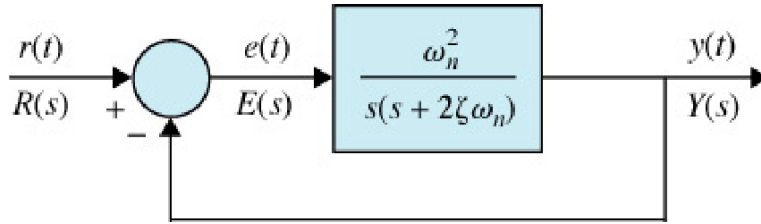


Figure 4.48: Our example of second order control system.

According to equation (4.16), we define the open loop transfer function of the system, which coincides with open loop gain of the amplifier, as:

$$G(s) = \frac{Y(s)}{E(s)} = \frac{\omega_n^2}{s(s + 2\zeta\omega_n)} \quad (4.17)$$

where ζ and ω_n are real constants. The closed loop transfer function of the system, can be obtained from equation (4.16):

$$\frac{Y(s)}{R(s)} = \frac{\omega_n^2}{s^2 + 2\zeta\omega_n s + \omega_n^2} \quad (4.18)$$

where, as already mentioned, $\beta = 1$.

Now, if the input signal is given by a unit step function $R(s) = 1/s$, the output response of the system is given by:

$$Y(s) = \frac{\omega_n^2}{s(s^2 + 2\zeta\omega_n s + \omega_n^2)} \quad (4.19)$$

Its temporal expression can be obtained by taking the inverse Laplace transform of (4.19) [39]:

$$y(t) = 1 - \frac{e^{-\zeta\omega_n t}}{\sqrt{1 - \zeta^2}} \sin(\omega_n \sqrt{1 - \zeta^2} t + \cos^{-1}\zeta) \quad t \geq 0 \quad (4.20)$$

Fig.4.49 shows the unit step responses of equation (equation 4.20) plotted as functions of the normalized time $\omega_n t$ for different values of ζ .

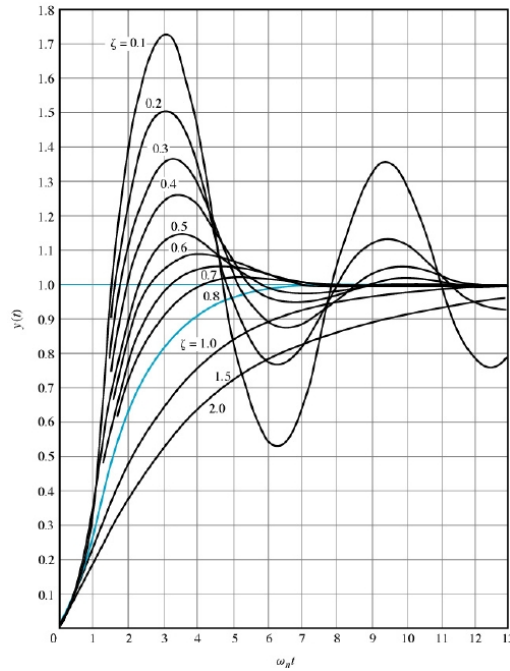


Figure 4.49: Representation of equation (6.8) for different ζ .

The parameter ζ is well known as *damping ratio*[5] and indicates how oscillations in a system decay. Depending on its value, the response of the system can be defined as:

- *overdamped* ($\zeta > 1$), the solution is simply a decaying exponential with no oscillation;
- *underdamped* ($0 < \zeta < 1$), the solution is a decaying exponential combined with an oscillatory portion;
- *critically damped* ($\zeta = 1$), the system returns to equilibrium as quickly as possible without oscillating.

It is interesting to notice that for the limit value $\zeta = 0$, equation (3.18) becomes:

$$y(t) = 1 - \sin(\omega_n t + 1) \quad (4.21)$$

and the step response degenerates to a sinusoidal wave.

In Fig. 4.50 we have implemented the same equation with MATLAB's *step* command, which plots the step response of a provided closed loop. In this case, the curves depend also on ω_n , which is called *damped natural (angular) frequency* and controls the frequency of the oscillation when the system is underdamped. In our model, a value $\omega_n = 10$ has been used. In the figure, the

underdamped responses are easily visualized because they oscillate around the x -axis and they interest the positive part of y -axis.

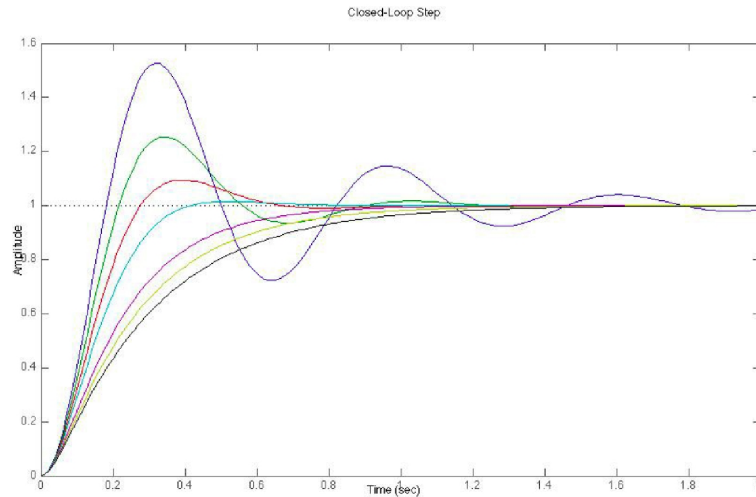


Figure 4.50: Unit step responses realized with MATLAB.

Analysis of the function

As already mentioned, the step response is defined as an output signal from a negative feedback loop where the input is given by a signal similar to a square wave. In most of the cases, the trend of this function increases when the input signal is applied and reaches, by oscillating, the final value given by the amplitude of the constant input signal. Several parameters control the way and the rapidity the step response approaches the final value.

A typical step response is characterized by different factors that describe its shape and trend (Fig 4.51):

Maximum overshoot. Being $y(t)$ the unit step response, y_{max} the maximum value of $y(t)$ and y_f the constant value of the input function (in the figure $y_f = 1$), the maximum overshoot of $y(t)$ is defined as:

$$\text{maximum overshoot} = y_{max} - y_f$$

This quantity is often represented as a percentage of the final value of the step response:

$$\text{percent maximum overshoot} = \frac{\text{maximum overshoot}}{y_f} \times 100\%$$

The maximum overshoot is used to measure the relative stability of a control system: higher is its value and lower is the stability of the response. Depending

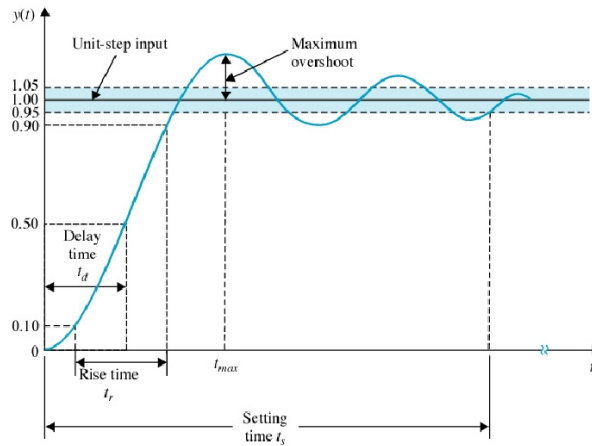


Figure 4.51: Characteristics of a unit step response. [104]

on the function used in the feedback, the maximum overshoot can occur at a later peak and can even be negative.

Delay time. The delay time, indicated with t_d , represents the time required for the step response to reach half of its final value.

Rise time. The rise time t_r is defined as the time required for the step response to rise from 10% to 90% of its final value.

Settling time. The settling time t_s indicates the time required for the step response to decrease and stay within a specified percentage of its final value (5% in the figure). In our case, the settling time can be approximated, if the damping ratio $\zeta \ll 1$, by:

$$t_s = -\frac{\ln(\text{tolerance fraction})}{\zeta\omega_n}$$

where the tolerance fraction indicates the fraction of percentage expressed above.

Steady state error. The steady state error is defined as the discrepancy between the output and the input, where the final value (steady state) is reached.

Comparison with our results

Our idea to connect the NF-kB expression with the step response was born from the considerations about negative feedback loop. In fact, two in particular are the reasons that allowed us to make this analogy in the behaviors:

1. NF-kB characterizes the transcription of a gene responsible for the production of the proteins that inhibit NF-kB activation (I κ B family, see Fig. 4.36);

- the input signal is a constant stimulus from $\text{TNF}\alpha$, $\text{IL-1}\beta$ or, like in our case, the perturbation produced by the medium change.

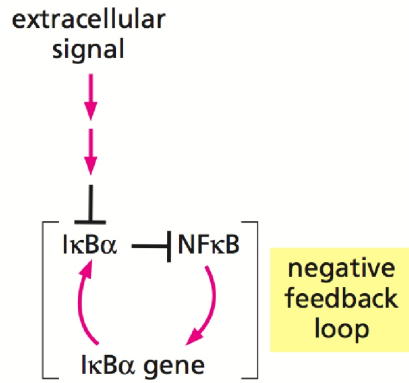


Figure 4.52: Stimulation of the transcription of $\text{I}\kappa\text{B}\alpha$ protein by activated NF- κB . [13]

The input stimulus responsible for the degradation of $\text{I}\kappa\text{B}$ is indicated in Fig. 4.57 as extracellular signal and is maintained along the loop. Converted into mathematical expressions, these two points can be represented by the informations in equation 4.20

Fit of our data

The best fit to our experimental data was made with *MINUIT*, a program written in Fortran 77 and developed in 1989 at CERN [177]. *MINUIT* is usually used to find the best values of a set of parameters, where best is defined as those values which minimize a given function fixed in the beginning by the user. This can be a general function with one or more unknown parameters; purpose of this program is to find these parameters according with the experimental data. The parameter errors will be proportional to the uncertainty in the data, and therefore measurement errors must be known in order to obtain meaningful parameters. The plot of the function containing the parameters found was realized with *gnuplot* program.

Fig. 4.53 shows the the best fit of our data developed with the functions described in the theoretical model above. We have decided to force the function for the irradiated samples to be equal to the one for sham irradiated before the time corresponding to the irradiation ($\sim 1\text{h}$). This choice has been made because there should be no differences between the response of the two samples before the irradiation occurs.

As clearly shown in the figures, the trend of our data is well approximated by a step response-like function, according to regulating behavior described

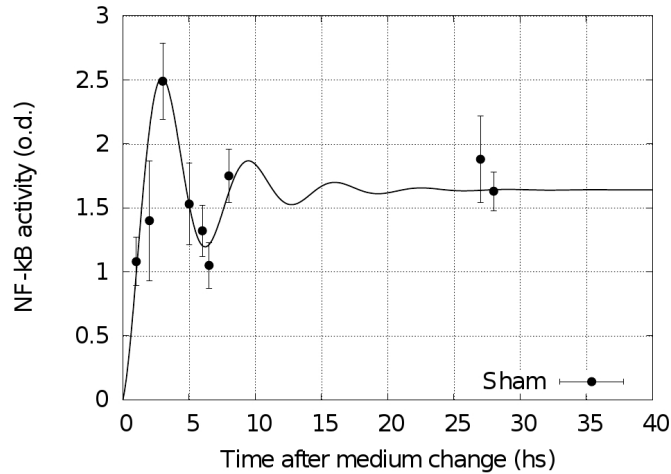


Figure 4.53: Best fit of our experimental data for sham irradiated cells using MINUIT.

previously. This is the result we expected because of the analogy between NF-kB and negative feedback amplifier previously seen. The only big difference consists on the time scale of the two processes: the MATLAB model is very rapid because of the parameters selected while the one based on our results is much slower because of the oscillation time of the mechanism, which can persist even for days.

An interpretation we have given to our model consists in the possibility that NF-kB, following a perturbation stress, is excited reaching a higher value of concentration and tries to maintain that value. This results in an oscillating trend around the final equilibrium point [107] [130] [170].

Although this association has never been done before, similar results in the trend of NF-kB concentration have been found experimentally in the literature [3] [39]. However, a big difference is given by the stronger experimental basis we obtained by using a high number of cells and the ELISA test.

Radiation exposition hypotheses

If we now plot on the same graph the curves for sham and irradiated samples (Fig. 4.55), two main differences are clearly seen:

1. the damping effect is much slower for the irradiated sample;
2. the first oscillation peak is more prominent for the sham irradiated sample;

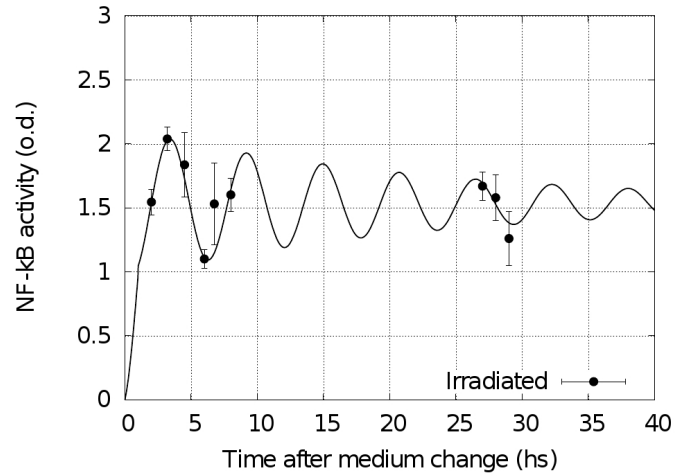


Figure 4.54: Best fit of our experimental data for irradiated cells using MINUIT.

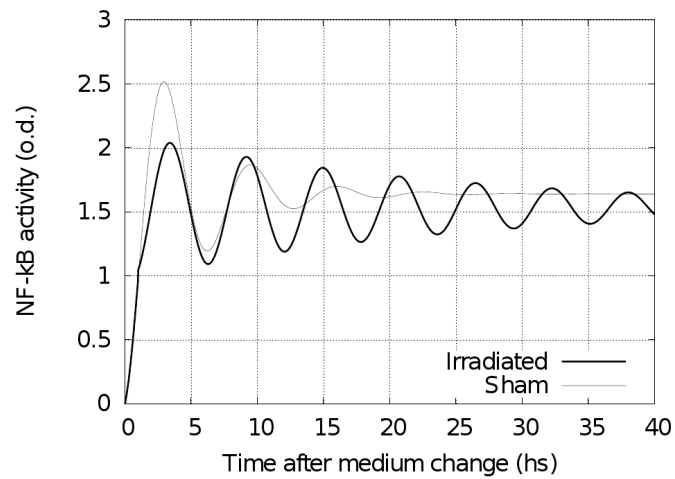


Figure 4.55: Best fit curves for sham irradiated and irradiated sample.

On the basis of these observations, we could hypothesize that a low dose irradiation keeps the oscillation of NF-kB concentration for a longer amount of time. While after 25 hours from the medium change the sham irradiated sample seems to have reached the final value, for the other one the oscillatory behavior is still dominating. Another possible interpretation concern the value of the damping ratio: since the amplitude of the first oscillation peak is smaller for the irradiated sample, the damping ratio ζ (see Fig. 4.51) is likely to be higher when a radiation exposition has occurred.

Since the dumping ratio is related to the efficacy of the amplification mechanism, a smaller value of this parameters (irradiated cells) can be related to a smaller efficiency of the regulating mechanisms, suggesting once again that the radiation can act as a perturbation that moves the systems from the equilibrium.

From our analysis the irradiated system seem to oscillate for longer time, reaching the final equilibrium condition well after 40 hours, whereas for unirradiated cells this value is reached at 15 hours.

In conclusion, this analysis is useful to explain the expression of nuclear activated NF-kB in terms of step response function. It is important to point out that these are only conclusions based on the model found with the least-squares fit, and they should be confirmed by using a higher number of points.

4.5 Receptor Expression as a function of Radiation Quality

In order to evaluate whether the different type of radiation has influence on the expression of the cytokines receptor on the cell membrane, we investigated by immunocytochemistry the pattern of expression for IL-6 and IL-8 receptors. Cells, fixed in cold 70% ethanol for 10 min at room temperature, were incubated with the monoclonal anti-human CD126 antibody (clone B-R6) at the dilution of 1:10 in a solution of 1% BSA in PBS 1X for 1 hours at room temperature.

We investigated receptor expression on AG01522 human fibroblasts sham irradiated and directly irradiated with different dosed of gamma rays and alpha particles 5 hours after irradiation or for cells conditioned with the medium collected after 20 hours form fibroblasts irradiated with different dosed of gamma rays and alpha particles.

These observations with the microscope were also confirmed by the quantitative analysis performed on the digital images randomly acquired.

Positive immunoreactive cells were observed with light microscope (Olympus BX 51) and image acquisition was carried out using a digital camera (Olympus Camedia). Digital images processed using Image Pro Plus software package (Media Cybernetics, Silver Spring, MD, USA) were converted in 16 gray scale



Figure 4.56: Example of IL-8 receptor expression obtained with immunohistochemistry analysis for fibroblast exposed at different radiation doses and in different conditions. The detailed quantification of the results are shown in the next Figures

and the brightness of at least five randomly chosen fields was calculated and expressed as arbitrary units (a.u.).

Additionally, in order to evaluate whether the presence of DMSO or c-PTIO has any influence on the expression of the receptors on the cell membrane, we investigated by immunocytochemistry the pattern of expression for this receptor 20 hours after incubation with one of the scavengers. The overall results are shown in the next set of Figures.

IL-8 receptor expression after low doses of gamma rays irradiation

In this section the results obtained for IL-8 receptors on cells directly irradiated (with gamma) and bystander are reported.

IL-6 receptor expression after low doses of gamma rays irradiation

In this section the results obtained for IL-8 receptors on cells directly irradiated(gamma) and bystander are reported .

IL-8 receptor expression after low doses of alpha particles irradiation

In this section the results obtained for IL-8 receptors on cells directly irradiated(alpha particles) are reported .

IL-6 receptor expression after low doses of alpha particles irradiation

In this section the results obtained for IL-6 receptors on cells directly irradiated(alpha particles) and bystander are reported .

The possible effect of radiation quality is presented in the next Figures.

As it is possible to see from the results shown above the effects of radiation (both direct and mediated through bystander signalling) is, if present, very small, without any possible clear indication of a dose response or of a radiation

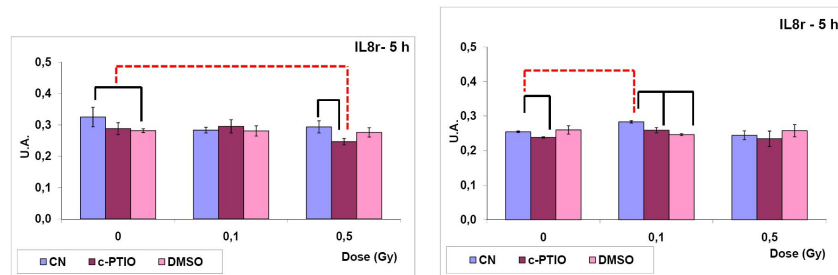


Figure 4.57: Left panel: Quantitative analysis of IL8 receptor expression from AG01522 human fibroblasts sham irradiated and directly irradiated with 0,1 Gy and 0,5 Gy of gamma rays 5 hours after irradiation; Right panel: Quantitative analysis of IL8 receptor expression from AG01522 human fibroblasts conditioned with the medium collected after 20 hours from fibroblasts irradiated with different doses of gamma rays. For each dose point an evaluation of the IL-8 receptor was performed also for cells conditioned with 20 nM of c-PTIO and 5% of DMSO. The lines above the data are guidelines to highlight the statistical significance of the results: the red dashed line represents a statistical significance ($p < 0.05$) due to radiation for the same condition, whereas the black solid line represents a statistical significance due to the different scavenger condition at the same radiation dose.

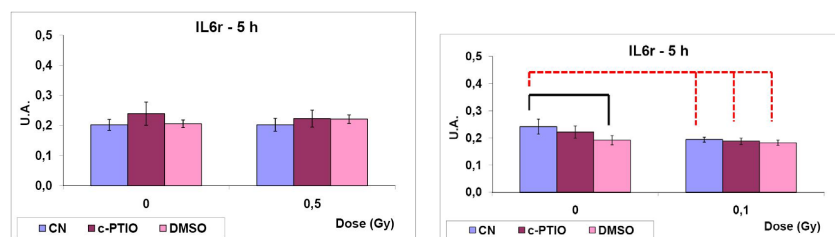


Figure 4.58: Left panel: Quantitative analysis of IL6 receptor expression from AG01522 human fibroblasts sham irradiated and directly irradiated with 0,1 Gy and 0,5 Gy of gamma rays 5 hours after irradiation; Right panel: Quantitative analysis of IL6 receptor expression from AG01522 human fibroblasts conditioned with the medium collected after 20 hours from fibroblasts irradiated with different doses of gamma rays. For each dose point an evaluation of the IL-6 receptor was performed also for cells conditioned with 20 nM of c-PTIO and 5% of DMSO. The lines above the data are guidelines to highlight the statistical significant data: the red dashed line represents a statistical significance ($p < 0.05$) due to radiation for the same condition, whereas the black solid line represents a statistical significance due to the different scavenger condition at the same radiation dose.

quality persistent effect. On the other hand, the presence of ROS and RNS scavengers seems to change the receptor profile (in terms of the covered area) in the irradiated and bystander cell, indicating a possible role for these molecules

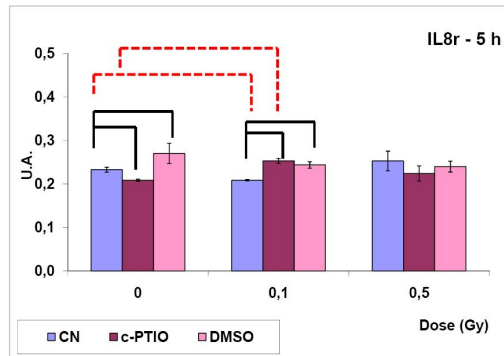


Figure 4.59: Quantitative analysis of IL8 receptor expression from AG01522 human fibroblasts sham irradiated and directly irradiated with 0,1 Gy and 0,5 Gy of alpha 5 hours after irradiation; For each dose point an evaluation of the IL-8 receptor was performed also for cells conditioned with 20 nM of c-PTIO and 5% of DMSO. The line above the data are guidelines to highlight the statistical significant data: the red dashed line represent a statistical significance ($p < 0.05$) due to radiation for the same condition, whereas the black solid line represent a statistical significance due to the different scavenger condition at the same radiation dose.

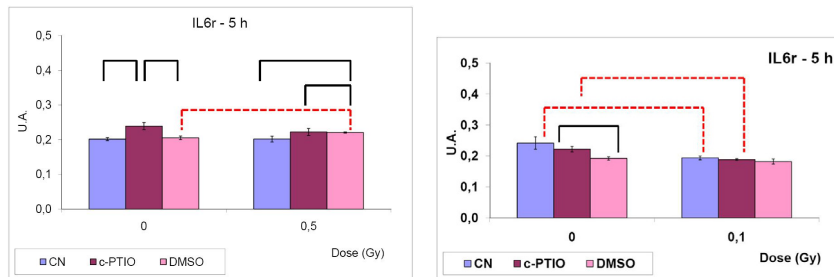


Figure 4.60: Left panel: Quantitative analysis of IL6 receptor expression from AG01522 human fibroblasts sham irradiated and directly irradiated with 0,1 Gy and 0,5 Gy of alpha particles 5 hours after irradiation; Right panel: Quantitative analysis of IL6 receptor expression from AG01522 human fibroblasts conditioned with the medium collected after 20 hours from fibroblasts irradiated with different doses of alpha particles. For each dose point an evaluation of the IL-6 receptor was performed also for cells conditioned with 20 nM of c-PTIO and 5% of DMSO. The line above the data are guidelines to highlight the statistical significant data: the red dashed line represent a statistical significance ($p < 0.05$) due to radiation for the same condition, whereas the black solid line represent a statistical significance due to the different scavenger condition at the same radiation dose.

in the pathway of receptor expression.

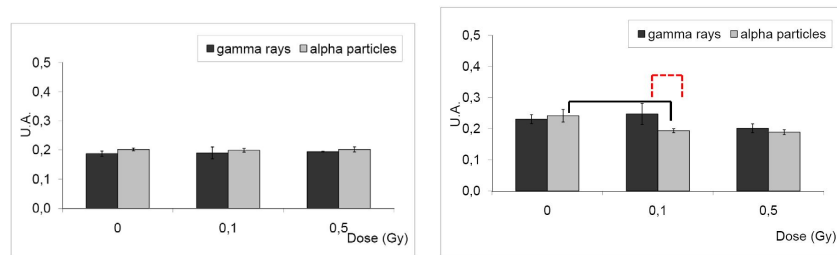


Figure 4.61: Left panel: comparison between the data obtained with gamma and alpha irradiation for IL-6 receptor for directly irradiated cells. No significant difference was found. Right panel: Comparison between the data obtained with gamma and alpha irradiation for IL-6 receptor for bystander conditioned cells. Differences in the behavior due to radiation quality effect were found for 0.1 Gy.

Chapter 5

Conclusions

The main objective of the thesis was devoted to the characterization and quantification of the induction of DNA-targeted and non-DNA-targeted molecular, cellular and multi-cellular radiobiological endpoints following irradiation of (mainly) normal human cells with different radiation qualities. The main aim of the work consisted of reaching a better understanding of the mechanisms governing the physical and biophysical pathways leading from the initial energy deposition by radiation in matter to the induction of observable radiobiological damage also at a *supra*-cellular level, with great focus on the role played by radiation quality (i.e. particle type and energy, and thus LET). General objective of the work was the characterization of the peculiar features of the biological system following the perturbation of the radiation insult: in particular we focused on the quantification of the robustness of the systems, investigating also the non-linear phenomena (such as negative feedbacks in protein expression) that might contribute to the overall stability of the systems. The investigations were carried out both experimentally and theoretically, with a continuous feedback and exchange of information and input between experimentalists and modellers: the outcomes provided fundamental information on the dependence on key conditions such as dose, time, radiation quality, cell type etc., whereas the theoretical approaches allowed us to test and validate assumptions on the underlying mechanisms, to perform predictions where the data are not easily available (e.g. at low doses and for small DNA fragments) and to suggest crucial experiments aimed to clarify specific open questions (e.g. the dependence of cytokine release on the cell number and spatial density). More specifically, we characterized the induction of DNA DSB within different fragment-size ranges experimentally and theoretically outlining the effectiveness of high-LET radiation in inducing small fragments (see Chapter 2). This reflects the clustering properties of radiation track structure and is correlated with the induction of severe damage. In the case of Nitrogen ions, we found a DSB yield per Gray equals to 81, compared to the value of 41 experimentally obtained, due to the limitations in technical methods. Furthermore, in the same chapter we investigated the effect of the uptake of in-

ternal emitters inside the cell. In particular we evaluated the dose distribution released by different cytoplasmic concentrations of the nuclides and the genomic damage (DSB, chromosomal aberration) induced by 2 different nuclides (Tritium and Nickel-63) characterized by a different spectra (and consequently different ranges) of beta particles.

Proceeding in the evolution of the biological damage, we focused our research (see Chapter 3) on the study of the cellular response due to DNA breaks, investigating in particular the phosphorylation of the hystone H2AX after exposure to different radiation qualities. The kinetics of foci formation and disappearance have been quantified both theoretically and experimentally, and a preliminary study on the foci size has been performed in case of anti protons irradiation, focusing on the damage induced at the pleateu or at the peak depth. These data have been correlated with a series of simulations realized with Geant4 program.

Concerning non-DNA-targeted damage (Chapter 4), we quantified the medium-mediated reduction of cell survival in bystander cells, which showed a significant decrease in the clonogenic survival at different time. To investigate the mechanisms underlying medium-mediated bystander damage, which are thought to be based on cell-to-cell communication via signalling molecules such as cytokines, we characterized the time- and dose-dependence of cytokine (e.g. IL-6, IL-8) concentration in the culture medium of sham-irradiated and irradiated cells, finding an initial increase followed by a saturation-like pattern at several hours after irradiation. The release, diffusion and internalization of cytokine was simulated developing an analytical model and a MC code which allows to test the basic hypothesis implemented, and to quantify the key parameters underlying the perturbation of cell communication. Furthermore with this approach it was possible to quantify some characteristic (in terms of cell communication) peculiar of the in vitro cellular system, such as the low robustness and stability of the systems, and the possible differences between the in vitro and in vivo process (e.g. signal degradation in the medium). The intrinsic characteristics of the cell signaling issue were investigated also in terms of the different activation of the NF-kB, one of the most crucial transcription factor involved in the inflammatory process. Thanks to the experimental results and the interpretation of the feedback loop that regulates the NF-kB activation (according to what found in the literature), we connected the pathway of this transcription factor with a negative feedback ideal amplifier. According to the model, when the input to the amplifier is a constant step function, the output's trend follows a characteristic behavior called *step response*. This function has as main characteristic the oscillation around a value that can coincide with the constant input, and its convergence to that value. The shape and the speed of convergence are mainly controlled by a parameter called *damping ratio*. By means of a fit of our experimental results, we hypothesized that the radiation stimulus acts reducing the value of the damping ratio.

In summary, the objective of this work was the investigation, in a reductionist fashion, of the different steps involved in the induction of the radio biological damage. The whole process of damage induction has been investigated separating the different steps of damage formation within an integrated experimental/theoretical approach, and for different radiation quality exposure. The reason for those investigation resided in the understanding of complex issue of the radiation exposure at low doses, and, more importantly, it was fun.

Bibliography

- [1] M. Belli R. Cherubini V. Dini G. Esposito W. Friedland S. Gerardi S. Molinell A. Ottolenghi² H. Paretzke G. Simon A. Campa, F. Ballarini and M. A. Tabocchini. Dna dsb induced in human cells by charged particles and gamma rays: Experimental results and theoretical approaches. *International Journal of Radiation Biology*, 81:841–854, 2005.
- [2] S.M. Bailey B.L. Marrone B.E. Lehnert A. Deshpande, E.H. Goodwin. Alpha particle-induced sister chromatid exchange in normal human lung fibroblasts: evidence for an extranuclear target. *Radiat. Res.*, 145:260–267., 1996.
- [3] M.L. Scott D. Baltimore A. Hoffmann, A. Levchenko. The ikbfn-kb signaling module: Temporal control and selective gene activation. *Science*, 298:1241–1245, 2002.
- [4] A. Halstensen P. Kierulf A. Waage, P. Brandtzaeg and T. Espevik. The complex pattern of cytokines in serum from patients with meningococcal septic shock. *J. Exp. Med.*, 169:333–338, 1989.
- [5] D.G. Alciatore. *Introduction to MechATronics and Measurement Systems*. McGraw Hill, 207.
- [6] D. Alloni, F. Ballarini, M. Belli, A. Campa, G. Esposito, W. Friedland, M. Liotta, A. Ottolenghi, and H. G. Paretzke. Modeling of dna fragmentation induced in human fibroblasts by 56fe ions. *Adv. Space Res.*, 40:1401–1407, 2007.
- [7] U. Alonn. *An Introduction to Systems Biology—Design Principles of Biological Circuit*. Chapman Hall/CRC, Boca Raton, FL, 2007.
- [8] R. M. Anderson, S. J. Marsden, E. G. Wright, M. A. Khadim, D. T. Goodhead, and C. S. Griffin. Complex chromosome aberrations in peripheral blood lymphocytes as a potential biomarker of exposure to high-let a-particles. *Int. J. Radiat. Biol.*, 76:31–42, 2000.

- [9] J.A. Aten, J. Stap, P.M. Krawczyk, C.H. van Oven, R.A. Hoebe, J. Es-sers, and R. Kanaar. Dynamics of dna double-strand breaks revealed by clustering of damaged chromosome domains. *Science*, 303:92–95, 2004.
- [10] E.I. Azzam, S.M. de Toledo, and J.B. Little. Direct evidence for the participation of gap junction-mediated intercellular communication in the transmission of damage signals from alpha-particle irradiated to nonir-radiated cells. *PNAS*, 98:473–478, 2001.
- [11] E.I. Azzam, S.M. de Toledo, and J.B. Little. Oxidative metabolism, gap junctions and the ionizing radiation-induced bystander effect. *Oncogene*, 102:7050–7057, 2003.
- [12] J. Lewis M.Raff K. Roberts P. Walter B. Alberts, A. Johnson. *Molecular Biology of the Cell*. Garland Science, 2007.
- [13] A.S. Baldwin. Nf-kb and ikk as key mediators of in ammation and onco-genic progression. *Handbook of Transcription Factor NF-kappaB*, 2007.
- [14] M. H. Barcellos-Hoff. Cancer as an emergent phenomenon in systems radiation biology. *Radiat. Environ. Biophys.*, 47:33–38, 2008.
- [15] M.H. Barcellos-Hoff. How do tissues respond to damage at the cellular level? the role of cytokines in irradiated tissues. *Radiation Research*, 150:109–120, 1998.
- [16] P.J. Barnes and M. Karin. Nuclear factor-kappab: A pivotal transcrip-tion factor in chronic in inflammatory diseases. *The New England Journal of Medicine*, 336:1066–1071, 1997.
- [17] J.S. Beckman and W.H. Koppenol. Nitric oxide, superoxide and per-oxynitrite: the good, the bad and ugly. *Am. J. Physiol. Cell. Physiol.*, 271:C1424–C1437, 1996.
- [18] M. Belli, R. Cherubini, M. Dalla Vecchia, V. Dini, G. Esposito, G. Mos-chini, O. Saporà, G. Simone, and M. A. Tabocchini. Dna fragmentation in v79 cells irradiated with light ions as measured by pfge. i experimntal results. *Int. J. Radiat. Biol.*, 284:475–483, 2002.
- [19] F. Belloni, D. Bettega, P. Calzolari, R. Cherubini, P. Massariello, and L. Tallone. Inactivation cross sections for mammalian cells exposed to charged particles: A phenomenological approach. *Radiat. Prot. Dosime-try*, 99:109–202, 2002.
- [20] O.V. Belyakov, S.A. Mitchell, D. Parikh, G. Randers-Pehrson, S.A. Marino, S.A. Amundson, C.R. Geard, and D.J. Brenner. Biological ef-fects in unirradiated human tissue induced by radiation damage up to 1 mm away. *PNAS*, 102:4203–1420, 2005.

- [21] L. Von Bertalanffy. The theory of open systems in physics and biology. *Science*, 111:23–29, 1950.
- [22] L. Von Bertalanffy. *General Systems Theory*. George Braziller, 1968.
- [23] K. E. Boulding. General systems theory-the skeleton of science. *Management Sci.*, 3:197–208, 1950.
- [24] M.A. Brach, R. Hass, M.L. Sherman, H. Gunji, R. Weichselbaum, and D. Kufe. Ionizing radiation induces expression and binding activity of the nuclear factor kb. *J. Clin. Invest.*, 88:691–695, 1991.
- [25] D.J. Brenner. The linear-quadratic model is an appropriate methodology for determining isoeffective doses at large doses per fraction. *Seminars in Radiation Oncology*, 18:234–239, 2008.
- [26] D.J. Brenner, R. Doll, D.T. Goodhead, E.J. Hall, C.E. Land, J.B. Little, J.H. Lubin, D.L. Preston, R.J. Preston, J.S. Puskin, E. Ron, R.K. Sachs, J.M. Samet, R.B. Setlow, and M. Zaider. Cancer risks attributable to low doses of ionizing radiation: Assessing what we really know. *PNAS*, 100(24):13761–13766, 2003.
- [27] S. Burdak-Rothkamm, K. Rothkamm, and K.M. Prise. Atm acts downstream of atr in the dna damage response signalling of bystander cells. *Cancer Res.*, 68:7059–7065, 2008.
- [28] J. Caamano and C.A. Hunter. Nf-kb family of transcription factors: Central regulators of innate and adaptive immune functions. *Clinical Microbiology Reviews*, 15:414–429, 2002.
- [29] A. Campa, D. Alloni, F. Antonelli, F. Ballerini, M. Belli, V. Dini, G. Esposito, A. Facoetti, W. Friedland, and M. A. Tabocchini. Dna fragmentation induced in human fibroblasts by 56fe ions: Experimental data and monte carlo simulations. *Radiat. Res.*, 171:438–445, 2009.
- [30] A. Campa, F. Ballarini, M. Belli, R. Cherubini, V. Dini, G. Esposito, W. Friedland, S. Gerardi, S. Molinelli, and M. A. Tabocchini. Dna dsb induced in human cells by charged particles and gamma rays: Experimental results and theoretical approaches. *Int. J. Radiat. Biol.*, 81:841–854, 2005.
- [31] F. Carlotti, R. Chapman, S.K. Dower, and E.E. Qwarnstrom. Activation of nuclear factor kb in single living cells. *The Journal of Biological Chemistry*, 274:7941–3794, 1999.
- [32] C.H. Chou, P.J. Chen, P.H. Lee, A.L. Cheng, H.C. Hsu, and J. C.H. Cheng. Radiation-induced hepatitis b virus reactivation in liver mediated by the bystander effect from irradiated endothelial cells. *Clin Cancer Res*, 13:851–857, 2007.

- [33] C.H. Chou, S.U. Chen, and J.C.H. Cheng. Radiation-induced interleukin-6 expression through mapk/p38/nf-kb signaling pathway and the resultant antiapoptotic effect on endothelial cells through mcl-1 expression with sil6-rna. *Int. J. Radiation Oncology Biol. Phys.*, 75:1553–1561, 2009.
- [34] Cutaia Claudia. Dipendenza del danno al dna da distribuzione subcellulare di radionuclidi emittitori di beta di bassa energia. *Master thesis, Supervisor: Ottolenghi A, Alloni D, Mariotti L*, 46:383–94, 2010.
- [35] J. E. Coogle. Effetti biologici delle radiazioni. *Ed. Minerva Medica*, 1998.
- [36] Anderson J. A. Harper J. V. Cucinotta F. A., Pluth J. M. and O’Neill P. Biochemical kinetics model of dsb repair and induction of gamma h2ax foci by non-homologous end joining. *Radiation Research*, 169:217–22, 2008.
- [37] Alloni D. Radiation biophysics modelling: track structure theoretical bases and monte carlo simulations of dna damage. *Ph.D thesis*, 2007.
- [38] M. Belli G Esposito L. Mariotti M. Liotta W. Friedland H. Paretzke D. Alloni, A. Campa and A Ottolenghi. Monte carlo evaluation of dna fragmentation spectra induced by different radiation qualities. *Micros 2009*, book of abstrac:12, 2009.
- [39] S.L. Werner C.S. Huang A. Hoffmann .D. Kearns, S. Basak. Ikbalpha provides negative feedback to control nf-kb oscillations, signaling dynamics, and inflammatory gene expression. *The Journal of Cell Biology*, 173:659–664, 2006.
- [40] Albert Van der Kogel and Micheal Joiner. *Basic Clilical Radiobiology*. Hodder Arnold, 2009.
- [41] N. Desai, E. Davis, P. O’Neill, M. Durante, F. A. Cucinotta, and H. Wu. Immunofluorescence detection of clustered h2ax foci induced by hze-particle. *Radiation Research*, 2005.
- [42] Y. Devary, C. Rosette, J.A. Di Donato, and M. Karin. Nf-kappa b activation by ultraviolet light not dependent on a nuclear signal. *Science*, 261:1442– 1445, 1993.
- [43] M. Dingfelder, M. Inokuti, and H. G. Paretzke. Inelastic-collision cross sections of liquid water for interactions of energetic protons. *Radiat. Phys. Chem.*, 59:255–275, 2000.
- [44] Newman DJi. A natural products chemist looks at the bystander effect. *Mutation Research*, 597:39–42, 2006.

- [45] M. Durante, K. George, G. Gialanella, G. Grossi, C. La Tessa, L. Manti, J. Miller, M. Pugliese, P. Scampoli, and F. A. Cucinotta. Cytogenetic effects of high-energy iron ions: Dependence on shielding thickness and material. *Radiat. Res.*, 164:571–576, 2005.
- [46] Abele A et al. Branching ratios for p^- p annihilation at rest into two-body final states. *Nuclear Physics A*, 679(2):563–571, 2001.
- [47] Ashley et al. Dynamic changes in rad51 distribution on chromatin during meiosis in male and female vertebrates. *Chromosoma*, 104:19–28, 1995.
- [48] Ashley et al. p53 binding protein 1 (53bp1) is an early participant in the cellular response to dna double-strand breaks. *J. Cell Biol.*, 151:1381–1390, 2000.
- [49] Bassler et al. The antiproton depth-dose curve in water. *Physics in Medicine and Biology*, 53:793–805, 2008.
- [50] Costes et al. Spatiotemporal characterization of ionizing radiation induced dna damage *foci* and their relation to chromatin organization. *Mutation Research*, 704:78–87, 2010.
- [51] Costes S. et al. Image-based modelling reveals dynamic redistribution of dna damage into nuclear sub-domains. *Plos Computation Biology*, 166:31–38, 2007.
- [52] Folkard et al. A charged-particle microbeam : I. development of an experimental system for targeting cells individually with counted particles. *International Journal of Radiation Biology*, 72(4):375–385, 1997.
- [53] Goodead et al. Report of the committee examining radiation risks of internal emitters (cerrie). http://www.cerrie.org/pdfs/cerrie_report_e-book.pdf, 2005.
- [54] Haff et al. Nuclear *foci* of mammalian rad51 recombination protein in somatic cells after dna damage and its localization in synaptonemal complexes. *Proc. Natl. Acad. Sci.*, 92:2298–2302, 1995.
- [55] Holzscheiter et al. The biological effectiveness of antiproton irradiation. *Radiotherapy and Oncology*, 86:233–242, 2006.
- [56] Kavanagh J et al. Experimental setup and first measurement of dna damage induced along and around an antiproton beam. *Eur. Phys. J D.*, Published on line, 2010.
- [57] Leatherbarrow et al. Induction and quantification of γ -h2ax *foci* following low and high let-irradiation. *International Journal of Radiation Biology*, 82(2):111–118, 2006.

- [58] Lobrich M et al. Gamma h2ax *foci* analysis for monitoring dna double strand breaks repair. strengths, limitations and optimization. *Cell Cycle*, 9(4):662–669, 2010.
- [59] Maser et al. hmre11 and hrad50 nuclear *foci* are induced during the normal cellular response to dna double-strand breaks. *Mol. Cell. Biol.*, 17:6087–6096, 1997.
- [60] Nelms et al. In situ visualization of dna double-strand break repair in human fibroblasts. *Science*, 280:590–592, 1998.
- [61] Nikjoo et al. Computational modelling of lowenergy electron-induced dna damage by early physical and chemical events. *Int. J. Radiat. Biol.*, 1997.
- [62] Nikjoo et al. Computational approach for determining the spectrum of dna damage induced by ionizing radiation. *Radiat. Res.*, 2001.
- [63] Rogakou et al. Dna double stranded breaks induce histone h2ax phosphorylation on serine 139. *J. Biol. Chem.*, 273(4):5858–5868, 1998.
- [64] Rogakou et al. Megabase chromatin domains involved in dna double-strand breaks in vivo. *J Cell Biol.*, 146(5):905–16, 1999.
- [65] Salles B et al. The loss of gamma h2ax signal is a marker of dna double strand breaks repair only at low levels of dna damage. *Cell Cycle*, 5(10):1116–1122, 2006.
- [66] Short et al. Dna damage response at low radiation doses. *Radiation Research*, 164:292–302, 2005.
- [67] W. Friedland et al. Monte carlo simulation of the production of short dna fragments by low-linear energy transfer radiation using higher-order dna models. *Radiat. Res*, 150:170–182, 1998.
- [68] Salazar et la. Multisite protein phosphorylation - from molecular mechanisms to kinetic models. *FEBS Journall*, 276:3177–3198, 2009.
- [69] A. Ottolenghi F. Ballarini, M. Biaggi and O. Sapura. Cellular communication and bystander effects: a critical review for modelling low-dose radiation action. *Mutation Research*, 501:1–12, 2002.
- [70] L Mariotti R Nano A Ottolenghi F Ballarini, A Facoetti. Cellular communication and non-targeted effects: Modelling approaches. *Advances in Space Research*, 44:917–925, 2009.
- [71] B.C. Kuo F. Golnaraghi. *Automatic Control Systemsl*. John Wiley and Sons, 2010.

- [72] A. Facoetti, L. Mariotti, F. Ballarini, A. Bertolotti, R. Nano, F. Pasi, E. Ranza, and A. Ottolenghi. Experimental and theoretical analysis of cytokine re-lease for the study of radiation-induced bystander effect. *Int. J. Radiat. Biol.*, 85:690–699, 2009.
- [73] A.A. Fowler, B.J. Fisher, and R Natarajan S.S. Ghosh S. Ghosh L.B. Sweeney, T.J. Wallace. Nitric oxide regulates interleukin-8 gene expression in acti- vated endothelium by inhibiting nf-kb binding to dna: effects on endothelial function. *Biochem. Cell Biol.*, 77:201–208, 1999.
- [74] D. Frankenberg, H. J. Brede, U. J. Schrewe, C. Steinmetz, M. Frankenberg-Schwager, G. Kasten, and E. Pralle. Induction of dna double-strand breaks by 1h and 4he ions in primary human skin fibroblasts in the let range of 8 to 124 kev mm²¹. *Radiat. Res.*, 284:540–549, 1999.
- [75] W. Friedland, P. Jacob, P. Bernhardt, H. G. Paretzke, and M. Dingfelder. Simulation of dna damage after proton irradiation. *Radiat. Res.*, 159:401–410, 2003.
- [76] W. Friedland, P. Jacob, H. G. Paretzke, M. Merzagora, and A. Ottolenghi. Simulation of dna fragment distributions after irradiation with photons. *Radiat. Environ. Biophys.*, 150:39–47, 1999.
- [77] W. Friedland, P. Jacob, H. G. Paretzke, A. Ottolenghi, F. *in vitro*, and M. Liotta. Simulation of light ion induced dna damage patterns. *Radiat. Prot. Dosimetry*, 122:116–120, 2006.
- [78] W. Friedland, P. Jacob, H. G. Paretzke, and J. Stork. Monte carlo simulation of the production of short dna fragments by low-linear energy transfer radiation using higher-order dna models. *Radiat. Res.*, 150:170–182, 1998.
- [79] Ilaikis G. Gamma h2ax in recognition and signaling of dna double-strand breaks in the context of chromatin. *Nucleic Acids Reserch*, 36:5678–5694, 2008.
- [80] B. R. Gaines. General systems research: Quo vadis? *Gen Syst.*, 24:1–9, 1979.
- [81] K. George, M. Durante, H. Wu, V. Willingham, and F. A. Cucinotta. In vivo and in vitro measurements of complex-type chromosomal exchanges induced by heavy ions. *Adv. Space Res*, 31:1525–1535, 2003.
- [82] S. Ghosh. The nf-kb pathway: A paradigm for inducible gene expression. *Handbook of Transcription Factor NF-kappaB*, 2007. CrC Press.
- [83] M.E. Ginn-Pease and R.L. Whisler. Redox signals and nf-kb activation in t cells. *Free Radical Biology Medicine*, 22:346–361, 1998.

- [84] G. Gloire, S. Legrand-Poels, and J. Piette. Nf-kb activation by reactive oxygen species: Fteen years later. *Biochemical Pharmacology*, 72:1493–1505, 2006.
- [85] L. Gray and T. E. Kalogeropoulos. Possible biomedical applications of antiproton beams: Focused radiation transfer. *Radiation Research*, 97(2):246–252, 1984.
- [86] F.R. Greten and M. Karin. The ikk/nf-kb activation pathway - a target for prevention and treatment of cancer. *Cancer LETters*, 206:193–199, 2004.
- [87] Cateau H and Tanaka S. Kinetic analysis of multisite phosphorylation using analytic solutions to michaelis-menten equations. *J. Theor. Biol*, 217:1–14, 2002.
- [88] Eric Hall and Amato Giaccia. *Radiobiology for the radiologist*. Lippincott Williams Wilkins, 2009.
- [89] W. Han, L. Wu, S. Chen, L. Bao, L. Zhang, E. Jiang, Y. Zhao, A. Xu, T.K. Hei, and Z. Yu. Constitutive nitric oxide acting as a possible inter-cellular signaling molecule in the initiation of radiation-induced dna double strand breaks in non-irradiated bystander cells. *Oncogene*, 26:2330–2339, 2007.
- [90] F. Hayot and C. Jayaprakash. Nf-kb oscillations and cell-to-cell variability. *Journal of Theoretical Biology*, 240:583–591, 2006.
- [91] T.K. Hei, H. Zhou, V.N. Ivanov, M. Hong, H.B. Lieberman, D.J. Brenner, S.A. Amundson, and C.R. Geard. Mechanism of radiation-induced bystander effects: A unifying model. *Journal of Pharmacy and Pharmacology*, 60:943–950, 2008.
- [92] M.A. Hill, D.L. Stevens, M. Kadhim, M. Blake-James, A.J. Mill, and T. Goodhead. Experimental techniques for studying bystander effects in vitro by high and low-let ionising radiation. *Radiation Protection Dosimetry*, 122:260–265, 2006.
- [93] Høglund and Stenerlow. Induction and rejoining of dna double-strand breaks in normal human skin fibroblasts after exposure to radiation of different linear energy transfer: Possible roles of track structure and chromatin organization. *Radiat. Res*, 155:818–823, 2001.
- [94] W. R. Holley and A. Chatterjee. Clusters of dna damage induced by ionizing radiation: Formation of short dna fragments. *Radiat. Res.*, 145:188–199, 1996.
- [95] <http://www.celprogen.com>.

- [96] [http://www.com/pathways/nk-kappab signaling.jsp](http://www.com/pathways/nk-kappab%20signaling.jsp). Cellsignal. 2008.
- [97] <http://www.epa.gov/radiation/radionuclides/cobalt.html>.
- [98] B. Hu, L. Wu, W. Han, L. Zhang, S. Chen, A. Xu, T.K. Hei, and Z. Yu. The time and spatial effects of bystander response in mammalian cells induced by low dose radiation. *Carcinogenesis*, 27:245–251, 2005.
- [99] L. Huang, A.R. Snyder, and W.F. Morgan. Radiation-induced genomic instability and its implications for radiation carcinogenesis. *Oncogene*, 22:5848–5854, 2003. 22.
- [100] Y. Ibuki, S. Mizuno, and R. Goto. Gamma-irradiation-induced dna damage enhances no production via nf-kb activation in raw264. *Biochemica et Bio- physica Acta*, 1593:159–167, 2003.
- [101] A.E.C. Ihekweba, D.S. Broomhead, R. Grimley, N. Benson, M.R.H. White, and D.B. Kell. Synergistic control of oscillations in the nf-kb signalling pathway. In *IEE Proc.-Syst. Biol*, volume 152, pages 153–160, 2005.
- [102] K.N. Islam, Y. Kayanoki, H. Kaneto, K. Suzuki, M. Asahi, J. Fujii, and N. Taniguchi. Tgf-beta1 triggers oxidative modifications and enhances apoptosis in hit cells through accumulation of reactive oxygen species by suppression of catalase and glutathione peroxidase. *Free. Radic. Biol. Med.*, 22:1007–1017, 1997.
- [103] V.N. Ivanov, H. Zhou, S.A. Ghandhi, T.B. Karasic, B. Yaghoubian, S.A. Amundson, and T.K. Hei. Radiation-induced bystander signaling pathways in human fibroblasts: A role for interleukin-33 in the signal transmission. *Cellular Signalling*, 22:1076–1087, 2010.
- [104] R. Iyer and B.E. Lehnert. Factors underlying the cell growth-related bystander responses to alpha particles. *Oncogene*, 27:1290–1298, 2000.
- [105] A. Jablonski. Über den Mechanismus der photolumineszenz von Farbstoffphosphoren. *Z. Phys*, 94:38–46, 1935.
- [106] Sokolnikov M, Khokhryakov VV, Vasilenko E, Jacob P, Meckbach R. Lung cancer risk of mayak workers: modelling of carcinogenesis and bystander effect. *Radiat Environ Biophys.*, 46:383–94, 2007.
- [107] A. Jain, C. Blum, and V. Subramaniam. Fluorescence lifetime spectroscopy and imaging of visible fluorescent proteins. *Advances in Biomedical Engineering*, 2009. Elsevier.
- [108] M.C. Joiner. Quantifying cell killing and cell survival basic clinical radiobiology. *Hodder Arnold*, 2002.

- [109] M.C. Joiner, B. Marples, and P. Lambin. Low-dose hypersensitivity: Current status and possible mechanisms. *Int J Radiat Oncol Biol Phys*, 49:379–389, 2001.
- [110] Suzuki K Matsuda N Kodama S Suzuki M Nagata K Kinashi Y Masunaga S Ono K Watanabe M. Kashino G, Prise KM. Effective suppression of bystander effects by dms0 treatment of irradiated cho cells. *J Radiat Res*, 48:327–333, 2007.
- [111] Jenrow KA Ryu S Kim JH, Brown SL. Mechanisms of radiation-induced brain toxicity and implications for future clinical trials. *Journal of Neurooncology*, 87:279–286, 2008.
- [112] J.R. Lakowicz. *Principles of Fluorescence Spectroscopy*. Springer, 2006.
- [113] J.R. Lazutka and S. Rudaitiene. Modulation by novobiocin of sister-chromatid exchanges induced by tumor necrosis factor in human lymphocytes. *Mutation Research*, 268:217–221, 1992.
- [114] J.K. Leach, S.M. Black, R.K. Schmidt-Ullrich, and R.B. Mikkelsen. Activation of constitutive nitric-oxide synthase activity is an early signaling event induced by ionizing radiation. *The Journal of Biological Chemistry*, 277:15400–15406, 2002.
- [115] R. Lee, E. Nasonova, and S. Ritter. Chromosome aberrations yields and apoptosis in human lymphocytes irradiated with feions of differing let. *Rad. Prot. Dos.*, 35:268–275, 2005.
- [116] B.E. Lehnert and E.H. Goodwin. Extracellular factor(s) following exposure to a particles can cause sister chromatid exchanges in normal human cells. *Cancer Research*, 57:2164–2171, 1997.
- [117] B.E. Lehnert and E.H. Goodwin. Extracellular factor(s) following exposure to a particles can cause sister chromatid exchanges in normal human cells. *Cancer Research*, 57:2164–2171, 1997.
- [118] B. Lewin. Il gene. *Zanichelli*, 2006.
- [119] D.A. Lewis, B.M. Mayhugh, Y. Qin, K. Trott, and M.S. Mendoca. Production of delayed death and neoplastic transformation in cgl1 cells by radiation- induced bystander effects. *Radiation Research*, 156:251–258, 2002.
- [120] T. Lipniacki, P. Paszek, A.R. Brasier, B. Luxon, and M. Kimmel. Mathematical model of nf-kb regulatory module. *Journal of Theoretical Biology*, 228:195– 215, 2004.
- [121] J.B. Little. Radiation carcinogenesis. *Carcinogenesis*, 21:397–404, 2000. 21 (3):.

- [122] Cooper P. K. Lobrich, M. and B. Rydberg. Joining of correct and incorrect dna ends at double-strand breaks produced by high-linear energy transfer radiation. *Radiation Research*, 150:619–626, 2000.
- [123] S.A. Lorimore, P.J. Coates, and E.G. Wright. Radiation-induced genomic instability and bystander effects: inter-related nontargeted effects of exposure to ionizing radiation. *Oncogene*, 4:7058–7069, 2003.
- [124] F.M. Lyng, C.B. Seymour, and C. Mothersill. Production of a signal by irradiated cells which leads to a response in unirradiated cells characteristic of initiation of apoptosis. *British Journal of Cancer*, 83:1223–1230, 2000.
- [125] M. Dalla Vecchia V. Dini G. Moschini C. Signoretti G. Simone M. A. Tabocchini P. Tiveron M. Belli, R. Cherubini. Dna dsb induction and rejoining in v79 cells irradiated with light ions: a constant field gel electrophoresis study. *Int. J. Rad. Biology*, 76:1095–1104, 2000.
- [126] P. Ma, X. Cui, S. Wang, J. Zhang, E.V. Nishanian, W. Wang, R.A. Wesley, and R.L. Danner. Nitric oxide post-transcriptionally up-regulates lps-induced il-8 expression through p38 mapk activation. *Journal of Leukocyte Biology*, 76:278–287, 2004.
- [127] Leonardi S Tanori M Rebessi S Di Majo V Pazzaglia S Toni MP Pimpinella M Covelli V Mancuso M, Pasquali E and Saran A. Oncogenic bystander radiation effects in patched heterozygous mouse cerebellum. *PNAS*, 105:12445–12450, 2008.
- [128] L. Mariotti, A. Facchetti, D. Alloni, A. Bertolotti, E. Ranza, and A. Ottolenghi. Effects of ionizing radiation on cell-to-cell communication. *Radiation Research*, 174:280–289, 2010.
- [129] N. Mohan and M.L. Meltz. Induction of nuclear factor kb after low-dose ionizing radiation involves a reactive oxygen intermediate signaling pathway. *Radiation Research*, 140:97–104, 1994.
- [130] A.M. Monk. Oscillatory expression of hes1, p53, and nf-kb driven by transcriptional time delays. *Current Biology*, 13:1409–1413, 2003.
- [131] C. Mothersill and C. Seymour. Radiation-induced bystander effects: Past history and future direction. *Radiation Research*, 155:759–767, 2001.
- [132] V. Bottero C. Didelot P. Van Houtte J. Gerard J. Peyron N N. Magne, R. Toillon. Nf-kb modulation and ionizing radiation: mechanisms and future directions for cancer treatment. *Cancer LETters*, 231:158–168, 2006.

- [133] S. Nagar, L.E. Smith, and W.F. Morgan. Characterization of a novel epigenetic effect of ionizing radiation: the death inducing effect. *Cancer Research*, 63:324–328, 2003.
- [134] H. Nagasawa and J.B. Little. Induction of sister chromatid exchanges by extremely low doses of alpha-particles. *Cancer Research*, 52:6394–6396, 1992. 52.
- [135] P.K. Narayanan, K.E.A. LaRue, E.H. Goodwin, and B.E. Lehnert. Alpha particles induce the production of interleukin-8 by human cells. *Radiation Research*, 152:57–63, 1999.
- [136] C. Nathan and M. Sporn. Cytokines in context. *The Journal of Cell Biology*, pages 981–986, 1991.
- [137] D. E. Nelson, A.E.C. Ihekweaba, M. Elliott, J.R. Johnson, C.A. Gibney, B.E. Foreman, G. Nelson, V. See, C.A. Horton, D.G. Spiller, S.W. Edwards, H.P. McDowell, J.F. Unitt, E. Sullivan, R. Grimley, N. Benson, D. Broomhead, D.B. Kell, and M.R.H. White. Oscillations in nf-kb signaling control the dynamics of gene expression. *Science*, 306:704–708, 2004.
- [138] H. C. Newman, K. M. Prise, M. Folkard, and B. D. Michael. Dna double-strand break distributions in x-ray and a-particle irradiated v79 cells: Evidence for non-random breakage. *Int. J. Radiat. Biol.*, 71:347–363, 1997.
- [139] S.M.E. Nugent, C.E. Mothersill, C. Seymour, B. McClean, F.M. Lyng, and J.E.J. Murphy. Increased mitochondrial mass in cells with functionally compromised mitochondria after exposure to both direct radiation and bystander factors. *Radiation Research*, 168:134–142, 2007.
- [140] M. A. O'Malley and J. Dupre. Fundamental issues in systems biology. *Bioessays*, 27:1270–1276, 2005.
- [141] A. Ottolenghi, M. Merzagora, L. Tallone, M. Durante, H. G. Paretzke, and W. E. Wilson. The quality of dna double-strand breaks: A monte carlo simulation of the end-structure of strand breaks produced by protons and alpha particles. *Radiat. Environ. Biophys.*, 34:239–244, 1995.
- [142] E.H. Goodwin B.E. Lehnert P. Narayanan, K.E.A. LaRue. Alpha particle-induced sister chromatid exchange in normal human lung fibroblasts: evidence for an extranuclear target. *Radiat. Res.*, 152:57–64, 1999.
- [143] Gotein M Paganetti H and Parodi K. A measurement of the local energy deposition by antiprotons coming to rest in tissue-like material. *Phys. Med. Biol.*, 30:1297–1232, 1985.

- [144] W.B. Parsons, C.H. Watkins, G.L. Pease, and D.S. Childs. Changes in sternal bone marrow following roentgen-ray therapy to the spleen in chronic granulo- cytic leukaemia. *Cancer*, 7:179–189, 1954. 7.
- [145] M. Pinto, K. M. Prise, and B. D. Michael. A monte carlo model of dna double-strand break clustering and rejoining kinetics for the analysis of pulsed-field gel electrophoresis data. *Radiat. Res.*, 162:453–463, 2004.
- [146] A. L. Ponomarev and R. K. Sachs. Radiation breakage of dna: a model based on random-walk chromatin structure. *J. Math. Biol.*, 43:356–376, 2001.
- [147] A.V. Prasad, N. Mohan, B. Chandrasekar, and M.L. Meltz. Activation of nuclear factor kappa b in human lymphoblastoid cells by low-dose ionizing radiation. *Radiation Research*, 138:367–372, 1994.
- [148] K.M. Prise, O.V. Belyakov, M. Folkard, and B.D. Michael. Studies of bystander effects in human broblasts using a charged particle microbeam. *Int J Radiat Biol*, 74:793–798, 1998.
- [149] K.M. Prise and J.M. O’Sullivan. Radiation-induced bystander signalling in cancer therapy. *Nature reviews*, 9:351–360, 2009.
- [150] K.M. Prise, G. Schettino, M. Folkard, and K.D. Held. New insights of cell death from radiation exposure. *Lancet Oncol.*, 6:520–528, 2005. 6.
- [151] M.B. Sowa Resat and W.F. Morgan. Radiation-induced genomic instability: A role for secreted soluble factors in communicating the radiation response to non-irradiated cells. *Journal of Cellular Biochemistry*, 92:1013–1019, 2004. 92:.
- [152] E.P. Rogakou, D.R. Pilch, A.H. Orr, V.S. Ivanova, and W.M. Bonner. Dna double-stranded breaks induce histone h2ax phosphorylation on serine 139. *The Journal of Biological Chemistry*, 273:5858–5868, 1998. 273, 10:.
- [153] B. Rydberg. Clusters of dna damage induced by ionizing radiation: Formation of short dna fragments. *Radiat. Res.*, 145:200–209, 1996.
- [154] R. K. Sachs, A. L. Ponomarev, P. J. Hahnfeldt, and L. R. Hlatky. Locations of radiation-produced dna double strand breaks along chromosomes: A stochastic cluster process formalism. *Math. Biosc.*, 159:165–187, 1999.
- [155] D. Salvemini, T.P. Misko, J.L. Masferrer, K. Seibert, and M.G. Currie. Nitric oxide activates cyclooxygenase enzymes. *Proc. Natl. Acad. Sci.*, 90:7240–7244, 1993.

- [156] J.A. Schmid, A. Birbach, R. Hofer-Warbinek, M. Pengg, U. Burner, P.G. Furtmuller, B.R. Binder, and R. de Martin. Dynamics of nf-kb and ikbalph studied with green fluorescent protein (gfp) fusion proteins. *The Journal of Biological Chemistry*, 275:7035–1704, 2000.
- [157] R. Schreck, P. Rieber, and P.A. Baeuerle. Reactive oxygen intermediates as appar- ently widely used messengers in the activation of the nf-kappa b transcription factor and hiv-1. *EMBO J*, 10:2247–2258, 1991.
- [158] R. Sen and D. Baltimore. Multiple nuclear factors interact with the immunoglob- ulin enhancer sequences. *Cell*, 1986.
- [159] C. E. Shannon. A mathematical theory of communication. *Bell Syst. Tech.*, 27:379–423, 1948.
- [160] C. Shao, M. Folkard, B.D. Michael, and K.M. Prise. Targeted cyto- plasmic irradiation induces bystander responses. *PNAS*, 101:3495–1350, 2004.
- [161] C. Shao, M. Folkard, and K.M. Prise. Role of tgf-1beta and nitric oxide in the bystander response of irradiated glioma cells. *Oncogene*, 27:434–440, 2008.
- [162] C. Shao, V. Stewart, M. Folkard, B.D. Michael, and K.M. Prise. Ni- tric oxide- mediated signaling in the bystander response of individually targeted glioma cells. *Cancer Research*, 63:8437–8442, 2003.
- [163] A. Hoffmann S.L. Werner, D. Barken. Stimulus specificity of gene expres- sion programs determined by temporal control of ikk activity. *Science*, 309:1857–1861, 2005.
- [164] Bentzen SM. Preventing or reducing late side effects of radiation therapy: radiobiology meets molecular pathology. *Nature Review Cancer*, 6:702– 713, 2006.
- [165] E.W. Son, C.K. Cho, D.K. Rhee, and S. Pyo. Inhibition of alpha- irradiation induced adhesion molecules and no production by alginate in human endothelial cells. *Arch. Pharm. Res.*, 24:466–471, 2001.
- [166] J.W.T. Spinks and R.J. Woods. *An Introduction to Radiation Chemistry*. John Wiley and Sons, 1990.
- [167] Z. Szallasi, J. Stelling, and V. Perival. *System Modelling in Cell Biology*. From Concepts to Nuts and Bolts. MIT Press, Cambridge, 2006.
- [168] L. Tartier, S. Gilchrist, S. Burdak-Rothkamm, M. Folkard, and K.M. Prise. Cy- toplasmic irradiation induces mitochondrial-dependent 53bp1 protein relo- calization in irradiated and bystander cells. *Cancer Re- search*, 67:5872– 5879, 2007.

- [169] V.J. Thannickal and B.L. Fanburg. Reactive oxygen species in cell signaling. *Am. J. Physiol. Lung Cell Mol. Physiol.*, 279:1005–1028, 2000.
- [170] A.J. Ting and D. Endy. Decoding nf-kb signaling. *Science*, 298:1189–1190, 2002.
- [171] H. Tsujii, T. Kamada, M. Baba, H. Tsuji, H. Kato, S. Kato, S. Yamada, S. Yasuda, T. Yanagi, and J. Mizoe. Clinical advantages of carbon-ion radiotherapy. *New J. Phys.*, 10:1–16, 2008.
- [172] Friedland W Jacob P Ottolenghi A Paretzke HG Valota A, Ballarini F. Modelling study on the protective role of oh radical scavengers and dna higher-order structures in induction of single- and double-strand break by gamma-radiation. *Int J Radiat Biol.*, 79:643–53, 2003.
- [173] L.H. Villarete and D.G. Remick. Nitric oxide regulation of il-8 expression in human endothelial cells. *Biochemical and Biophysical Research Communication*, 211:671–676, 1995.
- [174] Davide Volpi. Perturbation mechanisms of protein’s signalling induced by low doses of gamma irradiation. *Master thesis, Supervisor: Ottolenghi A, Mariotti L, Cappelletti D.*, 46:383–94, 2010.
- [175] Ace Collaboration website. <http://public.web.cern.ch/public/en/research/ace-en.html>.
- [176] Geant4 website. <http://geant4.cern.ch/>.
- [177] MINUIT website. <http://lcgapp.cern.ch/project/cls/work-packages/mathlibs/minuit/index.html>.
- [178] S.C. West. Molecular views of recombination proteins and their control. *Nat Rev Mol Cell Biol*, 4:435–45, 2003. 4 (6):.
- [179] B.G. Wouters and A.C. Begg. Irradiation induced damage and the dna damage response. *Basic clinical radiobiology*, 2002. Hodder Arnold.
- [180] Tadashi Fujita Nobuki Arai Ryuji Hayashi Jun Araya Shoko Matsui Naohiro Yamashita Eiji Sugiyama Yoshimasa Yoshida, Muneharu Maruyama and Masashi Kobayashi. Reactive oxygen intermediates stimulate interleukin-6 production in human bronchial epithelial cells. *Am J Physiol Lung Cell Mol Physiol*, 276:L900–L908, 1999.
- [181] H. Yue, M. Brown, J. Knowles, H. Wang, D.S. Broomhead, and D.B. Kellab. Insights into the behavior of systems biology models from dynamic sensitivity and identifiability analysis: A case study of an nf-kb signalling pathway. *Mol. BioSyst.*, 2:640–649, 2006.

- [182] H. Zhu, S. Huang, and P. Dhar. The next step in systems biology: Simulating the temporal-spatial dynamics of molecular network. *Bioessays*, 26:68–72, 2003.

List of publications

Publication in peer review papers (International)

1. L. Mariotti, Facoetti, A. Bertolotti, R. Nano, F. Pasi, A. Ottolenghi, Effects of ionizing radiation on cell-to-cell communication: a systems biology approach in view of a comprehensive description of signaling perturbation. *Radiat Res.* 174, 280-289 (2010)
2. D. Alloni, A. Campa, A Facoetti, W Friedland, M Liotta, L Mariotti, H G Paretzke, A Ottolenghi, A Monte Carlo study of radiation quality dependence of DNA fragmentation spectra. *Radiat. Res.* 173(3):263-271 (2010)
3. Facoetti, L. Mariotti, F. Ballarini, A. Bertolotti, R. Nano, F. Pasi, A. Ottolenghi, Experimental and theoretical analysis of cytokine release for the study of radiation induced bystander effect. *Int. J. Radiat. Biol.*, Vol 85 (8):690-699 (2009)
4. F. Ballarini, A. Facoetti, L. Mariotti, R. Nano, A. Ottolenghi, Role of cellular communication in the pathways of radiation-induced biological damage. *Advance in Space Research*, Vol 44: 917-925 (2009).
5. D. Alloni, F. Antonelli, F. Ballarini, M. Belli, A. Bertolotti, A. Campa, V. Dini, L. DàErcole, G. Esposito, A. Facoetti, W. Friedland, C. Giovannini, S. Grande, L. Guidoni, M. Liotta, F. Lisciandro, A. M. Luciani, L. Mantovani, L. Mariotti, R. Nano, A. Ottolenghi, A. Palma, H.G. Paretzke, F. Pasi, A. Rosi, O. Saporà, D. Scannicchio, G. Simone, E. Sorrentino, M.A. Tabocchini, V. Viti âCharged particle effects: experimental and theoretical studies on the mechanisms underlying the induction of molecular and cellular damage and the modulation of intercellular signallingâ. *Nuovo Cimento* 2008, Vol 31 C(1), 20-38
6. F. Pasi, A Bertolotti, A. Facoetti, L. Mariotti, A Ottolenghi, R Nano. Study of cytokines bystander signalling in human glioblastoma cells after exposure to gamma radiation. *Anticancer Research* 2008. Volume 28 (5C), 3439-3440

7. E Ranza, F.Pasi, A Bertolotti, A. Facchetti, L. Mariotti, A Ottolenghi, R Nano. Influence of IMATINIB mesylate on radiosensitivity on astrocytoma cells. *Anticancer Research* 2009, vol. 29 no. 11 4575-4578.
8. Bertolotti A, Ranza E, Mariotti, Pasi F, Facchetti A, Nano R, Mazzini G, Ottolenghi A. Mechanism of radiation effects at cellular level: bystander effects and modulation of the cytokine signaling. *Cytometry* 2010. PART A, vol. 77A; p. 155-156.
9. D. Alloni, A. Campa, M. Belli, G Esposito, L. Mariotti, M. Liotta, W. Friedland, H. Paretzke and A Ottolenghi. Monte Carlo evaluation of dna fragmentation spectra induced by different radiation qualities. *Rad Prot Dosimetry* , accepted (2010)
10. L Mariotti, A Facchetti, A Bertolotti, E Ranza, D Alloni, A Ottolenghi. Radiation induced perturbation of cell-to-cell signaling and communication. *Rad Prot Dosimetry*, accepted (2010)
Publication on national journals
11. Luca Mariotti. Modellizzazione dell'effetto bystander: come la radiazione modula la comunicazione cellulare. *SIRR 2008 Volume XI* (2), 6-9.
Invited Talks
12. Luca Mariotti. A systems radiation biology approach to investigate cell-to-cell signaling and its modulation by radiation. Invited talk, Bari, 25/09/2009. *XCV SIF (Italian Physical Society) Book of abstract*, p. 50 (2009)
13. Luca Mariotti Systems Radiation Biology: definitions and example useful for the investigation of biological effect induced by low dose irradiation. Invited talk, Roma. 26/10/2010, *XV SIRR (Italian Society for Radiation Research)*
14. Luca Mariotti, D. Alloni, A. Ottolenghi. Modelling cell-to-cell communication in a systems radiation biology framework. Invited talk, Bremen, Germany. 38th COSPAR Scientific Assembly. *Book of abstract*
15. Luca Mariotti. Un approccio integrato teorico-sperimentale per lo studio del cell signalling perturbato da radiazioni di diversa qualità . Invited talk, Roma, 14/05/2010, *La Radiobiologia degli adroni carichi con acceleratori INFN: ricerca, sviluppo, applicazioni*.
Abstract and participation to congresses
16. A Facchetti, D Alloni, F Ballarini, A Mairani, L Mariotti, R Nano, A Ottolenghi, How do experimental conditions and radiation affect cytokine signals ? *Int Cong. Radiat Res*, S. Francisco, July 2007, *Book of Abstracts*.

17. F. Ballarini, A. Facoetti, L. Mariotti, R. Nano, A. Ottolenghi, Role of cellular communication in the pathways of radiation-induced biological damage. 2008 COSPAR Meeting, Montreal, Canada, July 2008. Book of Abstracts
18. L. Mariotti (on behalf of UniPv).WP-2 WP-5 Contribution. 2nd NOTE meeting, Galway Ireland, 15 September 2008
19. Pasi F, Mariotti L, Bertolotti A, Facoetti A, Nano R, Ottolenghi A. Experimental and theoretical methodologies for cytokines bystander signaling. 2nd NOTE meeting, Galway Ireland, 15 September 2008
20. Mariotti L. Modelling the mechanisms of cell communication induced by radiation. Radiobiology Radiobiological Modelling in Radiotherapy 28 April à 1 May 2009. Chester UK.
21. A Bertolotti , L Mariotti et al, Studio dei messaggeri cellulari coinvolti nell'effetto bystander: influenza delle condizioni sperimentali. XIV Convegno nazionale SIRR, Trieste, Italy, 24 - 27 June 2008. Book of Abstracts, page 18.
22. A. Facoetti, L. Mariotti, A. Bertolotti, E. Ranza, F. Pasi, R. Nano, A. Ottolenghi. Experimental and theoretical study of the cytokine release after gamma irradiation of human fibroblasts. ISSBB (Italian Society for Space Biomedicine and Biotechnology) National Conference 31 March 2009, abstract. Book of abstract, page 41.
23. L. Mariotti (on behalf of UniPv).WP-2 WP-5 Contribution. 3rd NOTE meeting, Rome Italy, 29 June à 1 July 2009
24. D. Alloni, A. Campa, M Belli, G Esposito, A Facoetti, W Friedland, M Liotta, L Mariotti, H G Paretzke, A Ottolenghi,. Monte Carlo evaluation of DNA fragmentation induced by heavy ions. IBIBAM congress, Koln, 6-10 July 2009. Book of Abstracts
25. E Sorrentino, A Bertolotti, G Esposito, A Facoetti, S Grande, L Mariotti, R Nano, A Ottolenghi, E Ranza, MA Tabocchini. Investigation of signal transmission and bystander effects in relation to radiation quality. IBIBAM congress, Koln, 6-10 July 2009. Book of Abstracts
26. A. Ottolenghi, A Facoetti, L Mariotti. La valutazione dei rischi sanitari delle basse dosi di radiazioni ionizzanti: la ricerca italiana e le sue prospettive nel contesto europeo. Il contributo della modellistica. ISS,Roma, 27/02/2009.
27. D Alloni, A Campa, M Belli, G Esposito, A Facoetti, W Friedland, M Liotta, Luca Mariotti, H Paretzke, A Ottolenghi. Monte Carlo simulation of DNA fragmentation induced by heavy ions. XCV SIF (Italian Physical Society) Book of abstract, p. 20 (2009)

28. L. Mariotti, A. Facchetti, A. Bertolotti, E. Ranza, D. Alloni, A. Ottolenghi. Radiation induced perturbation of cell-to-cell signaling and communication. MICROS 2009, Book of abstract, p. 40 (2009)
29. D. Alloni, A. Campa, M. Belli, G. Esposito, L. Mariotti, M. Liotta, W. Friedland, H. Paretzke and A. Ottolenghi. Monte Carlo evaluation of dna fragmentation spectra induced by different radiation qualities. Micros 2009, book of abstract, p. 12 (2009)
30. A. Bertolotti, G. Esposito, A. Facchetti, S. Grande, L. Mariotti, A. Ottolenghi, E. Ranza, G. Simone, E. Sorrentino, M. A. Tabocchini, Radiation quality dependence of signal transmission and bystander induced cell killing, 38th COSPAR Scientific Assembly Bremen, Germany, 18-25 July 2010. Book of Abstracts
31. A. Campa, F. Antonelli, G. Esposito, L. Mariotti, M. Belli, P. Giardullo, G. Simone, M.A. Tabocchini, A. Ottolenghi, DNA DSB measurements and modelling approaches based on gamma-H2AX foci time evolution, 38th COSPAR Scientific Assembly, Bremen, Germany, 18-25 July 2010. Book of Abstracts
32. C. Cutaia, D. Alloni, L. Mariotti, A. Ottolenghi. Dna damage dependence on the subcellular distribution of low-energy beta- emitters. 38th COSPAR Scientific Assembly. Bremen, Germany, 18-25 July 2010. Book of Abstracts
33. L. Mariotti (on behalf of UniPv). WP-2 WP-5 Contribution. 4th NOTE meeting, Stockholm, Sweden, 6 September 2010
34. L. Mariotti, D. Alloni, A. Ottolenghi. How does radiation perturb cell communication? Radiation Research Annual Meeting, Maui, Hawaii, 25-29 September 2010. Book of Abstracts
35. G. Schettino, K. Savage, L. Mariotti, D. Richard and K.M. Prise, Spatio-temporal investigations of DNA damage repair following low LET radiation., Radiation Research Annual Meeting, Maui, Hawaii, 25-29 September 2010. Book of Abstracts
36. L. Mariotti, D. Alloni, D. Scannicchio, A. Ottolenghi. An integrated stochastic/deterministic modeling approach to investigate the radiation-induced perturbation of cell signaling. 4th Systems Radiation Biology Workshop, New York, 19-22 May 2010. Book of Abstracts
37. L. Mariotti, D. Alloni, D. Scannicchio, A. Ottolenghi. Simulation of cell signalling perturbation induced by radiation. 38th Annual Meeting - ERR 2010 Stockholm, Sweden, September 5-9, 2010. Book of Abstracts

38. L. Mariotti, F. Antonelli, G. Esposito, G. Simone, A. Campa, M. Belli, D. Cappelletti, A. Bertolotti, E. Ranza, M.A. Tabocchini, A. Ottolenghi. Bystander effects in human fibroblasts as a function of radiation quality. 38th Annual Meeting - ERR 2010 Stockholm, Sweden, September 5-9, 2010. Book of Abstracts
39. F. Antonelli, S. Grande, L. Mariotti, A. Rosi, G. Esposito, G. Simone, A. Campa, M. Belli, A. Ottolenghi, D. Cappelletti, A. Bertolotti, E. Ranza, A. Facoetti, M.A. Tabocchini. Early and late mediators of the signalling chain leading to bystander effects. 38th Annual Meeting - ERR 2010 Stockholm, Sweden, September 5-9, 2010. Book of Abstracts
40. C. Cutaia, D. Alloni, L. Mariotti, W. Friedland, A. Ottolenghi. Modelling of dose and dna damage due to low-energy b- emitters within cell nucleus and cell cytoplasm. 38th Annual Meeting - Err 2010 Stockholm, Sweden, September 5-9, 2010. Book of Abstracts
41. Cutaia C., Alloni D., Mariotti L., Friedland W., Ottolenghi A. Dipendenza del danno al DNA dalle distribuzioni di emettitori di beta- di bassa energia nel nucleo e nel citoplasma cellulare. XCVI SIF (Italian Physical Society), Bologna, September 20, 2010 Book of abstract
42. Alloni D., Mariotti L., Friedland W., Ottolenghi A. Track structure, radiation quality and initial events in radiobiological damage, MC2010, Stockholm, 9-12 November 2010

Acknowledgments

This work was partially supported by **European Commission**:

- **RISC RAD** project (DNA damage responses, genomic instability and radiation-induced cancer: the problem of risk at low and protracted doses)
- **NOTE** project (Non-targeted effects of ionising radiation: A new paradigm of Radiation Biology)
- **ALLEGRO** project (Early and late health risks to normal/healthy tissues from the use of existing and emerging techniques for radiation therapy)
- **DOREMI** project (Low Dose Research towards Multidisciplinary Integration)

This work was also partially supported by the **National Institute of Nuclear Physics (INFN)**:

- **EPICA** project (Effetti delle particelle cariche: meccanismi di induzione di danno molecolare e cellulare, e modulazione del signalling intercellulare)
- **TENORE** project (Meccanismi di danno e di risposta (a livello molecolare, cellulare e sovracellulare) negli effetti targeted e non-targeted delle radiazioni ionizzanti: dipendenza dalla qualita' della radiazione)

and by the **Italian Space Agency (ASI)**: **COUNT** project (Countermeasures for the exposure to Galactic Cosmic Rays in deep space).